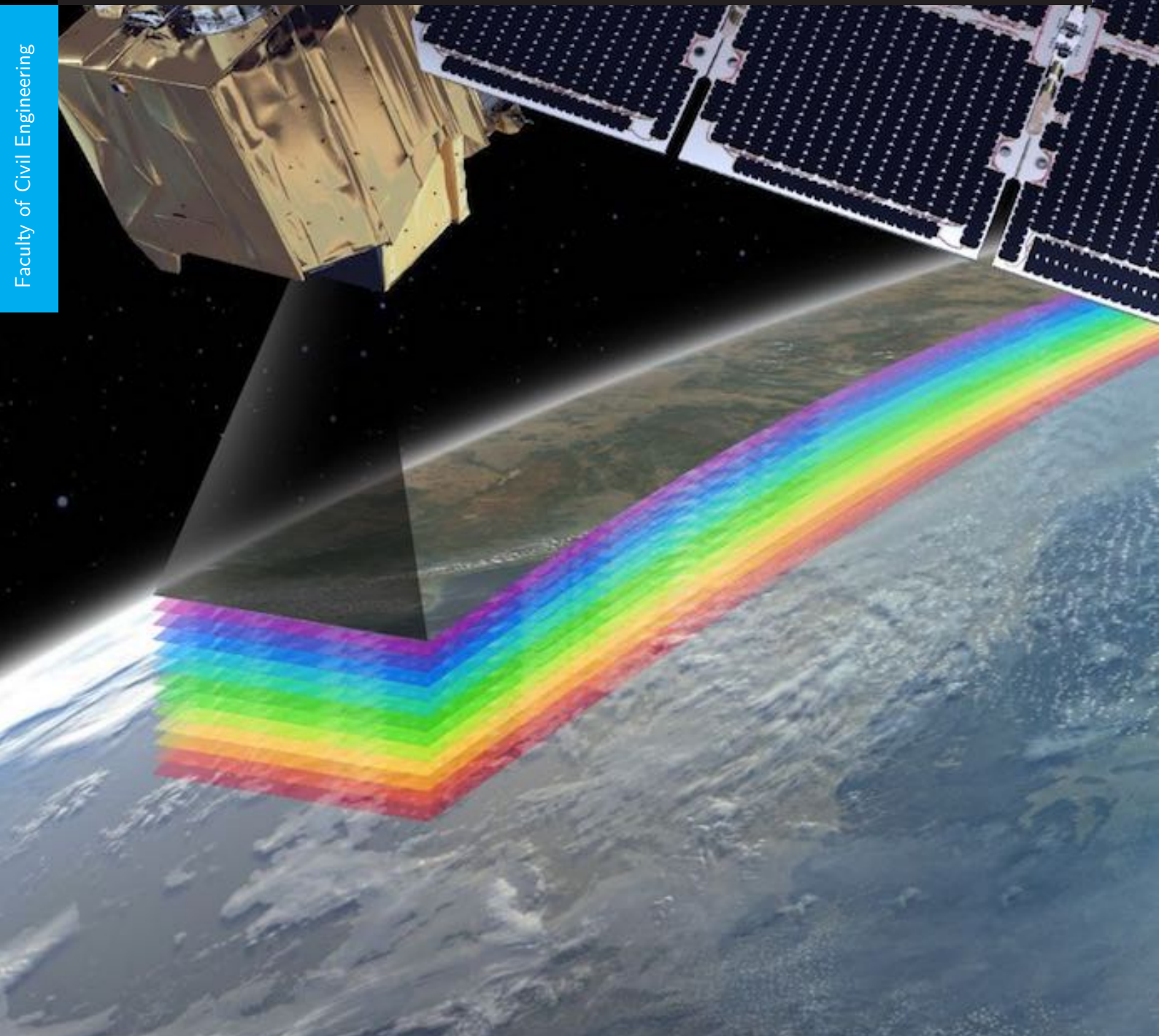


Master's Thesis

Constructing a One-Minute Video from a 2.586 Seconds Burst of Sentinel-2 Imagery to Show the Potential for Estimating Wave-Derived Nearshore Bathymetry by Using a Spatio-Temporal Cross-Correlation Method and a DMD-Based DIA

H. de Lange



Faculty of Civil Engineering

MASTER'S THESIS

Constructing a One-Minute Video from a 2.586 Seconds Burst of Sentinel-2 Imagery to Show the Potential for Estimating Wave-Derived Nearshore Bathymetry by Using a Spatio-Temporal Cross-Correlation Method and a DMD-Based DIA

by

H. de Lange

In fulfillment of the requirements for the degree of

Master of Science
Civil Engineering

at the Delft University of Technology,

Date:	12 July 2021	
Supervisors:	Dr. R. Almar	LEGOS (IRD)
	Dr. ir. E. W. J. Bergsma	LEGOS (CNES)
Thesis Committee:	Prof. dr. ir. S.G.J. Aarninkhof	TU Delft
	Dr. ir. S. de Vries	TU Delft
	Dr. J.F. Lopez Dekker	TU Delft
	Ir. M. Gawehn	TU Delft



PREFACE

Dear reader,

Sometimes life is a wave, just like the study to become a Civil Engineer. It has peaks and troughs, supported by the (sea)bottom that lies beneath.

You have just started reading the master's thesis of Rikus de Lange, master student Hydraulic Engineering at the Faculty of Civil Engineering and Geosciences of the Delft University of Technology. The research, described in this thesis took place in close collaboration with the research institute LEGOS (IRD/CNES) in Toulouse, France, from September 2020 to March 2021. Unfortunately, the research could not take place at the LEGOS laboratory in Toulouse as planned due to the Covid-19 pandemic. Nevertheless, close and constructive cooperation has continuously been delivered, consumed and enjoyed.

From LEGOS I like to thank my supervisor Rafael Amar. His in-depth knowledge of satellites and waves has enabled me to get the most out of this research. Also my special thanks goes to Erwin Bergsma. As a Dutchman working at Legos and a substantive expert, he was able to break down barriers and, if necessary, to provide me with a peptalk every day.

From TU Delft, I would like to thank my thesis committee for reviewing and grading this project. With special thanks to Stefan Aarninkhof. In addition to his inspiring substantive qualities, I also highly appreciate his personal involvement. He called me personally late in the evening in Toulouse, just after my arrival, to inform me that due to a change in Covid regulations I had to return the other day. I would like to thank Matthijs Gawehn for the daily supervision and the many sparring moments in Rotterdam. I am very grateful for his first-hand tips and tricks and the fundamental discussions we could have about the subject. I would also like to express my special thanks to Sierd de Vries, who made it possible for me to be physically present at TU Delft once a week. And to Paco Lopez Dekker for his expertise in Remote Sensing and his critical questions during our meetings.

From my inner circle I like to express my big thanks to my housemates Ruben, Olivier and Lucas who always managed to motivate me when I was tired of working alone in my student room. I would also like to thank Tracy for her support and critical eye. And my dear sister Florian with her listening ear, and for lending me her Macbook at the last minute to make it possible to perform the final time-consuming computer runs. Finally, I would like to express my warm gratitude to my parents for their faith, trust and support during so many years and for giving me the opportunity to enjoy a real student life, while growing up to become a genuine Delft Civil Engineer.

I wish you a pleasant reading and I hope you enjoy my research report. I really enjoyed working on it and I am pleased to have been able to contribute to prediction models for future floods and thus to the protection of the inhabitants of coastal areas. If you have any questions afterwards, feel free to contact me. Finally, remember:

The deeper the sea, the higher the waves; every obstacle leads to rising opportunities!

*H. de Lange
Rotterdam, July 2021*

ABSTRACT

To effectively mitigate environmental changes and to manage coastal environments, a good understanding of nearshore bathymetry and its evolution is required. The coastal zone is expected to be vulnerable in the foreseeable future due to the combined effects of increased coastal impacts and a growing coastal population. The use of spaceborne remote sensing methods has been developed in recent decades to estimate nearshore bathymetry. Compared to traditional methods, spaceborne remote sensing techniques offer a relatively large spatial coverage as well as frequent temporal monitoring. The Sentinel-2 mission is potentially able to provide regular bathymetry estimations, mainly due to its significant revisit time and freely accessible data.

This research focuses on the development of a spatio-temporal cross-correlation model in order to construct a one-minute wave-representing video. The video is used to show the potential for wave-derived bathymetry estimation, exploiting a depth inversion algorithm (DIA) based on dynamic mode decomposition (DMD) to invert depth. The model is applied to two distinct datasets: a synthetic FUNWAVE dataset and Sentinel-2 imagery. The Sentinel-2 imagery covers research sites in Saint-Louis, Senegal and Capbreton, France.

Three model requirements are created based on the research objectives. The model should show wave propagation for at least one minute and, moreover, the waves in the video should accurately represent the wave field. Both requirements are demanded by the use of a DMD-based DIA. Lastly, the resulting video should enable an accurate bathymetry estimation. Based on the requirements, the developed spatio-temporal cross-correlation model includes four model parts: pre-processing, image resolution augmentation, wave characteristics estimation and video construction.

The research has led to a range of insights. A discrepancy between the quality of constructed videos and related bathymetry estimations is observed. The videos as constructed by the model generally show a good representation of average wave propagation for a sufficiently long duration, while the bathymetry estimations are less accurate. The low quality of bathymetry estimations is explained by three main error sources: celerity estimation errors, the applied filtering methods and the way in which the video is constructed. These three error sources together lead to videos that lack pixel-wise detail and therefore decrease the bathymetry estimation quality. The developed application framework shows that estimating wave characteristics from Sentinel-2 imagery by means of the model is at the edge of possibilities. In temporal sense, relatively large celerity estimation errors are expected for wave periods lower than 5 s and higher than 8 s. The model is less sensitive for spatial parameters: as long as wavelengths are larger than circa 150 m the celerity estimation error is acceptable.

All together, the developed model and related video constructions offer added value, although not for the purpose of a bathymetry estimation by means of a DMD-based DIA. The constructed videos represent wave propagation in an average sense and can therefore be exploited for wave-related purposes, e.g. obtaining wave spectra, estimating dominant wave direction and estimating wave climates. In general, the video offers a way to enlarge the temporal range of Sentinel-2 imagery. It is furthermore concluded that the model is probably more suitable for use in combination with other types of imagery, including satellite imagery with larger burst duration and increased spatial resolution as well as standard video imagery.

CONTENTS

Preface	i
Abstract	ii
List of Symbols and Acronyms	vi
Glossary	vii
List of Figures	ix
List of Tables	xii
I Base	1
1 Introduction	3
1.1 Sentinel-2 Mission	5
1.2 Research Gap	6
1.3 Problem Statement and Research Objectives	8
1.4 Research Questions	10
1.5 Structure of the Report.	10
2 Waves and Sentinel-2 Imagery	12
2.1 Sentinel-2 Imagery	12
2.2 Sentinel-2 User Products	14
2.3 Observing Waves from Sentinel-2 Imagery	15
3 Datasets	16
3.1 Dataset 1: Synthetic FUNWAVE Dataset	16
3.2 Dataset 2: Sentinel-2 Imagery	18
4 Research Methodology	20
4.1 Methodology: Spatio-Temporal Cross-Correlation Model	20
4.1.1 Model Overview and Model Parts	20
4.1.2 Model Requirements	22
4.1.3 Model Variants	22
4.2 Methodology: Dataset Analysis	23
4.2.1 Analysis of Dataset 1, Synthetic FUNWAVE Dataset	23
4.2.2 Analysis of Dataset 2, Sentinel-2 Imagery.	23
4.2.3 Evaluating the Model Performance based on the Model Requirements	23
4.3 Summary of Methodology	24
II Results	25
5 Spatio-Temporal Cross-Correlation Model	26
5.1 Overview of the Spatio-Temporal Cross-Correlation Model.	26
5.2 Illustrating Sinusoidal Wave	28
5.3 Main Mathematical Principle of the Model: Cross-Correlation.	29
5.4 Model Part 0: Pre-Processing	31
5.4.1 Manual Selection of the Area of Interest	31
5.4.2 Selection of Usable Imagery	31
5.4.3 Equalisation of the Time Lag between Spectral Bands.	31

5.4.4	Determination of the Order of Spectral Bands	32
5.4.5	Detrending and Normalising	32
5.4.6	Filtering the Imagery Using a 2D Fourier Transform	32
5.5	Model Part 1: Image Resolution Augmentation	33
5.6	Model Part 2: Wave Characteristics Estimation	35
5.6.1	Estimation of Dominant Wave Direction	35
5.6.2	Estimation of Wavelength	37
5.6.3	Estimation of Wave Celerity	37
5.7	Model Part 3: Video Construction	39
5.7.1	Median Filtering of Estimated Wave Characteristics	39
5.7.2	Creation of Time Vectors and Video Construction	39
5.8	Summary Chapter 5: Spatio-Temporal Cross-Correlation Model.	43
6	Dataset Analysis	45
6.1	Results: Synthetic FUNWAVE Dataset	46
6.1.1	Wave Direction Estimations	46
6.1.2	Wavelength Estimations	47
6.1.3	Celerity Estimations	48
6.1.4	Wave Spectra	49
6.1.5	Video Duration	49
6.1.6	Bathymetry Estimations	50
6.2	Results: Sentinel-2 Imagery in Saint-Louis	51
6.2.1	Wave Direction Estimations	51
6.2.2	Wavelength Estimations	51
6.2.3	Wave Celerity Estimations	52
6.2.4	Wave Spectra	52
6.2.5	Video Duration	53
6.2.6	Bathymetry Estimations	53
6.3	Results: Sentinel-2 Imagery in Capbreton	54
6.3.1	Wave Direction Estimations	54
6.3.2	Wavelength Estimations	54
6.3.3	Wave Celerity Estimations	55
6.3.4	Wave Spectra	55
6.3.5	Video Duration	56
6.3.6	Bathymetry Estimations	56
6.4	Interpretation of Dataset Analysis.	57
6.4.1	Interpretation of Synthetic FUNWAVE Dataset Analysis.	57
6.4.2	Interpretation of Sentinel-2 Imagery Analysis in Saint-Louis	57
6.4.3	Interpretation of Sentinel-2 Imagery Analysis in Capbreton	58
III	Reflection	59
7	Discussion	60
7.1	Interpretation of Results	60
7.1.1	Wave Propagation in the Constructed Videos	60
7.1.2	Bathymetry Estimations	61
7.1.3	Estimation of Wave Characteristics in the FUNWAVE Domain	62
7.1.4	Estimation of Wave Characteristics in Sentinel-2 Imagery	66
7.1.5	Filtering	68
7.1.6	Average Representation of Wave Characteristics in the Video.	70
7.1.7	Video Duration	70
7.1.8	Celerity, Video and Bathymetry	71

7.2	Delimitations and Assumptions.	72
7.2.1	Scope of the Thesis	72
7.2.2	Datasets	72
7.2.3	Ground-Truth Wave Spectrum.	72
7.2.4	Ground-truth Bathymetric Data.	72
7.2.5	Currents and Wind	73
7.3	Retrospection.	73
7.4	Added Value of the Research.	73
8	Conclusion	75
9	Recommendations	77
9.1	Improving the Model.	77
9.1.1	In-depth Research on Celerity Estimation	77
9.1.2	In-depth Research on Image Resolution Augmentation	77
9.1.3	In-depth Research on Video Construction Method	78
9.1.4	Research using Detailed Datasets	78
9.2	Other Applications of the Model	78
9.2.1	Research on Other Types of Imagery	78
9.2.2	Research on the Value of Other Applications	78
9.3	Sentinel-2 Imagery and Bathymetry Estimation	78
9.3.1	Keep Focusing on a Wave-Derived Bathymetry	79
9.3.2	Keep Focusing on a Cross-Correlation in Space-Time Domain	79
9.3.3	Focus on Celerity Estimation by Improving Resolution Augmentation.	79
9.3.4	Make the Celerity Estimation Perfect for Sinusoidal Waves	79
9.3.5	Avoiding Video Construction for Bathymetry Estimation Purposes	79
	References	80
	Appendices	87
A	Wave Climate Capbreton, France, March 2018	88
B	Wave Climate Saint-Louis, Senegal, March 2019	89
C	Theoretical Application Range of the Model	90
C.1	Motivation to Define a Theoretical Application Range	90
C.2	Dataset 3: Set of Synthetic Sinusoidal Waves.	90
C.3	Methodology: Theoretical Application Range of the Model.	91
C.3.1	Percent Error and Dimensionless Parameters	91
C.3.2	Temporal and Spatial Analysis.	91
C.3.3	Wave Phase Differences	92
C.4	Results: Theoretical Application Range.	93
C.4.1	Results: Temporal Analysis Wavelength Estimations.	93
C.4.2	Results: Spatial Analysis Wavelength Estimations	94
C.4.3	Results: Temporal Analysis Celerity Estimations	95
C.4.4	Results: Spatial Analysis Celerity Estimations	96
C.5	Interpretation of Theoretical Application Range	97
D	Celerity Fields in Saint-Louis	98
E	Bathymetry Estimations in Saint-Louis	101

LIST OF SYMBOLS AND ACRONYMS

Symbol	Description	Unit
θ	Angle	degree
ω	Angular frequency	rad/s
Dur	Burst duration	s
c	Celerity	m/s
x	Cross-shore distance	m
d_{int}	Deep water limit	m
Radius	Domain radius	m
g	Gravitational acceleration	m/s ²
d	Local depth	m
y	Longshore distance	m
L_o	Offshore wavelength of water waves	m
T_p	Peak wave period	s
ρ	Pearson correlation coefficient	-
PE	Percent error	%
RMSE	Root-mean-square error	m
d_{sh}	Shallow water limit	m
H_s	Significant wave height	m
ϕ	Spatial phase change	m
Res	Spatial resolution	m
η	Surface height	m
t	Time	s
Δt	Time lag	s
a	Wave amplitude	m
Dir	Wave direction	degree
k	Wave number	rad/m
k_x	Wave number in x-direction	rad/m
k_y	Wave number in y-direction	rad/m
T	Wave period	s
λ	Wavelength of light waves	m
L	Wavelength of water waves	m

GLOSSARY

Acoustic Doppler current profiler (ADCP) Instrument for observing waves and ocean currents based on sampling the range-gated Doppler return of acoustic beams.

Bathymetry The ocean's depth relative to sea level, the study of the 'submarine topography'.

Burst duration The overall temporal offset between the first and last band of satellite imagery.

Constellation A group of artificial satellites working together as a system.

Cross-correlation Measuring the similarity of two (time) series as a function of the displacement of one relative to the other.

Depth inversion algorithm (DIA) Technique that analyses wave features in order to obtain depth.

Domain radius Radius that defines the size of the calculation domain: the area that is used to provide information for the estimation of wave characteristics at a certain pixel.

Dynamic Mode Decomposition (DMD) A post-processing technique that extracts dynamic information of a physical process from snapshots.

Echo-sounding Determining the depth of the seabed by measuring the time taken for sounds echoes to return to the listener/observer.

EMODnet The European Marine Observation and Data Network, an organisation that aims to provide a single access point to a range of available marine measurements, such as bathymetric charts.

GEBCO The General Bathymetric Chart of the Oceans.

Imagery A collection of visual images.

In-situ Measurements performed on site.

LiDAR Light Detection and Ranging, a remote sensing method that uses light in the form of a pulsed laser to measure variable distances to the Earth.

Low-elevation coastal zone (LECZ) The contiguous and hydrologically connected zone of land along the coast and below 10 m of elevation.

Metadata A set of data that describes other data (imagery) and/or provides background information.

Multi Spectral Instrument (MSI) An instrument that measures the Earth's reflected radiance in multiple spectral, or frequency bands.

Multi-spectral Consisting of multiple frequency bands.

Nearshore The zone extending from the offshore zone (where waves and seabed hardly interact) to the breaker, or swash zone (where waves start to dissipate and break) [1].

Ortho-image A computer-generated image of an aerial photograph in which displacements and distortion due to terrain relief and camera tilts have been removed.

Radar A detection system that uses radio waves to determine the range, angle or velocity of objects.

Remote sensing The process of detecting the physical characteristics of an area by measuring its reflected and emitted radiation at a distance, typically from an aircraft or satellite.

Revisit Time The time elapsed between observations of the same point on Earth by a satellite.

Satellite An artificial body placed in an orbit around the earth or moon or another planet for communication or monitoring purposes.

Spatial Relating to information regarding position, area or size.

Spatial resolution The physical dimension that represents a pixel of an image. Can be interpreted as the linear spacing between each pixel.

Spectral Relating to frequencies or analysis in the frequency domain.

Sun-synchronous orbit Circulating around the Earth while being in the same 'fixed' position relative to the sun, which means in practical that a certain location at the Earth is always visited at the same time of the day and therefore experiences the same light circumstances.

Synthetic dataset A dataset that is artificially manufactured instead of generated from real-world measurements.

Temporal Relating to information regarding time.

Time lag The temporal offset between each separate band of satellite imagery.

Video A recording of moving visual images.

Wave characteristics (Statistical) parameters that define the propagation of waves.

Wave parameters (Statistical) parameters that define the propagation of waves. Is used interchangeably with the term 'wave characteristics'.

LIST OF FIGURES

1.1	Estimated population in the low-elevation coastal zone (LECZ) by 2060.	3
1.2	Examples of the Sentinel-2 constellation and its imagery.	5
1.3	Structure of the report.	11
2.1	Example of Sentinel-2 imagery off the coastline of Senegal.	12
2.2	Schematic representation of the focal plane configuration of the Sentinel-2 satellite.	13
2.3	Sentinel-2 imagery off the coast of Saint-Louis, Senegal, projected in varying resolutions.	15
2.4	Sentinel-2 image showing the propagation of waves	15
3.1	Input bathymetry and free surface height of the FUNWAVE simulation.	17
3.2	Decreasing the resolution of FUNWAVE bands from 1 m to 10 m and 20 m.	17
3.3	Overview of the research sites: Capbreton and Saint-Louis	18
3.4	Site selection of the coast off Capbreton and Saint-Louis.	19
4.1	Schematic overview of methodology	21
5.1	Overview spatio-temporal cross-correlation model.	27
5.2	Illustrating sinusoidal wave defined over a 3D domain (x, y, η) with corresponding cross-section.	28
5.3	A cross-section of the illustrating sinusoidal wave, together with 10 snapshots that show wave propagation.	29
5.4	Time series of the illustrating wave.	30
5.5	Time series of the illustrating sinusoidal wave	30
5.6	Interpolation of a irregular time vector.	31
5.7	Satellite imagery showing the distinction between sea and land areas.	32
5.8	Schematic of Radon transform [2].	34
5.9	Example of a Radon transform.	35
5.10	Cross-correlation for a pixel of interest.	36
5.11	Overview of estimated wave direction for a range of pixels of the illustrating sinusoidal wave.	36
5.12	Estimation of wavelength for a pixel of the hypothetical sinusoidal.	37
5.13	Correlation images and isolated signals	38
5.14	Celerity estimation of a certain pixel of the illustrating sinusoidal wave.	39
5.15	Perpendicular distance from a surrounding point to the wave crest in the point of interest.	40
5.16	Example showing the difference between two distances of interest.	42
6.1	Wave direction estimations for the entire domain of the synthetic FUNWAVE dataset.	46
6.2	Cross-correlation images corresponding to a wave direction estimation for pixel $(X = 450 \text{ m}, Y = 900 \text{ m})$ of the synthetic FUNWAVE dataset.	46
6.3	Wavelength estimations for the entire domain of the synthetic FUNWAVE dataset.	47
6.4	Wavelength estimation for pixel $(X = 450 \text{ m}, Y = 900 \text{ m})$ of the synthetic FUNWAVE dataset.	47
6.5	Celerity estimations for the entire domain of the synthetic FUNWAVE dataset.	48
6.6	Celerity estimation for pixel $(X = 450 \text{ m}, Y = 900 \text{ m})$ of the synthetic FUNWAVE dataset.	48
6.7	Wave spectra related to the synthetic FUNWAVE dataset.	49

6.8	Snapshots of the constructed video that relates to the synthetic FUNWAVE dataset. . .	49
6.9	Bathymetry estimation for the domain of the synthetic FUNWAVE dataset.	50
6.10	Bathymetry estimation comparison related to the synthetic FUNWAVE dataset.	50
6.11	Estimations of wave direction applied to the domain of the research site off the coast of Saint-Louis.	51
6.12	Estimations of wavelength applied to the domain of the research site off the coast of Saint-Louis.	51
6.13	Celerity estimations for the domain of Saint-Louis.	52
6.14	Wave spectra corresponding to the video in Saint-Louis.	52
6.15	Snapshots of the constructed video that relates to the Sentinel-2 imagery in Saint-Louis.	53
6.16	EMODnet ground-truth bathymetry and bathymetry estimations in Saint-Louis. . . .	53
6.17	Estimations of wave direction applied to the domain of the research site off the coast of Capbreton.	54
6.18	Estimations of wavelength applied to the domain of the research site off the coast of Capbreton.	54
6.19	Celerity estimations for the domain of Capbreton.	55
6.20	Wave spectra for the domain of Capbreton.	55
6.21	Snapshots of the constructed video that relates to the Sentinel-2 imagery in Capbreton.	56
6.22	Bathymetry estimations in Capbreton.	56
7.1	Comparison of in-situ measured and video-obtained 2D variance-density spectrum in Saint-Louis.	61
7.2	Cross-section of ground-truth bathymetry and estimated bathymetries related to the synthetic FUNWAVE dataset.	61
7.3	Cross-correlation images corresponding to a wave direction estimation for pixel ($X = 450$ m, $Y = 900$ m) of the synthetic FUNWAVE dataset.	62
7.4	Cross-sections of the synthetic FUNWAVE domain, presenting celerity and wavelength estimations.	63
7.5	Theoretical application range of the model.	63
7.6	Theoretical application range of the model in relation to the estimation of wavelength.	64
7.7	Theoretical application range of the model in relation to the estimation of celerity. . .	65
7.8	Average celerity estimation errors for varying wavelength.	65
7.9	Theoretical application range of the model in relation to the estimation of wavelength for Sentinel-2 Imagery.	66
7.10	Theoretical application range of the model in relation to the estimation of celerity for Sentinel-2 Imagery.	67
7.11	Celerity estimations for the domain of Saint-Louis.	69
7.12	Celerity estimations for the domain in Saint-Louis.	69
7.13	Theoretical application range corresponding to celerity estimation errors.	74
A.1	GFS-Wave wave climate of Capbreton, France, in March 2018 [3, 4]	88
B.1	GFS-Wave wave climate of Dakar, Senegal, a city nearby Saint-Louis, in March 2019 [3, 4]	89
C.1	Example of a sinusoidal wave snapshot ($L = 240$ m).	91
C.2	Wave phase differences and pixel positions.	92
C.3	Overview of results temporal analysis regarding wavelength estimations.	93
C.4	Overview of results spatial analysis regarding wavelength estimations.	94
C.5	Overview of results temporal analysis regarding celerity estimations.	95
C.6	Overview of results spatial analysis regarding celerity estimations.	96
D.1	Celerity Field in Saint-Louis.	98
D.2	Celerity Field in Saint-Louis.	99

D.3 Celerity Field in Saint-Louis. 100

E.1 Bathymetry Estimations in Saint-Louis. 101

E.2 Bathymetry Estimations in Saint-Louis. 102

E.3 Bathymetry Estimations in Saint-Louis. 103

LIST OF TABLES

2.1	Overview of spectral bands of the Sentinel-2 constellation.	13
3.1	Overview input and output parameters FUNWAVE simulation.	16
3.2	Overview of Sentinel-2 imagery in Saint-Louis and Capbreton.	19
4.1	Model requirements	22
4.2	Model requirements and evaluation criteria	23
6.1	Model requirements and evaluation criteria	45
6.2	Overview of Pearson correlation coefficients (ρ) and RMSE between estimated bathymetry and ground-truth in Saint-Louis.	53
6.3	Overview of pearson correlation coefficients (ρ) and RMSE between estimated bathymetry and ground-truth in Capbreton.	56
C.1	Overview of dimensionless temporal and spatial parameters.	92

I

BASE

1

INTRODUCTION

To effectively mitigate environmental changes and to manage coastal environments, a good understanding of bathymetry and its evolution is required [5, 6]. The coastal environment is more frequently and more intensely exposed to a range of climatological extremes and coastal hazards due to global climate change [5]. Local impacts, such as sea-level rise, increased storm surge and severe wave load, lead to an increase of coastal floodings and the change of erosion/sedimentation patterns within the coastal zone [5, 7, 8]. Moreover, the coastal areas are inhabited by a large amount of citizens. These coastal zones house a significant part of the world's population; nearly 2.4 billion people - about 40% of the total number of people on earth (2009) - live within 100 km of the coast [9]. Furthermore, the population density in the coastal areas is larger than the population density in non-coastal environments [10]. This difference is only expected to increase, since globally, people tend to migrate seawards: the population of the **Low-Elevation Coastal Zone (LECZ)** is predicted to more than double from 625 million in 2000 to 1.4 billion by 2060 [7].

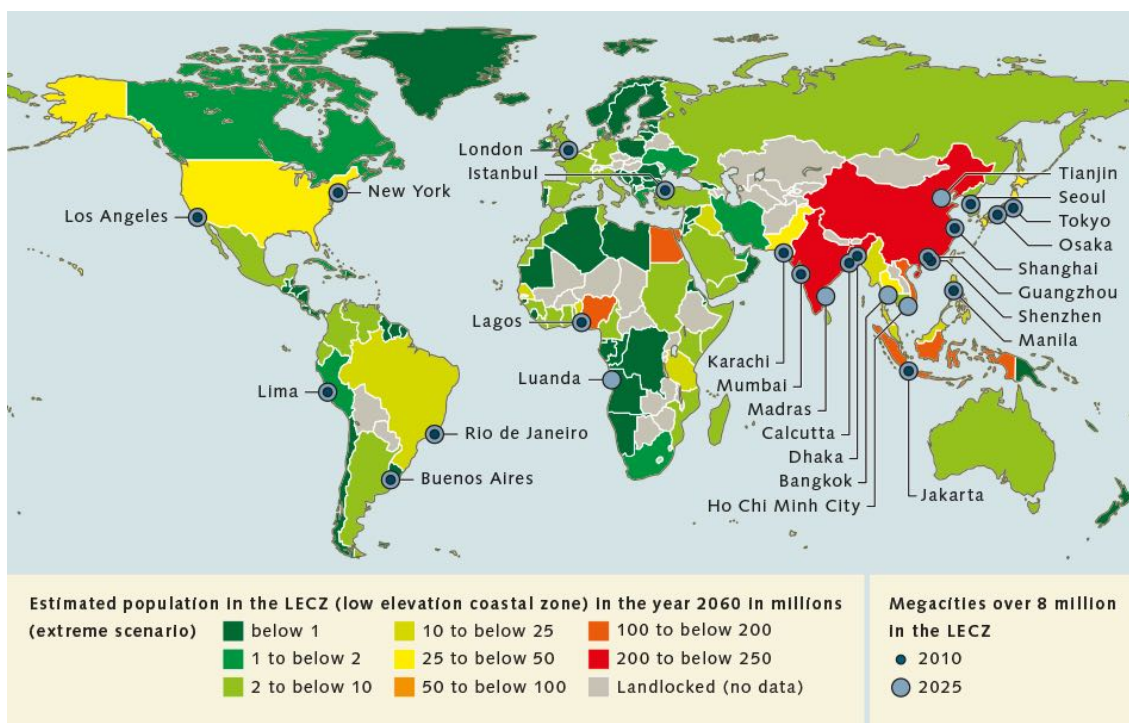


Figure 1.1: Estimated population in the low-elevation coastal zone (LECZ) by 2060. Following the most extreme scenario, a total LECZ population increase from 625 million (2000) to 1.4 billion (2060) is expected [7].

As a consequence of the combined effects of increased impacts on the coastal zone and a rapidly growing coastal population, the coastal communities are expected to be highly vulnerable in the

foreseeable future [11, 12]. To develop adequate adaptation and mitigation policies, a broad understanding of the coastal zone and its processes is indispensable [13]. Among other characteristics, there is specific interest in the [nearshore bathymetry](#), mainly because it dictates the storm surge and wave impact; sea level height, [wave characteristics](#) and coastal bathymetry are strongly related to each other [5, 14, 15]. It should be acknowledged that understanding coastal bathymetry is paramount for effective coastal management strategies such as nourishment programs as well [6]. Assessing the nearshore bathymetry is therefore essential to managing coastal areas [7, 8, 11, 12], as well as to the enhancement of economy, recreation and ecology in the coastal zone [6].

ESTIMATING NEARSHORE BATHYMETRY

A range of methods exists to estimate the local nearshore bathymetry. Ship-based [in-situ](#) techniques have been quite popular in the past centuries. Historically, a conventional pre-measured rope or leadline was used to measure the local depth [16, 17]. Although recently, more advanced techniques based on [echo-sounding](#) [18] and [radar](#) technology [19] have been commonly applied when measuring from ships or other moving vessels. Airborne [remote sensing](#) techniques have been around for a long time as well. One of the first known missions to assess the local bathymetry from the air was performed during World War II in an attempt to identify the gradients of enemy-held beaches using aerial photographs to recognise wave patterns [20, 21]. In the last few decades these airborne techniques have been improved significantly. Nowadays, techniques based on laser technology ([LiDAR](#)) provide accurate measurements [22–24]. A more recent development is the usage of shore-based remote sensing methods. The main technological approaches within this field are based on [video imagery](#) [25–27] and radar technology [28–30].

Each measuring method comes with its own advantages and limitations. Although relatively accurate, ship-based measurements are generally time-consuming and expensive, while their [spatial](#) and [temporal](#) range is quite low [17, 27]: it is relatively costly to do regular ship-based measurements on a small and local spatial scale. Since the coastal zone is known for its highly dynamic environment, the need for cost-effective and frequently repeated measurements is clear [5, 25, 31]. In this way the main disadvantage of ship-based measurements is disclosed. Airborne ([LiDAR](#)) technologies make a decent attempt to overcome these issues by providing an increase of spatial scale while preserving the same order of accuracy as ship-based measurements. However, these airborne technologies are still quite expensive, especially when a high measuring frequency is demanded [16, 32]. On the other hand, shore-based remote sensing systems (video and radar) provide an accurate, cost-effective alternative that measures continuously [27, 29], but these methods are restricted by their local spatial coverage [5, 33].

SPACEBORNE REMOTE SENSING FOR NEARSHORE BATHYMETRY ESTIMATION

A development over the last few years is the use of [satellite](#) imagery to estimate coastal bathymetry [5, 16, 33, 34]. These spaceborne remote sensing techniques provide significant advantages compared to traditional methods: a large spatial coverage, together with frequent temporal monitoring [33]. Most satellite missions cover (nearly) the entire planet, while still visiting each location on a frequent basis (in the order of days or weeks). This provides useful long-term datasets for the monitoring of coastal processes [35]. When the data of those satellite missions is used for the retrieval of intermediate to shallow water nearshore bathymetry the estimation is generally based on one of two different concepts: 1) the recognition of radiative transfer in water to produce optical images of the bathymetry based on reflectance and absorption and 2) the recognition of hydrodynamic processes (waves, currents etc.) to estimate the bathymetry, using the relation between those processes and the nearshore bathymetry. Within this last method, both optical and radar images could be used to assess the hydrodynamic processes [33].

Imagery of a range of satellite missions has the potential, or has already been used, to estimate nearshore bathymetry. Some examples of those missions are the SPOT, LandSat-8, Worldview, Quickbird, IKONOS, Pleiades, ERS-1, ERS-2, TerraSar-X, Sentinel-1 and Sentinel-2 missions [33]. Although

very auspicious, the main challenge within this field of remote sensing is achieving bathymetry estimations of the same order of vertical accuracy as the most accurate traditional measuring methods, or at least obtaining an order of accuracy that is meeting the user requirements [33]. The Sentinel-2 mission [36] has proven to be one of the promising missions in providing such reliable information for the purpose of nearshore bathymetry estimation, mainly since it delivers freely accessible data with a significant revisit time [5, 32, 37–39].

1.1. SENTINEL-2 MISSION

The Sentinel-2 mission consists of a constellation of two polar-orbiting satellites. The two satellites are placed in the same sun-synchronous orbit, experiencing a 180 degree phase difference [36]. The revisit time of the total constellation is five days at the equator [40], corresponding with two to three days at mid-latitudes [36]. This revisit time is high in comparison with e.g. the popular LandSat-8 satellite (16 days [41]). The mission is part of the Copernicus programme, which is an Earth observation programme, headed by the European Commission (EC) and the European Space Agency (ESA) [42]. Copernicus is formerly known as the Global Monitoring for Environment and Security (GMES) programme [38]. The goal of it is to "provide accurate, timely and easily accessible information to improve the management of the environment, understand and mitigate the effects of climate change and ensure civil security" [42], from which the three key mission objectives of the Sentinel-2 mission are distilled: 1) delivering global high-resolution multi-spectral imagery with a high revisit frequency, 2) continuing the multi-spectral imagery of the SPOT mission and 3) providing information of next generation operational products, such as land-cover maps [38].



Figure 1.2: Examples of the Sentinel-2 constellation and its imagery. In (a) an artist impression of a Sentinel-2 satellite [36] is provided, while (b) shows an example of Sentinel-2 optical imagery: a projection of the Bahamas in blue, green and red light [43].

In order to fulfill the objectives of the mission, the design of Sentinel-2 has led to a set of relevant specifications. The constellation could be characterised as a multi-spectral Earth-observation system, which means that it features a multi spectral instrument (MSI) with 13 spectral bands [38]. The MSI of Sentinel-2 is an instrument that measures the radiance that is reflected by the Earth in 13 colour bands; each of the bands measures a fraction of the total spectrum of the radiation returned by the Earth [44]. The spatial resolution on the ground of those bands varies from 10 m to 60 m, while each band provides a field of view of 290 km [38]. Four of the bands deliver a spatial resolution of 10 m, six bands provide a 20 m resolution and the last three bands are of 60 m resolution [38]. A last relevant property of the Sentinel-2 imagery is the time lag that exists between each spectral band. For example, the total lag between the first and last band amounts 2.586 s [36]. In practice, above specifications mean that the provided imagery of Sentinel-2 consists of a set of 13 images of differing resolutions, picturing a certain location on Earth with a total time lag of 2.586 s. This protocol is repeated every few days.

1.2. RESEARCH GAP

The imagery of the Sentinel-2 mission has already been used for a broad range of Earth monitoring purposes. These applications reach from geological [40, 45], hydrological [46–48], benthic mapping [39] and snow-cover monitoring [49] purposes, to the detection of vegetation [50, 51] and land-use patterns [52, 53]. Given the broad variety in applications, the description of the research gap in this thesis solely focuses on the usage of Sentinel-2 and other remote sensing methods for the assessment of nearshore bathymetry.

COLOUR-BASED BATHYMETRY ESTIMATION

Most spaceborne bathymetry estimation techniques are based on the physical principle of recognising radiative transfer in water to estimate depth: the 'colour-based bathymetry estimation'. Simply stated, this measures the water-leaving reflectance of light at several spectral bands (the water colour) to provide the local bathymetry [54]. Casal *et al.* [55] applied this concept to Sentinel-2 data for the estimation of nearshore bathymetry using two different traditional empirical algorithms: the linear band model [56] and the log-transformed band ratio model [57]. Others improved these so-called empirical algorithms by processing the Sentinel-2 data using neural networks [58], machine learning models [54], random forest models [59] and Support Vector Machine (SVM) techniques [60, 61]. More examples using the same physical principle are of Chybicki [32], Kabiri [62] and Traganos *et al.* [63]. Note that these methods are not solely used in the coastal zone; there are applications of Sentinel-2 imagery in other aquatic environments like coral reefs [39].

WAVE-DERIVED BATHYMETRY ESTIMATION

A significantly different approach is the so-called 'wave-derived bathymetry estimation' [64]. Instead of directly translating the optical images to a bathymetry, it uses a two-step strategy. First, the wave characteristics are estimated from (satellite) imagery and secondly, these wave parameters can be converted to a local bathymetry by using the linear dispersion relation [5, 64, 65], relating wave characteristics to local depth (d):

$$\omega^2 = gk \tanh(kd) \quad (1.1)$$

in which g represents the gravitational acceleration, ω is angular frequency ($\frac{1}{T}$) and k is wave number ($\frac{1}{L}$). T and L respectively represent wave period and wavelength and are related to each other through celerity, or phase speed ($c = L/T = \omega/k$). Since bathymetry only dictates the wave parameters when waves are propagating in intermediate to shallow water depths, the deep and shallow water limits act as boundary for the applicability of this approach. Both limits depend on the wavelength and are typically expressed by $d_{int} = \frac{L}{2}$ and $d_{sh} = \frac{L}{20}$ [65]. The main advantage of this wave-derived method is that it avoids the challenges of above depth-by-colour routines that are induced by e.g. the turbidity of coastal waters and the need of in-situ calibrations [64]. It also has the potential to estimate depths beyond the limitations of colour-based methods (typically 10 to 20 m) [5, 66].

Work has been done in the past few years regarding the field of wave-derived coastal bathymetry estimation, using Equation 1.1 as basis for the method. One segment of these techniques relies on shore-based video systems [25] or drones [67, 68]. The advantage of these techniques is the availability of longer duration video imagery instead of single images, which makes the estimation of wave characteristics and therefore depth, more straightforward. Wave characteristics could also be obtained from high resolution satellite imagery with larger temporal range, such as the Pleiades mission in persistent mode [64, 69]. Although very promising, there are only a few satellites that could offer such high resolution data of a certain location on Earth (e.g. Pleiades [69] and WorldView-2 [70]) and moreover, the use of those satellites is generally expensive [71].

The Sentinel-2 mission offers a low-cost and freely accessible, open source alternative to these expensive "high-performance" satellites [5, 41]. However, like most other satellite missions, Sentinel-2 provides very limited data. Only a short burst of lower resolution images is taken instead of a longer,

high resolution sequence or video [71]. This leads to restricted temporal information of a relatively low spatial resolution. Although some recent efforts have been made to get wave-derived coastal bathymetry using limited Sentinel-2 imagery [72] as well as to develop a method for the processing of restricted temporal information [73], it remains challenging to accurately estimate wave-derived nearshore bathymetry from this sparse source of information. However, given the open source and widely available character of the data, there is broad consensus regarding the potential of utilising Sentinel-2 images for these purposes [5, 41, 73].

Wave-derived nearshore bathymetry estimation using Sentinel-2 imagery is considered a promising technique due to the freely accessible and widely available data, while avoiding the complications of colour-based routines. Nonetheless, the main challenge to overcome is the lack of temporal information in combination with a low spatial resolution.

MATHEMATICAL APPROACHES TO ESTIMATE WAVE CHARACTERISTICS

Determining wave-derived bathymetry relies on solving Equation 1.1. Knowing two of five **wave parameters** (L, T, ω, k, c), either in the spatio-temporal domain (L, T, c) or in the spectral domain (ω, k, c) leads to an estimation of the local depth (d) [5]. Several types of mathematical approaches have proven to obtain these wave parameters from different kinds of datasets.

Several methodologies are based on spectral methods, which generally aim to solve phase differences in the spectral wave number domain (ω, k) [5, 66, 72, 74–76]. Although very powerful, a clear disadvantage of these methods is the need for sufficient temporal or spatial information (in the order of a few wavelengths) to solve wave characteristics; multiple waves have to be 'observed' to accurately derive spectral information [64]. A second, possibly more important complication of spectral methods is induced by the shape of the raw signal. Since the acquisition of spectral wave characteristics depends on Fourier [77] or Wavelet [78] transformations, deviations of the signal from a perfect sinusoidal wave introduces errors [64].

A way to overcome these issues is provided by methods based on **cross-correlation** in the space-time domain. Instead of obtaining wave characteristics in spectral form (ω, k, c), the analysis is performed by applying correlations in temporal or spatio-temporal sense (L, T, c). Since correlation in space and time does not depend on signal shape, it is expected that these approaches better handle non-linear wave features [64]. The first results using a method based on these principles are achieved by Almar *et al.* [79], who present a protocol to solve wave celerity from video imagery based on temporal correlation. A comparison of this method with a spectral approach is done thereafter in Bergsma and Almar [80]. A large advantage of these applications to video imagery is the temporal range of the datasets, which makes the assessment of wave characteristics less challenging. Almar *et al.* [64] did a first application to much shorter time series by using the imagery of the Pleiades constellation in persistent mode (12 images, 8 s apart, 0.5 m resolution). This research has led to good agreement between estimated and measured bathymetry: a correlation of 0.92 and root-mean-square error of 1.4 m for the COMBI 2017 Capbreton experiment [64], which is stated to be the best performance obtained for regional spatial bathymetry [73].

The question that arises is whether these kinds of spatio-temporal cross-correlation methods are applicable to datasets of significantly shorter temporal duration and/or lower spatial resolution, such as Sentinel-2 imagery (13 images, in total 2.586 s apart and 60 to 10 m resolution). Recently, the potential has been shown by estimating wave parameters from a **synthetic dataset**, mimicking Sentinel-2 data [73]. The conclusion is justified that it remains challenging to obtain accurate results for less-than-a-wave-period time series [73]. Furthermore, Almar *et al.* [73] used a synthetic dataset of 1 m resolution, instead of actual Sentinel-2 resolutions. The development of a spatio-temporal cross-correlation model for the estimation of wave parameters from real Sentinel-2 data is therefore a natural and valuable next research step. It thereby forms a part of the objective of this research.

Further details about the spatio-temporal cross-correlation model are provided in the methodology section.

DEPTH INVERSION FROM WAVE CHARACTERISTICS

A wave-derived bathymetry estimation consists roughly of two parts: 1) the estimation of wave characteristics and 2) a depth inversion. When wave characteristics are obtained, the plainest way of inverting depth is by explicitly using Equation 1.1. More sophisticated ways of solving bathymetry are offered by a [Depth Inversion Algorithm \(DIA\)](#). DIAs are techniques that have been developed to estimate depth by utilising a range of different methods. Most of the DIAs are frequency-based: they exploit the linear dispersion relationship by decomposing the wave signal in harmonics [75, 81]. Enabling a wave-derived nearshore bathymetry estimation from Sentinel-2 data by combining a spatio-temporal cross-correlation and a DIA makes sense. The cross-correlation is applied to derive wave parameters, while a DIA converts the parameters to depth.

When deploying a DIA, the main complication is found in the required temporal range. Most DIAs are designed as post-processing techniques [82]. That implies they could rely on longer duration information: an increased temporal range eases the decomposition of harmonics [82]. A relatively new approach that aims to solve depth on the fly is developed by Gawehn *et al.* [82], by proposing an algorithm that utilises [dynamic mode decomposition \(DMD\)](#) [83, 84]. Although less demanding, the algorithm still requires a minimum time serie of 40 to 60 s [82]. To combine a spatio-temporal cross-correlation of Sentinel-2 data with the DMD-based DIA, the challenge is therefore to enlarge the temporal range of information. That introduces the need to construct a longer duration video from the Sentinel-2 imagery, representing the propagation of waves. The video then acts as a link between the satellite imagery and depth estimation.

Developing a spatio-temporal cross-correlation model to obtain wave characteristics from Sentinel-2 imagery is a natural next research step. The potential to estimate depth could possibly be shown by using a DMD-based DIA, of which the use is enabled by enlarging the temporal range of information: from a 2.586 s burst to a longer duration video (40 - 60 s).

1.3. PROBLEM STATEMENT AND RESEARCH OBJECTIVES

Due to the combined effects of increased coastal impacts and a rapidly growing coastal population, the coastal zone is expected to be highly vulnerable in the foreseeable future. A good understanding and assessment of the nearshore bathymetry is essential for the effective management of coastal areas. The use of spaceborne remote sensing methods has been developed in recent decades to estimate nearshore bathymetry. Compared to traditional methods, spaceborne remote sensing techniques offer a relatively large spatial coverage as well as frequent temporal monitoring. The Sentinel-2 mission - part of the Copernicus programme and initiated by the European Commission and the European Space Agency - offers potential to enable regular bathymetry estimations, mainly due to its significant revisit time and freely accessible data.

This research focuses on the development of a spatio-temporal cross-correlation model in order to construct a video representing wave propagation. The motivation is to show the potential of the video for the estimation of a wave-derived nearshore bathymetry from Sentinel-2 imagery. Enabling *wave-derived* bathymetry avoids the complications of *colour-based* routines, i.e. turbidity challenges and limitations to relatively shallow water. On the other hand, the choice for a spatio-temporal cross-correlation method is induced by the expected potential of the method to better handle non-linear wave signals, as well as the need for less temporal information. The developed spatio-temporal cross-correlation model is used to construct a longer duration video that shows the propagation of waves. The video forms a link between the raw satellite imagery and the potential bathymetry estimation. A DMD-based DIA is used to invert depth, leading to the research objective statement:

The explicit aim of this research is to construct a one-minute^a video from a short burst of Sentinel-2 imagery (2.586 s), a video that accurately represents the propagation of waves. In addition, the potential of the video to estimate wave-derived nearshore bathymetry is shown. A DMD-based DIA is exploited for that purpose. The video is constructed by developing a spatio-temporal cross-correlation model.

^aThe required temporal range to enable the use of the DMD-based DIA is case-dependent and somewhere between 40 and 60 s [82]. It is therefore decided to use a duration of one minute in the research objective statement as well as in the main research question.

DISTINCTION BETWEEN VIDEO CONSTRUCTION AND DEPTH ESTIMATION

In the research objective statement, a clear distinction is made between the video construction and depth estimation. This thesis focuses on the video construction and is therefore explicitly stated as the sole aim of the research. The motivation to construct a video is formed by enabling wave-derived depth estimation; the video acts as a connection between Sentinel-2 imagery and the exploiting of a DMD-based DIA. It thereby forms a way to combine the available spatial information of the satellite imagery towards a product of significant temporal range. Therefore, the potential to assess bathymetry is shown in this research as well. Another advantage of a video construction is that it possibly allows for a range of other applications, beyond the purpose of bathymetry estimation: a video construction is a way to project Sentinel-2's short burst of temporal information in a form that potentially unlocks a wider range of applications. The demands for a video construction and a *wave-derived* bathymetry estimation both are requirements that have been imposed by the facilitator of this research: the Laboratory of Space Geophysics and Oceanography Studies (LEGOS) [85].

DEVELOPING A SPATIO-TEMPORAL CROSS-CORRELATION MODEL

A second part of the objective to be emphasised is the development of a spatio-temporal cross-correlation model. As argued, these kinds of methods have been proven to be promising in accurately solving wave characteristics, mainly due to the ability of assessing non-linear wave features. While acknowledging the strength and advantages of other mathematical approaches, e.g. spectral methods, this research focuses therefore on the development of a spatio-temporal cross-correlation model.

RESEARCH SUB-OBJECTIVES

The full spatio-temporal cross-correlation model - from raw Sentinel-2 imagery to a video construction that represents wave propagation - can be subdivided upfront in three consecutive steps:

1. The enabling of the use of more temporal Sentinel-2 information by **augmenting the resolution** of the satellite's lower resolution spectral bands;
2. The estimation of **wave characteristics**;
3. The construction of a **video** that represents the propagation of waves;

A fourth step can be added to show the potential of the model for the estimation of wave-derived bathymetry:

4. The use of the DMD-based DIA to estimate **nearshore bathymetry**.

One of the key points of this work is to enlarge the temporal information that is obtained from Sentinel-2 data. The first step is therefore to allow for the use of more temporal information by augmenting the resolution of the satellite's lower resolution bands. The obtained imagery is then used to estimate wave characteristics in the second step. From these wave characteristics a video is constructed that significantly enlarges the range of temporal information. Step 3: a video representing the propagation of waves. When the temporal range of the video is sufficient, the DMD-based DIA [82] is used to show the potential in estimating wave-derived depth. The four steps can be seen as the sub-objectives of this thesis. A full description of the methodology and the spatio-temporal cross-correlation model is provided in Chapters 4 and 5.

1.4. RESEARCH QUESTIONS

Developing a set of methods to fulfill each of the above introduced sub-objectives, and knowing the accuracy of the particular method, together lead to an answer to the research question. The main research question underlining the sub-objectives is the following:

Is it possible to construct a one-minute video that represents the propagation of waves, from a 2.586-second burst of Sentinel-2 satellite imagery, by developing a spatio-temporal cross-correlation model, in order to show the potential for the estimation of wave-derived nearshore bathymetry using a DMD-based DIA?

To be able to answer the main research question, it is divided into 10 sub-questions. The first three questions aim to develop a spatio-temporal cross-correlation model:

1. What is an adequate way to augment the resolution of Sentinel-2's lower resolution spectral bands in order to enable the use of more temporal information?
2. What is an adequate way to estimate wave characteristics from the available Sentinel-2 imagery following the mathematical principle of spatio-temporal cross-correlation?
3. What is an adequate way to construct a longer duration video that represents the propagation of waves from Sentinel-2 imagery and the obtained wave characteristics?

The constructed video should be able to represent wave propagation for at least one minute, leading to the following sub-questions:

4. Does the constructed video show wave propagation for at least one minute?
5. What is the accuracy of the waves that are represented by the video?

The potential of the constructed video for bathymetry estimation purposes is shown by using a DMD-based DIA. The model is therefore applied to a synthetic dataset as well as to Sentinel-2 imagery. This introduces the questions:

6. What is the accuracy of a bathymetry estimation when a DMD-based DIA is used to invert depth from the created video, when applied to a synthetic dataset?
7. What is the accuracy of a bathymetry estimation when a DMD-based DIA is used to invert depth from the created video, when applied to Sentinel-2 imagery?

Furthermore, it is interesting to benchmark the bathymetry estimations by using the model to directly invert wave characteristics to depth, avoiding the use of a video:

8. What is the accuracy of a bathymetry estimation when estimated wave characteristics are directly inverted to depth, without using a video, when applied to a synthetic dataset?
9. What is the accuracy of a bathymetry estimation when estimated wave characteristics are directly inverted to depth, without using a video, when applied to Sentinel-2 imagery?

At last, the validity of the developed spatio-temporal cross-correlation model is defined by finding the theoretical application range of the model:

10. What is the theoretical application range of the proposed spatio-temporal cross-correlation model?

1.5. STRUCTURE OF THE REPORT

In this thesis a spatio-temporal cross-correlation model is developed. The report consists of three parts: a 'Base' part, a 'Results' part and a 'Reflection' part. In the 'Base' part, Chapter 2 provides background information regarding the Sentinel-2 constellation as well as information regarding the observation of waves from satellite imagery. Chapter 3 subsequently introduces the datasets that are

used in the context of this thesis. The next chapter, Chapter 4, proposes the methodology of the research. The methodology consists of the development of a spatio-temporal cross-correlation model and the application of the model to two different datasets. The results of these two methodology parts are presented in the 'Results' part of the report. First, the spatio-temporal cross-correlation model is discussed in Chapter 5. Next, the results of the second methodology part, the application to two datasets, are elaborated upon in Chapter 6. Both, Chapters 5 and 6 are concluded by a summarising section. The last part of the report is the 'Reflection' part. The research results are discussed and put in perspective in Chapter 7, the Discussion. Starting from the discussion, the research questions and sub-questions are answered and an overall conclusion is formed in Chapter 8. Lastly, recommendations for further research are proposed in Chapter 9. An overview of the report structure is presented in Figure 1.3.

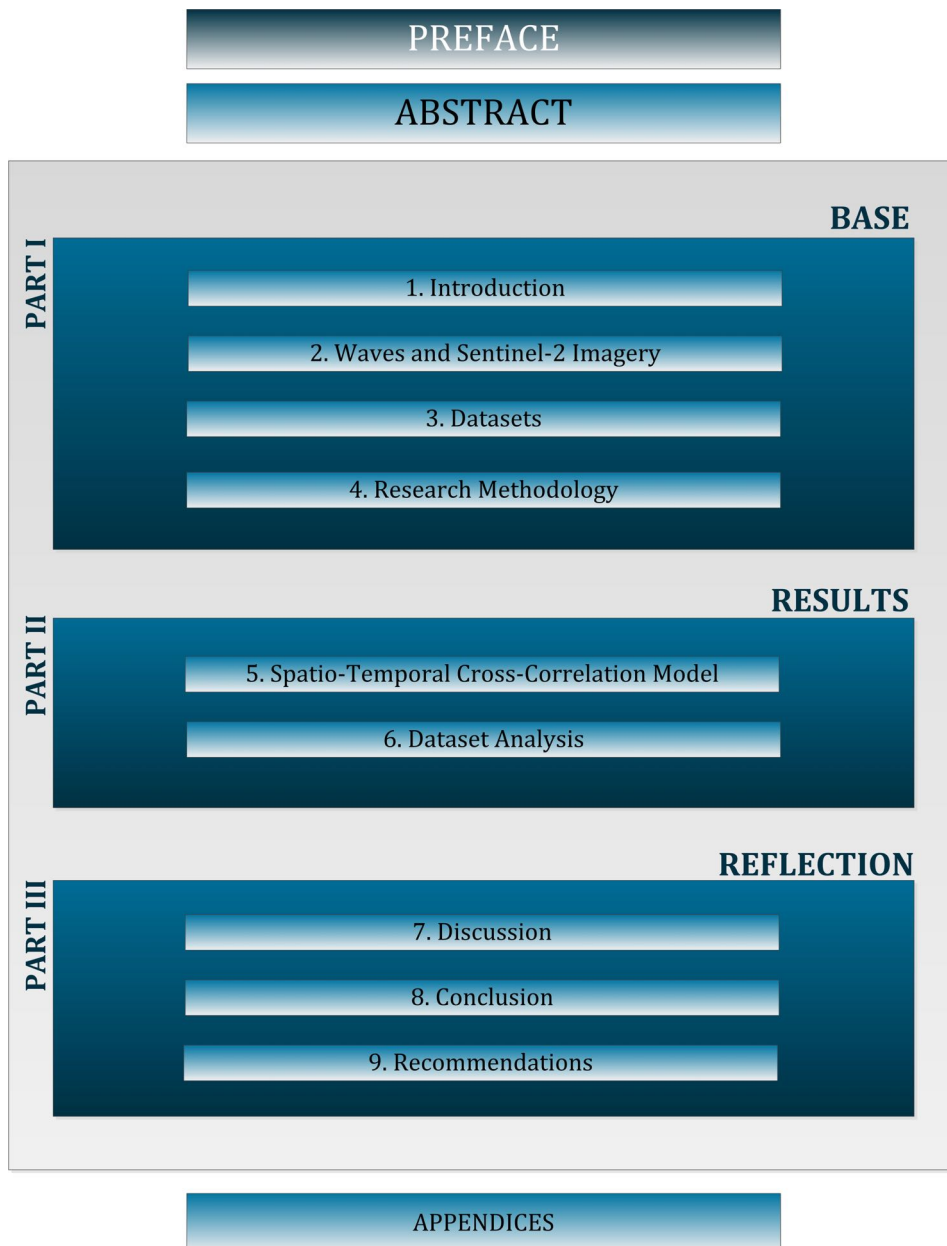


Figure 1.3: Structure of the report.

2

WAVES AND SENTINEL-2 IMAGERY

In order to obtain wave characteristics from Sentinel-2 imagery it is required to observe actual waves in the satellite images. A thorough understanding of the imagery of Sentinel-2 and the way waves are revealed is therefore essential. Section 2.1 elaborates upon the characteristics of the Sentinel-2 imagery, after which Section 2.2 discusses the specific user products of the Sentinel-2 mission. Lastly, Section 2.3 explains how waves and their propagation are observed from these user products.

2.1. SENTINEL-2 IMAGERY

The multi spectral instrument of the Sentinel-2 constellation provides observations in 13 separate spectral bands. Every time a location on Earth is revisited, a particular part of the Earth's reflected radiance is measured by each of these bands: the radiance is split into 13 spectral channels covering the visible, near infrared and shortwave infrared ranges. The total spectral domain varies from wavelengths (λ)¹ of 400 nm (visible radiance) to wavelengths of 2400 nm (shortwave infrared radiance) [86]. For the purpose of (water) wave observations the specific details of the measured radiative wavelengths are not of interest. More details are provided in Cazaubiel *et al.* [86].

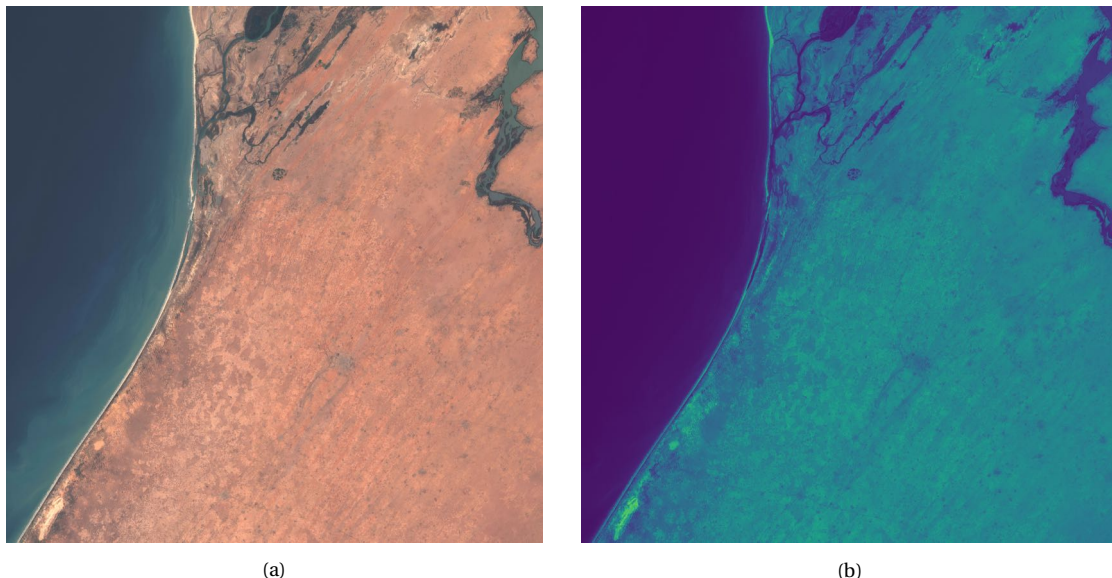


Figure 2.1: Example of Sentinel-2 imagery off the coastline of Senegal. In (a) blue ($\lambda \approx 492$ nm), green ($\lambda \approx 559$ nm) and red ($\lambda \approx 664$ nm) colour bands are combined to produce one resulting image, while (b) represents the near infrared ($\lambda \approx 704$ nm) colour band [43]. The total coverage of both images is 109.8 km by 109.8 km.

¹Note that the wavelengths of light observed by the MSI - for which λ is chosen as abbreviation - are meant. This differs from the wavelength of water waves (L), which is an essential parameter in the remainder of this thesis.

Each of the 13 spectral bands is characterised by a spatial resolution and a temporal offset. An overview of these is provided in Table 2.1 [36].

Table 2.1: Overview of spectral bands of the Sentinel-2 constellation. Note that the temporal offset and reversed (rev.) temporal offset are presented with respect to B02. The central wavelength is the mid-wavelength of the particular band's bandwidth [36]. The bands are presented in order of detection.

Spectral Band	Central Wavelength (λ)	Temporal Offset	Rev. Temporal Offset	Spatial Resolution
B02	492.4 nm	0.000 s	0.000 s	10 m
B08	832.8 nm	0.264 s	-0.264 s	10 m
B03	559.8 nm	0.527 s	-0.527 s	10 m
B10	1373.5 nm	0.851 s	-0.851 s	60 m
B04	664.6 nm	1.005 s	-1.005 s	10 m
B05	704.1 nm	1.269 s	-1.269 s	20 m
B11	1613.7 nm	1.468 s	-1.468 s	20 m
B06	740.5 nm	1.525 s	-1.525 s	20 m
B07	782.8 nm	1.790 s	-1.790 s	20 m
B8A	864.7 nm	2.055 s	-2.055 s	20 m
B12	2202.4 nm	2.085 s	-2.085 s	20 m
B01	442.7 nm	2.314 s	-2.314 s	60 m
B09	945.1 nm	2.586 s	-2.586 s	60 m

The difference in spatial resolution between bands is the result of three engineering considerations [36]. First of all, the signal-to-noise ratio is of relevance. Each of the bands has a different bandwidth: the spectral range that it detects. This is a consequence of the varying purposes of different bands. Bands with larger bandwidth detect more light and can therefore observe higher resolutions, while preserving a sufficient signal-to-noise ratio. A second argument can be found in the observed wavelength (λ). In general, the observation of larger wavelengths leads to lower allowable resolutions. The last consideration is one of data transfer size. Since the amount of data transfer per day from satellite to Earth is large, an attempt is made to decrease the total data size. Therefore, the most frequently used bands (e.g. visible light) are provided in a higher resolution rather than less frequently needed bands (e.g. bands for the purpose of atmospheric correction of other bands). More details can be found in the Sentinel-2 Mission Guide [36] and in Cazaubiel *et al.* [86].

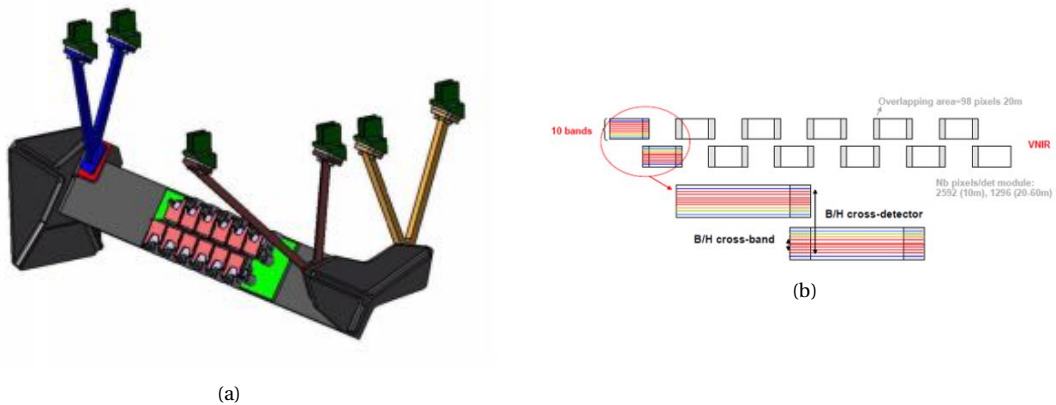


Figure 2.2: Schematic representation of the focal plane configuration showing the visible and near infrared detectors (a) [86]. In (b) the detectors are shown in more detail, including the stacked colour bands [36].

Another feature is the temporal offset between the spectral bands: the bands do not observe the Earth's surface at the exact same moment in time. This is due to the layout of the focal plane, the plane at which the detectors of the satellite are placed [36]. There are two focal planes, each containing 12 detectors.² One focal plane contains the detectors that measure the visible and near

²Note that detectors and spectral bands are two different concepts.

infrared radiance (i.e. the spectral bands B01, B02, B03, B04, B05, B06, B07, B08, B8A, B09), while the other one contains the shortwave infrared detectors (i.e. the spectral bands B10, B11, B12). This distinction is made because a different kind of detector and electronic set-up is needed for the measurements of these radiative wavelengths [36]. Figure 2.2a and Figure 2.2b show a schematic of the focal plane containing the detectors for visible and near infrared radiance. The focal plane for short wave infrared radiance looks similar. As can be seen, each detector measures all 10 spectral bands - in the case of visible and near infrared radiance - and these bands are stacked horizontally above each other. This staggered configuration, together with the angle of the focal plane with respect to the Earth's surface leads to the temporal offsets as shown in Table 2.1 [36].

The design consisting of 12 detectors is invented to enable the wide field of view (290 km), hence the high revisit time of the Sentinel-2 constellation [36]. Since the detectors are placed alternately, as can be seen in Figure 2.2b, a complication for the processing of the data is induced: the sequence of band detection switches from detector to detector. This means that, given the 12 detectors together cover the total field of view, the order of temporal offset switches approximately every 10 kilometers within a single satellite image. This reversed order is indicated in Table 2.1 as well. It is an important concept to account for in the developed spatio-temporal cross-correlation model.

Sentinel-2 imagery consists of 13 spectral bands varying in spatial resolution. The bands are characterised by a temporal offset with respect to each other. An important concept to account for is the switching of the order of this offset within the field of view of a satellite image.

2.2. SENTINEL-2 USER PRODUCTS

The Sentinel-2 constellation regularly provides imagery of locations on Earth [43]. The information is obtained in the form of different user products, of which Level-1C and Level-2A are made freely available. The processing of Sentinel-2 products is more extensive as the number-letter combination of the product name increases. In short, Level-0 products deliver the raw sensing data, while in Level-1A products a rough pixel alignment between the spectral bands as well as between the detectors is added. Level-1B products are subsequently radiometrically corrected, which means that the raw instrument measurements are converted to radiances. All three products (Level-0, Level-1A and Level 1-B) are projected in sensing geometry [87].

The creation of Level-1C products starts with the reprojection of Level 1-B products in a cartographic reference frame. It is represented in the form of granules, or tiles. A tile is an [ortho-image](#), a geometrically corrected satellite image, of 109.8 km by 109.8 km. The reference frame of the tiles is the Universal Transverse Mercator / World Geodetic System 1984 (UTM/WGS84) projection. For the gridding of the tiles, the US-Military Grid Reference System (US-MGRS) is used, which introduces the tiles' naming conventions [36, 87, 88]. Separate tiles are created for each of the 13 spectral bands. The processing of Level-2A products mainly adds an atmospheric correction to the imagery [36, 88]. The Level-2A products are projected in the same cartographic reference frame and are provided in the same structure as the Level-1C products. For more details, see S2P [88] and Gascon *et al.* [87].

CLOUD COVERAGE

The indicator of cloud coverage [%] is an important parameter to assess the usability of a certain set of imagery. A large cloud coverage significantly complicates the observation of free surface height, since the clouds reflect radiance and therefore hide the sea surface. An indication of the cloud coverage is found in the [metadata](#) of the imagery.

RESOLUTIONS OF SENTINEL-2 USER PRODUCTS

As is explained in Table 2.1 the Sentinel-2 products are provided in tiles of 10 m, 20 m and 60 m resolution. Figure 2.3 shows the effect of the varying resolutions to the imagery of a particular location on Earth, a 3000 m by 3000 m, nearshore location off the coast of Saint-Louis, Senegal. Note

the disappearance of smaller wave features in Figure 2.3b (20 m resolution). In Figure 2.3c (60 m resolution) almost all wave features are unrecognisable.

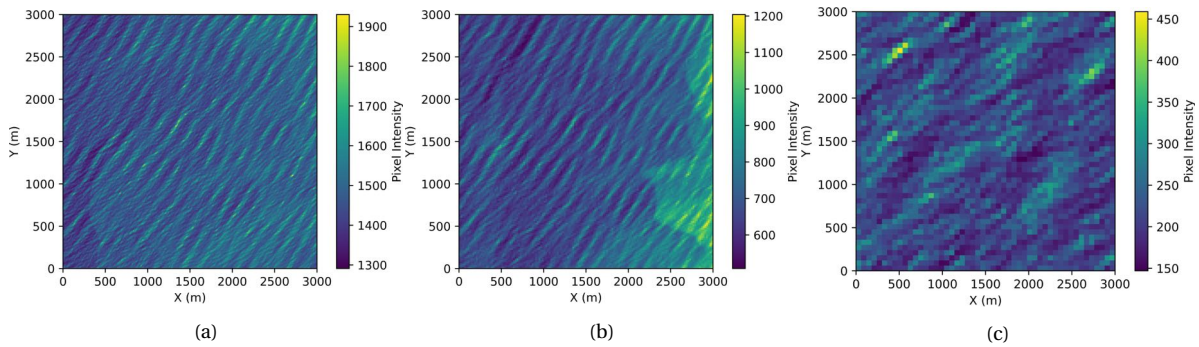


Figure 2.3: Sentinel-2 imagery off the coast of Saint-Louis, Senegal. In (a) the spectral band B02 (10 m resolution) is shown. (b) Represents B05 (20 m resolution) and (c) shows B10 (60 m resolution).

2.3. OBSERVING WAVES FROM SENTINEL-2 IMAGERY

The temporal offset of Sentinel-2 imagery allows for observing the propagation of waves [41, 73, 80]. Single wave features can be obtained from the images since the water surface reflects solar radiance, which is measured by the MSI. Therefore, a Sentinel-2 image of a waterbody can be interpreted as a representation of surface height in a 3D plane (x, y, η) , e.g. Figure 2.4a. The actual propagation of waves becomes visible when the sequence of images is analysed. Even in raw satellite data this propagation is already visible, as is shown in Figure 2.4b. Note that the most distinct wave feature in this example shows up just to the right of 400 m cross-shore distance. A simple calculation indicates a displacement of the crest of the particular wave of ca. $20 * \sqrt{2} \approx 30$ m (wave direction is diagonally to the lower right). This would correspond with a celerity of $c \approx 30/2.055 \approx 15$ m/s, given the temporal offset between B02 and B8A of 2.055 s.³ Although it is only a rough example for illustration purposes, the possibilities of Sentinel-2 imagery to obtain wave characteristics are clearly demonstrated.

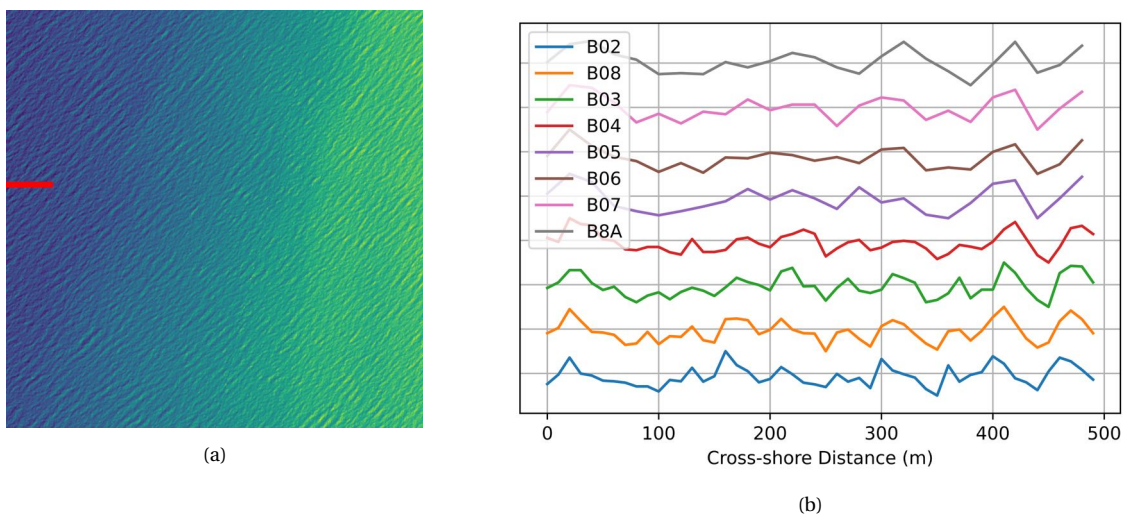


Figure 2.4: Sentinel-2 image (B02) showing wave patterns that are visible due to the reflection of solar radiance (a). The red line indicates the cross-section that is focused on in (b), which shows the propagation of waves from B02 to B8A in positive cross-shore direction.

³NB: the methodology of this thesis does not follow this specific approach for the estimation of the actual wave celerity. For the actual methodology see Chapter 4.

3

DATASETS

Two distinct datasets are analysed in this thesis. Each of the datasets provides for a specific set of input parameters and therefore forms a different kind of research environment. The two datasets are: a synthetic FUNWAVE dataset (Section 3.1) and actual Sentinel-2 imagery (Section 3.2).

In the context of this thesis, three terms are frequently used to characterise a certain dataset, e.g. Sentinel-2 imagery. The **burst duration** indicates the overall temporal offset between the first and last snapshot - or band - of the imagery. In the case of Sentinel-2 imagery, the burst duration is 2.586 s. The **time lag** represents the temporal offset between two specific subsequential snapshots. That means, all time lags of a dataset together accumulate to the burst duration. The term **spatial resolution** is used to indicate the spatial sampling of an image.

3.1. DATASET 1: SYNTHETIC FUNWAVE DATASET

The synthetic FUNWAVE dataset is produced by a simulation using FUNWAVE: a nonlinear Boussinesq wave model [89, 90]. This implies that it numerically solves Boussinesq-type equations to model the propagation of water waves [89]. The exact nature of FUNWAVE and other Boussinesq-type models is beyond the scope of this thesis¹. The input data of the FUNWAVE simulation consists of a set of statistical wave parameters, together with a forced bathymetry for a certain domain. Furthermore, the spatial resolution, time lag and burst duration of the output file are imposed. An overview is provided in Table 3.1.

Table 3.1: Overview input and output parameters FUNWAVE simulation.

Name	Parameter	Value
Significant Wave Height	H_s	1.4 m
Wave Peak Period	T_p	10 s
Wave Direction	Dir	15 °
Domain Size	-	900 by 1400 m
Spatial Resolution Output	-	1 m
Temporal Time Lag Output	-	0.5 s
Burst Duration	-	4.5 s

The bathymetry acting as input for the FUNWAVE simulation is shown in Figure 3.1a. Note that a complex bathymetry is used, featuring an arrhythmic sandbar. When the FUNWAVE simulation is performed, using the bathymetry and wave parameters as input, a free surface height is obtained. This is shown in Figure 3.1b. The resulting free surface height forms the actual dataset for the purpose of this thesis. This dataset, consisting of 10 frames representing a free surface height, is modified to improve the similarity with Sentinel-2 imagery, as well as to be better able to analyse the

¹For more details please see other relevant literature (e.g. Kirby *et al.* [89], Brocchini [91]).

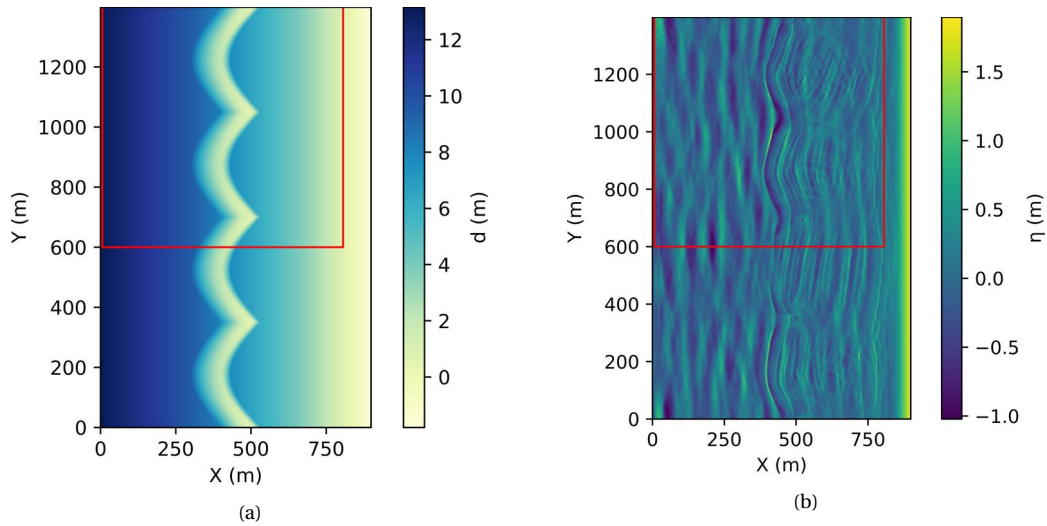


Figure 3.1: Input bathymetry of the FUNWAVE simulation (a). The red square indicates the newly created domain. (b) Shows the free surface height as a result of the FUNWAVE simulation.

dataset. Two changes are made. First of all, the total domain size is decreased to a square of 800 m by 800 m, covering the upper left part of the domain. The square is indicated in Figure 3.1a and Figure 3.1b. The motivation is to cut off the shoreline from the domain: the developed spatio-temporal cross-correlation model is not expected to solve bathymetry at the boundary between sea and shore. A second change is made to the resolution of the dataset. Sentinel-2 imagery is characterised by resolutions of 10 m, 20 m and 60 m. The dataset is therefore resampled to similar characteristics: four snapshots of 10 m resolution, four snapshots of 20 m resolution and two snapshots of 60 m resolution. The snapshots are sampled in similar order as the first 10 bands of Sentinel-2 imagery. The original FUNWAVE simulation provides frames of 1 m resolution, therefore the resolution is decreased to lower resolutions (10 or 20 m) by a simple averaging method: the intensity of all 'old' pixels that together form a 'new' pixel is averaged to produce the intensity of the 'new' pixel. For example: to decrease the resolution from 1 m to 10 m, the average of a square of 10 by 10 pixels is taken to calculate the intensity of the resulting pixel. Figure 3.2 shows the result of this approach.

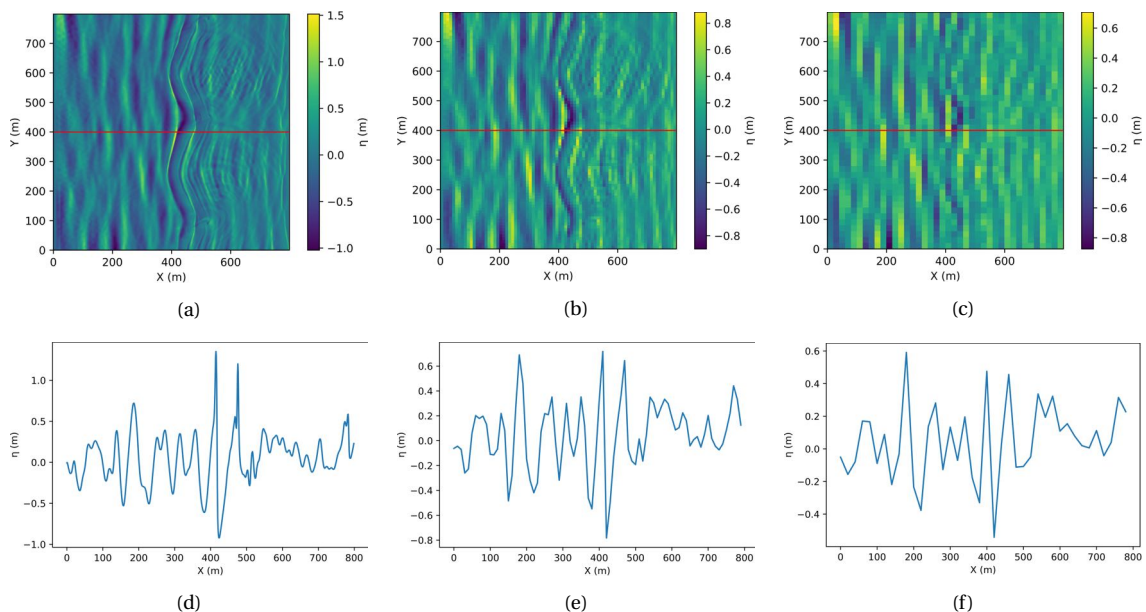


Figure 3.2: Decreasing the resolution of FUNWAVE bands from 1 m (a) to 10 m (b) and 20 m (c). The red line shows the cross-sections that are plotted in (d), (e) and (f).

3.2. DATASET 2: SENTINEL-2 IMAGERY

The Sentinel-2 dataset consists of imagery from two different research sites: Capbreton, France and Saint-Louis, Senegal. The research locations, the available bathymetry data and the imagery itself are discussed separately.

DATES AND LOCATIONS OF INTEREST: CAPBRETON, FRANCE AND SAINT-LOUIS, SENEGAL

Both research sites, Capbreton and Saint-Louis, are situated on the Atlantic Ocean. The locations are indicated in Figure 3.3. The dates of interest are 30/03/2018 for the location of Capbreton and 04/03/2019 for the location of Saint-Louis. The wave climate of the locations differs slightly. In general, the wave climate in Capbreton is characterised by shorter waves (lower peak wave period, T_p) than the wave climate in Saint-Louis. Both wave climates are generally dominated by swell waves however. Appendix A shows the GFS-Wave model wave measurements of Capbreton in March 2018, while Appendix B does the same for Saint-Louis in March 2019 [3, 4]. The date in Saint-Louis is one of which in-situ (Acoustic Doppler current profiler (ADCP)) wave measurements are available: the Saint-Louis 2019 field experiment. The date in Capbreton is chosen because it is characterised by preferable wave conditions [5].

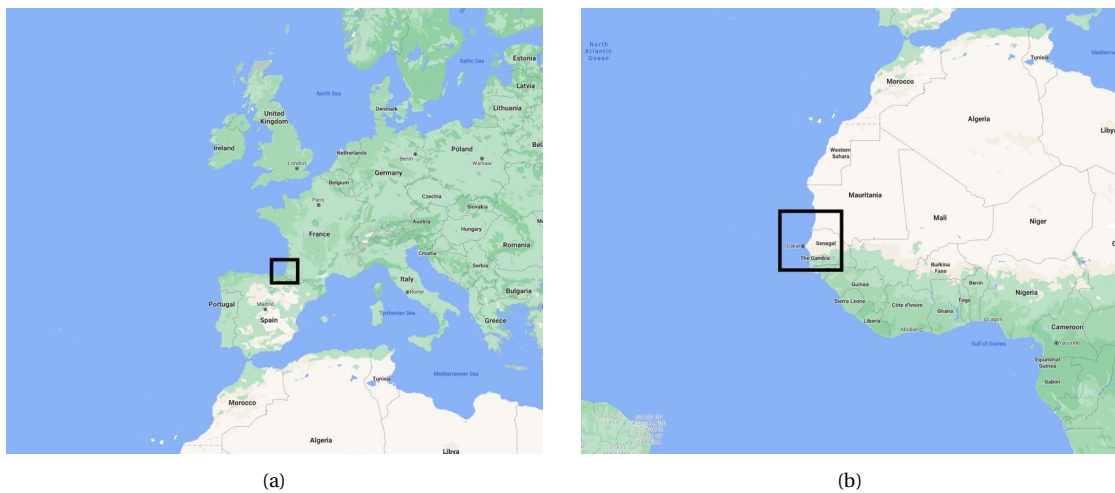


Figure 3.3: Both research sites: the area of Capbreton (a), as well as the area of Saint-Louis (b) [92].

BATHYMETRY DATA IN CAPBRETON AND SAINT-LOUIS

For both locations bathymetry data is made available by the European Marine Observation and Data Network (EMODnet) [93], an organisation that aims to provide a single access point to a range of available measurements, such as bathymetric products. EMODnet provides a digital terrain model (DTM): a map of the bathymetry and topography in coastal areas. These DTMs are based on the combination of three different sources [94]:

1. Bathymetric surveys: multi- and singlebeam surveys and echosoundings;
2. Composite datasets: a set of surveys merged and gridded together;
3. An integration of the worldwide GEBCO [95] data grid.

The bathymetric data of EMODnet is provided every two years. For both research locations the bathymetric maps of 2018 are used.

SENTINEL-2 IMAGERY IN CAPBRETON AND SAINT-LOUIS

The specific tile names corresponding to the locations of Capbreton and Saint-Louis are T30TXP and T28PCC respectively. The cloud coverage is an important parameter to assess the usability of a certain set of imagery; a large cloud coverage significantly complicates the observation of free surface height since the clouds reflect radiance and therefore hide the sea surface. An indication of

the cloud coverage is found in the metadata of the imagery. In Table 3.2 an overview of the Sentinel-2 imagery and corresponding cloud coverage is provided. A first estimate of the wave height and wave period per day is presented as well. It is chosen to use the median significant wave height and median peak wave period of the hourly measurements of GFS-wave for that purpose [3, 4].

Table 3.2: Overview of Sentinel-2 imagery in Saint-Louis and Capbreton. Wave height and wave period are represented by the median values of the GFS-wave measurements [3, 4].

Date	Location	Product	Cloud Coverage	Wave Height	Wave Period
30/03/2018	Capbreton, France	Level 1C	8.18 %	2.9 m	13 s
04/03/2019	Saint-Louis, Senegal	Level 1C	18.04 %	2.0 m	15 s
04/03/2019	Saint-Louis, Senegal	Level 2A	1.93 %	2.0 m	15 s

SITE SELECTION

In both locations a specific site has been selected to analyse. The selection is based on the available ground truth bathymetric data, using an area that is probably located in intermediate water depths. Since the expected wavelengths are in the range of 50 to 300 m, the depth range lies in between 15 m and 25 m. Therefore Area SL.1 is introduced as research site off the coast of Saint-Louis. The area is indicated by the red square in Figure 3.4f. The total size of the area is 2320 m by 2320 m. Analogously, the red square in Figure 3.4c shows the specific area: CPB.1, of which the size is 4240 m by 4240 m. The site selection is such that it corresponds to the location of the wave buoy measurements. Furthermore, the well-known deep water canyon [64] is an interesting area to focus on; it possibly ranges from deep water to intermediate and shallow water.

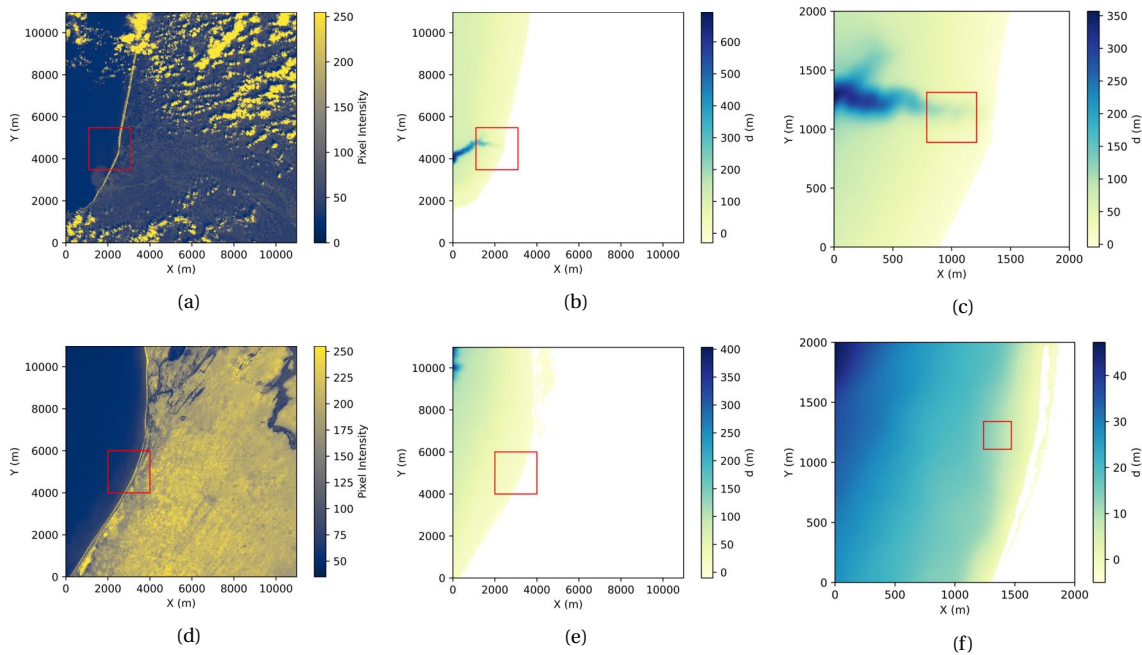


Figure 3.4: Site selection of the coast off Capbreton and Saint-Louis. In (a) an overview of the specific tile, T30TXP, from the Sentinel-2 imagery of Capbreton is shown. (b) presents the corresponding bathymetry, obtained from EMODnet 2018 data. The red square in (b) indicates the area in (c), which shows the specific site location: Area CPB.1. In (d), (e), and (f) the site in Saint-Louis (SL.1, T28PCC) is shown in a similar way.

4

RESEARCH METHODOLOGY

This research aims to determine whether constructing a longer duration video from a short burst of Sentinel-2 imagery is possible. The video should accurately represent the propagation of waves. Afterwards, the potential for the estimation of a wave-derived nearshore bathymetry is shown by exploiting a DMD-based DIA [82]. The research is separated into two parts. At first, a spatio-temporal cross-correlation model¹ is developed. Secondly, in the 'Dataset Analysis', the model is applied to two distinct datasets and bathymetry estimations are performed. The model, as well as the results of the 'Dataset Analysis' are presented in the 'Results' part of this thesis, consisting of the following chapters:

- **Chapter 5: Spatio-Temporal Cross-Correlation Model.** An overview of the developed model;
- **Chapter 6: Dataset Analysis.** The application of the developed model to two different datasets: Dataset 1, a synthetic FUNWAVE dataset and Dataset 2, Sentinel-2 imagery.

Below, the specific research methodology is discussed for each of the two research parts. Figure 4.1 provides a schematic overview of the methodology. The methodology is summarised in Section 4.3.

4.1. METHODOLOGY: SPATIO-TEMPORAL CROSS-CORRELATION MODEL

The spatio-temporal cross-correlation model forms the core of this work. Fundamentally, the principle of the model is based on Almar *et al.* [64], although it is emphasised that the model is specifically designed and developed for this thesis. Moreover, the application to Sentinel-2 imagery is a novelty as well. The main model parts are introduced first (Section 4.1.1), after which model requirements are defined (Section 4.1.2). Lastly, the development of model variants is discussed (Section 4.1.3).

4.1.1. MODEL OVERVIEW AND MODEL PARTS

Four model parts are introduced:

- **Model part 0:** Pre-processing;
- **Model part 1:** Image resolution augmentation;
- **Model part 2:** Wave characteristics estimation;
- **Model part 3:** Video construction.

These four predefined model parts relate to the research sub-objectives that are introduced in Chapter 1. The development of the entire model is based and structured on these parts. The model is designed to handle raw Sentinel-2 user products. It is therefore first needed to **pre-process** the products in model part 0. The second step results from the essence of the model: the aim to enlarge the range of temporal information, from a short burst of Sentinel-2 imagery to a longer duration

¹In the remainder of this thesis the spatio-temporal cross-correlation model is also referred to as 'the model'.

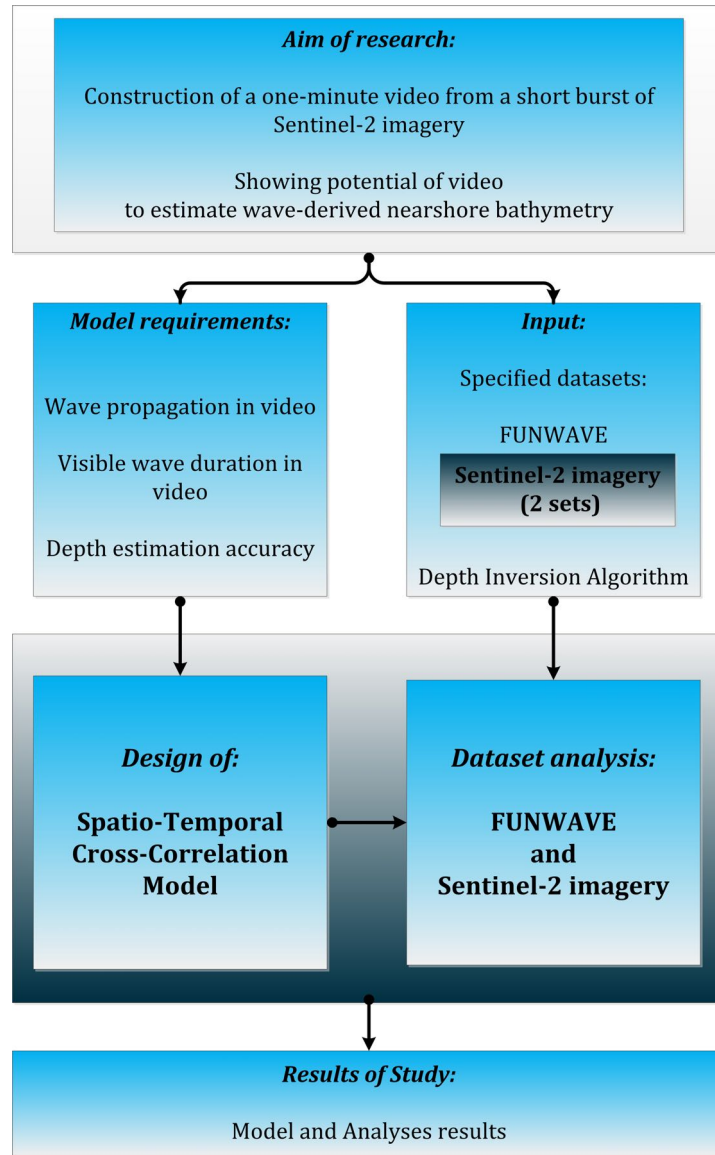


Figure 4.1: Schematic overview of methodology

video. Therefore, model part 1, **image resolution augmentation**, is required to increase the amount of available temporal information upfront. Model part 2 is introduced as a result of the aim to construct a video that represents the propagation of waves; a **wave characteristics estimation** in the space-time domain acts as basis of the video. Model part 3 eventually performs the last part: **the video construction** itself.

BATHYMETRY ESTIMATION

The motivation behind the research is to show the potential of a video construction in order to estimate wave-derived nearshore bathymetry. The depth inversion itself is performed using a DMD-based DIA [82], exploiting frequency-based solving of the linear dispersion relation [65]:

$$\omega^2 = gk \tanh(kd) \quad (4.1)$$

in which ω is angular frequency, g is gravitational acceleration, k is the wave number and d is local depth. The constructed video acts as input for the DIA. That is why an accurate representation of wave propagation in the video is an essential aspect the model. The bathymetry could also be assessed without the use of a video: directly converting the estimated wave characteristics of model part 2 to a local depth. To that end, the linear dispersion relation is rewritten in the space-time domain, since the model solves wave characteristics in the space-time domain as well:

$$L = \frac{gT^2}{2\pi} \tanh\left(\frac{2\pi d}{L}\right) \quad (4.2)$$

in which L is wavelength and T is wave period. Note that Equations 4.1 and 4.2 are two different forms of the same equation, since $\omega = 1/T$ and $k = 1/L$. The latter method is introduced to benchmark the performance of the DMD-based DIA. It is expected that solving the linear dispersion relation based on a wave-representing video construction and a DMD-based DIA leads to more accurate results, because it solves the linear dispersion relation for multiple harmonics [75, 82].

MODEL GRID

The model defines wave characteristics (model part 2) per single location, or pixel on a grid, e.g. the grid of Sentinel-2 imagery which is defined by a pixel every 10, 20 or 60 m. The resulting video construction (model part 3) and resulting bathymetry estimation are defined on the same grid.

4.1.2. MODEL REQUIREMENTS

Considering the motivations behind the video construction - showing the potential to estimate a nearshore wave-derived bathymetry estimation - there are three requirements to the developed model. These three requirements are presented in Table 4.1.

Table 4.1: Model requirements

Model Requirement
1. Accurate representation of wave propagation in the resulting video
2. One minute duration of wave visibility in the resulting video
3. Accurate bathymetry estimation as result of the video

MODEL REQUIREMENT: 1. WAVE PROPAGATION IN VIDEO

The first requirement is based on the aim to solve a *wave-derived* bathymetry, which means that bathymetry is estimated using the linear dispersion relation (Equations 4.1 and 4.2) [65]. These equations show that the quality of bathymetry estimation is dependent on the accuracy of the represented wave characteristics in the video. The first requirement is therefore an accurate representation of wave propagation in the video.

MODEL REQUIREMENT: 2. VISIBLE WAVE DURATION IN VIDEO

The second requirement is imposed by the choice to estimate bathymetry using a DMD-based DIA: a minimal duration of visible waves of 40 - 60 s is needed [82]. In the research question this requirement is stated as the need to construct a one-minute video. The second requirement is therefore a minimal duration of wave visibility in the video of one minute.

MODEL REQUIREMENT: 3. ACCURACY OF BATHYMETRY ESTIMATION

The third requirement is formed by the accuracy of the bathymetry estimation as result of the video. As said, the motivation of this research is to show the potential of a video construction for bathymetry estimation. This aim leads to the last requirement.

4.1.3. MODEL VARIANTS

The model as presented in the main report, results from the development and comparison of a range of variants. Each of these variants consists of a combination of different methods. The resulting, proposed model consists of the combination of methods that best performs. Three tests have been designed to evaluate the performance of the variants, respectively related to model parts 1, 2 and 3: the first test has evaluated the quality of image resolution augmentation, the second test has evaluated the performance to estimate wave characteristics and the third test has analysed the video construction. This report only presents the best performing model variant, while leaving the other variants and designed tests out of scope.

4.2. METHODOLOGY: DATASET ANALYSIS

The model is applied to two distinct datasets: Dataset 1, a synthetic FUNWAVE dataset (Section 4.2.1), and Dataset 2, Sentinel-2 imagery (Section 4.2.2). The motivation to use two different datasets is given by the different characteristics of both. The performance of the model in relation to the 'Dataset Analysis' is evaluated based on the introduced model requirements (Section 4.2.3).

4.2.1. ANALYSIS OF DATASET 1, SYNTHETIC FUNWAVE DATASET

The synthetic FUNWAVE dataset provides a research environment of which the input and output parameters are known upfront. The input parameters consist of a set of short-term wave statistics (H_s and T_p) [65] and an input bathymetry, while the output is a resulting surface height over time, structured in a Sentinel-2 mimicking way. The model is designed to analyse surface height, resulting in a wave-representing video and a bathymetry estimation. The input bathymetry of the FUNWAVE simulation therefore acts as ground-truth for the bathymetry estimation, while the input short-term wave statistics are used to compare with the video construction. As a result, analysing the synthetic FUNWAVE dataset leads to a step-wise insight into the performance and bottlenecks of the model.

4.2.2. ANALYSIS OF DATASET 2, SENTINEL-2 IMAGERY

Dataset 2, the Sentinel-2 imagery, is used to test the performance of the model when applied to real satellite data. In general, the irregularity of satellite data leads to more complications [5]. Both research sites are analysed. The ground-truth of the Sentinel-2 imagery is formed by the ADCP measurements and EMODnet bathymetric data. The research site in Saint-Louis acts as a more in-depth research environment compared to the case in Capbreton, since ADCP measurements are only available for the research site of Saint-Louis. The site in Capbreton is added to the research to show the capabilities of the model in relation to a wave environment that is generally dominated by relatively shorter waves.

4.2.3. EVALUATING THE MODEL PERFORMANCE BASED ON THE MODEL REQUIREMENTS

The performance of the model in relation to the 'Dataset Analysis' is evaluated based on the requirements as introduced in Table 4.1. Table 4.2 shows these model requirements in abbreviated form together with proposed quantitative and qualitative evaluation criteria.

Table 4.2: Model requirements, together with quantitative evaluation criteria (quant. criteria) and qualitative evaluation criteria (qual. criteria).

Model Requirement	Quant. Criteria	Qual. Criteria
1. Wave propagation in video	-	1) Pixel-wise wave char. assessment 2) Wave spectra assessment
2. Visible wave duration in video	Visible wave duration [s]	-
3. Accuracy of depth estimation	ρ [-] & RMSE [m]	Visual assessment

EVALUATING MODEL REQUIREMENT 1: WAVE PROPAGATION IN VIDEO

The accuracy of wave propagation representation is evaluated based on two distinct indicators. A first indication is provided by assessing the pixel-wise estimation of the specific wave characteristics in model part 2 since these estimations form the basis of the video. Secondly the resulting 2D variance-density spectra and frequency-direction spectra of the video [65] are estimated and compared to available ground-truth data, which are the input short-term wave statistics in the case of the synthetic FUNWAVE dataset and ADCP measurements in the case of Sentinel-2 imagery. Both indicators are evaluated in a qualitative sense.

EVALUATING MODEL REQUIREMENT 2: VISIBLE WAVE DURATION IN VIDEO

The performance of the model in relation to model requirement 2 is evaluated based on a quantitative evaluation criterion. The temporal range between the start of wave visibility and the end of

wave visibility in the resulting video is measured. To that end, screenshots of the resulting videos showing the start of wave propagation and the end of wave propagation are presented as results.

EVALUATING MODEL REQUIREMENT 3: ACCURACY OF BATHYMETRY ESTIMATION

The accuracy of bathymetry estimation is evaluated based on three indicators: two quantitative parameters, the Pearson correlation coefficient (ρ) and the root-mean-square error (RMSE), and a qualitative visual assessment. The ground-truth data is provided by the input bathymetry in the case of the synthetic FUNWAVE dataset and by the EMODnet bathymetric data in the case of Sentinel-2 imagery.

In the context of this research, the Pearson correlation coefficient is expressed as²:

$$\rho = \frac{\text{cov}(X, Y)}{\sigma(X)\sigma(Y)} \approx \frac{\sum_{i=1}^N (X_i - \bar{X})(Y_i - \bar{Y})}{\sqrt{\sum_{i=1}^N (X_i - \bar{X})^2} \sqrt{\sum_{i=1}^N (Y_i - \bar{Y})^2}} \quad (4.3)$$

in which X represents the pixel values of the estimated bathymetry, Y the pixel values of the ground-truth, N is the number of data points and i indicates the data point number with $i = 1, 2, 3, \dots, N$. The data point numbers represent the pixels of the model grid.

The root-mean-square error is represented by:

$$\text{RMSE} = \sqrt{\sum_{i=1}^N \frac{(X_i - Y_i)^2}{N}} \quad (4.4)$$

in which again X represents the pixel values of the estimated bathymetry, Y the pixel values of the ground-truth, N is the number of data points and i indicates the data point number with $i = 1, 2, 3, \dots, N$.

The visual assessment is performed by looking for similarities between estimated and ground-truth bathymetry. Both, similarities in absolute sense as well as similarities in gradients are of interest.

4.3. SUMMARY OF METHODOLOGY

The methodology of this research consists of two parts: 1) the development of a spatio-temporal cross-correlation model and 2) the application of the developed model to two distinct datasets. The datasets of interest are a synthetic FUNWAVE dataset and Sentinel-2 imagery. The performance of the model in relation to the datasets is evaluated based on three model requirements: 1) the representation of wave propagation in the resulting videos, 2) the duration of wave visibility in the videos and 3) the accuracy of bathymetry estimations that result from the videos. The model requirements relate to quantitative and qualitative evaluation criteria.

²Note that the standard convention is to use ρ as abbreviation of the Pearson correlation coefficient with respect to an entire population, while r is used to quantify the correlation of a certain sample. In this thesis it is chosen to use ρ as standard abbreviation.

II

RESULTS

5

SPATIO-TEMPORAL CROSS-CORRELATION MODEL

The spatio-temporal cross-correlation model is based on the fundamental principle in Almar *et al.* [64]. It is emphasised that the model is specifically designed and developed for this research. An overview of the model is provided in Section 5.1. To illustrate the concept of the model, a so-called illustrating sinusoidal wave is introduced afterwards in Section 5.2. Section 5.3 explains the main mathematical principle in the model: cross-correlation. The following four sections, Sections 5.4, 5.5, 5.6 and 5.7, separately discuss the four model parts. A summary of the chapter and the developed model is provided in Section 5.8. Although the model is designed to analyse FUNWAVE imagery and Sentinel-2 imagery, the description of the model focuses on Sentinel-2 imagery. The model code is written in Python.

5.1. OVERVIEW OF THE SPATIO-TEMPORAL CROSS-CORRELATION MODEL

Four model parts have been introduced in Chapter 4. An overview of the model is provided in Figure 5.1. Each of these model parts consists of a set of specific operations:

Model Part 0: Pre-Processing

1. Manual selection of the area of interest;
2. Selection of usable imagery;
3. Equalisation of the time lag between spectral bands;
4. Determination of the order of spectral bands;
5. Detrending and normalising;
6. Filtering the imagery using a 2D Fourier transform.

Model Part 1: Image Resolution Augmentation

1. Augmentation of lower resolution spectral bands.

Model Part 2: Wave Characteristics Estimation

1. Estimation of dominant wave direction;
2. Estimation of wavelength;
3. Estimation of wave celerity.

Model Part 3: Video Construction

1. Median filtering of estimated wave characteristics;
2. Creation of time vectors and video construction.

SPATIO-TEMPORAL CROSS-CORRELATION MODEL

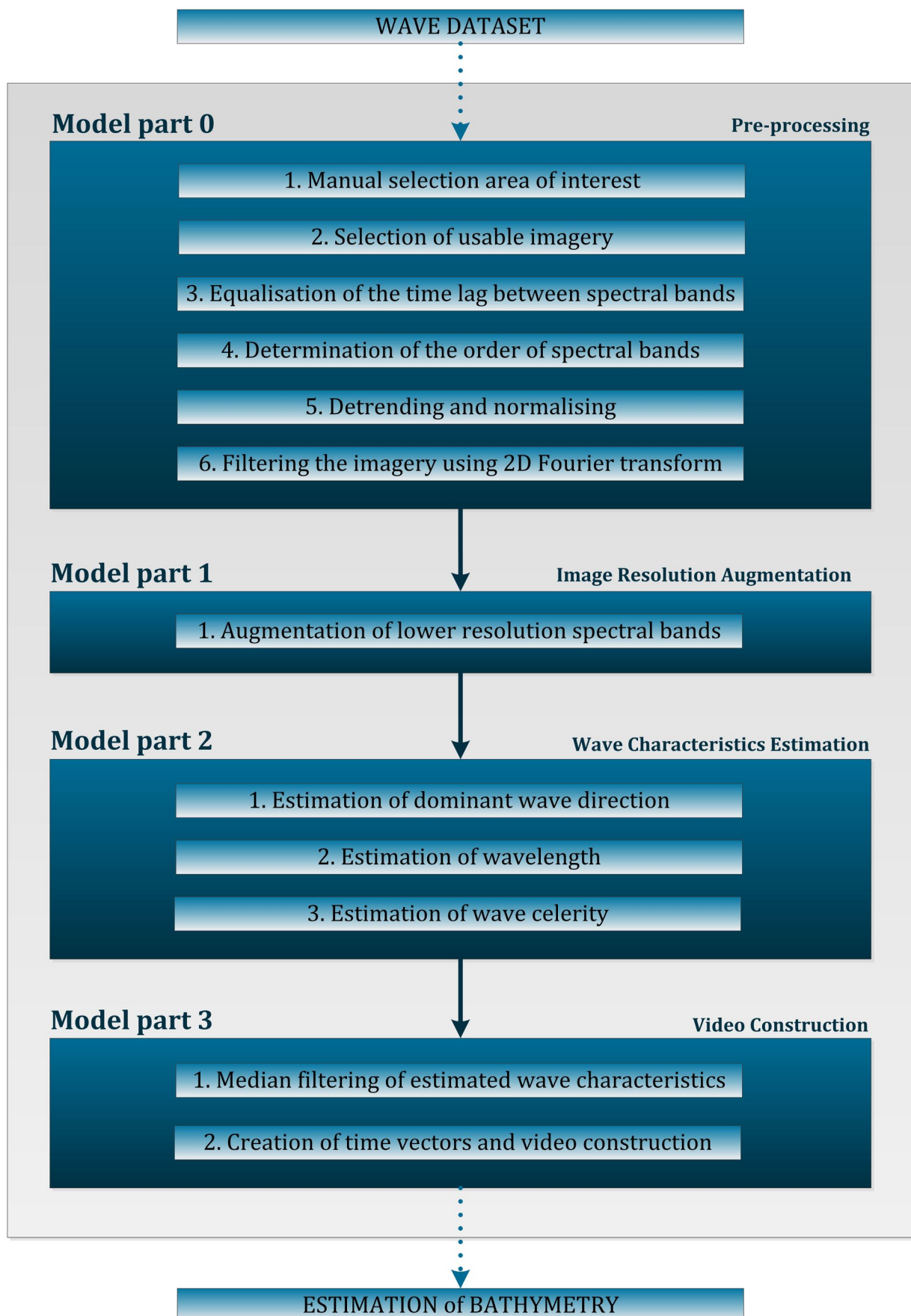


Figure 5.1: Overview spatio-temporal cross-correlation model.

DESIGN CHOICES

Design choices are introduced in the description of the model parts. These design choices represent case-dependent parameter settings of the model: the design choices are based on the specific dataset of interest. The design choices are clearly indicated and the corresponding parameter settings are provided when presenting the related results.

The spatio-temporal cross-correlation model consists of four model parts in order to analyse (FUNWAVE / Sentinel-2) imagery: 0) pre-processing, 1) image resolution augmentation, 2) wave characteristics estimation and 3) video construction. A set of design choices is introduced in the description of the model. These design choices are case-dependent parameter settings.

5.2. ILLUSTRATING SINUSOIDAL WAVE

The illustrating sinusoidal wave is solely used to illustrate the concept of the model. It is represented in a 3D plane (x, y, η) by:

$$\eta(x, y, t) = a \sin(\omega t - k_x x - k_y y) \quad (5.1)$$

in which η is surface height, x is the cross-shore direction, y is the longshore direction, t is time, a is wave amplitude, ω is angular frequency and k_x and k_y represent the wave number in x- and y-direction, respectively. The wavelength (L) and wave period (T) of the illustrating sinusoidal wave are set to be constant at $L = 100$ m and $T = 10$ s, respectively, while the wave direction is imposed to be constant at 0° with respect to the positive x-axis. That means, the wave is propagating in positive x-direction having a celerity of $c = L/T = 10$ m/s. The amplitude of the wave is set to be $a = 1$ m. The wave, defined over a 3D domain (x, y, η) of 1000 by 1000 m is shown in Figure 5.2a and a cross-section of the wave in Figure 5.2b.

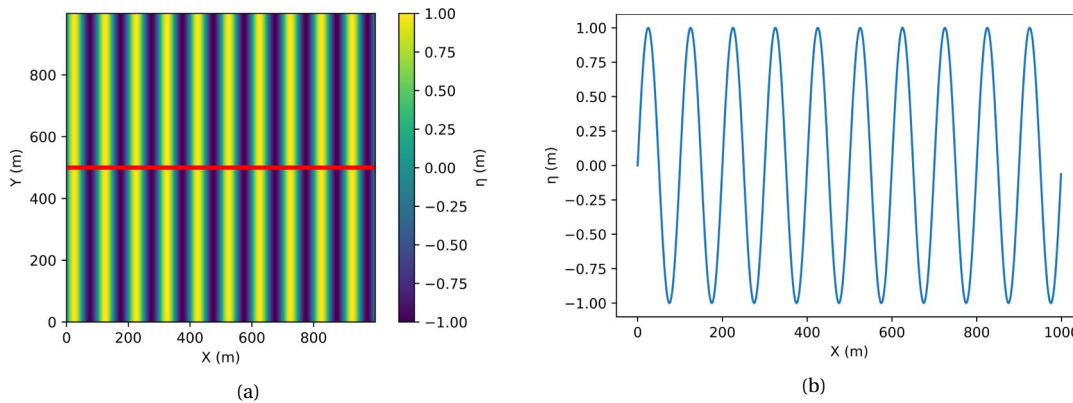


Figure 5.2: Illustrating sinusoidal wave defined over a 3D domain (x, y, η) of 1000 by 1000 m, $L = 100$ m and $T = 10$ s (a). In (b) the cross-section indicated by the red line in (a) is provided.

According to the linear dispersion relationship (Equation 4.2) [65] such a wave could only exist when the wave is propagating over a constant bathymetry, of which the depth amounts: $d \approx 12.08$ m. An important note here is that the wave propagates in intermediate water depth ($d_{sh} < d < d_{int} \rightarrow L/20 < d < L/2 \rightarrow 5 < d < 50$). A schematic of the wave in a 2D plane (x, η) , including the position of the bottom, is provided in Figure 5.3a. The structure in which the sinusoidal wave is provided more or less mimics Sentinel-2 imagery. It is presented as a set of 10 snapshots, with a constant time lag of 0.5 s. That means the wave propagates from snapshot to snapshot over a total duration of 4.5 s. An impression of that propagation is shown in Figure 5.3b in which cross-sections of 10 snapshots from $t = 0.0$ s (dark blue line) to $t = 4.5$ s (light blue line) are provided. The dataset is sampled in 10 m resolution.

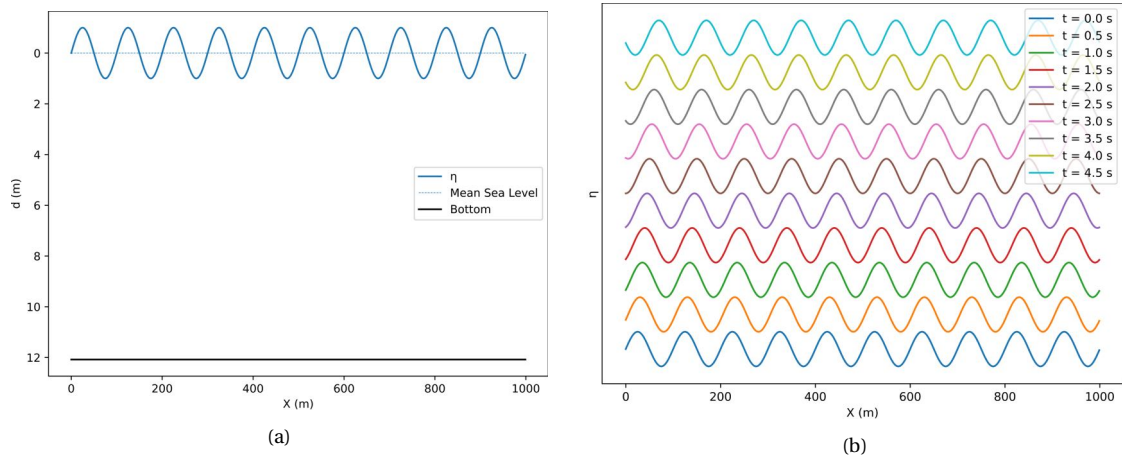


Figure 5.3: In (a) a cross-section of the illustrating sinusoidal wave is shown. The bottom and mean sea level are indicated as well. (b) shows 10 snapshots of the sinusoidal wave in which the propagation of the wave can be observed.

5.3. MAIN MATHEMATICAL PRINCIPLE OF THE MODEL: CROSS-CORRELATION

The main mathematical principle in the model is the correlation of time series in a spatial sense: a cross-correlation. In model part 2, time series per pixel are correlated with each other in order to estimate wave characteristics. The other three model parts consist of steps that improve or prepare the correlation, or make use of the estimated wave characteristics. A general introduction of cross-correlation is therefore provided first before discussing the specific model parts in the following sections.

PEARSON CORRELATION COEFFICIENT

Time series are correlated with each other using the Pearson correlation coefficient [96]. In general form it is expressed as:

$$\rho = \frac{\text{cov}(X, Y)}{\sigma(X)\sigma(Y)} \approx \frac{\sum_{i=1}^N (X_i - \bar{X})(Y_i - \bar{Y})}{\sqrt{\sum_{i=1}^N (X_i - \bar{X})^2} \sqrt{\sum_{i=1}^N (Y_i - \bar{Y})^2}} \quad (5.2)$$

where X and Y represent two variables that are possibly correlated, N is the number of data points and i indicates the data point number with $i = 1, 2, 3, \dots, N$. In the context of time series correlation, X and Y could be seen as the representatives of two time series and i as a certain moment in time. When time series are considered, ρ can be written as:

$$\rho = \frac{\text{cov}(TS_1, TS_2)}{\sigma(TS_1)\sigma(TS_2)} \approx \frac{\sum_{i=1}^N (TS_{1,i} - \overline{TS_1})(TS_{2,i} - \overline{TS_2})}{\sqrt{\sum_{i=1}^N (TS_{1,i} - \overline{TS_1})^2} \sqrt{\sum_{i=1}^N (TS_{2,i} - \overline{TS_2})^2}} \quad (5.3)$$

in which TS_1 and TS_2 both represent a certain time series. The value of ρ is always defined between -1 and 1. When two timeseries, TS_1 and TS_2 , are fully positively correlated ($\rho = 1$), it means that the relation between both time series could be described perfectly as a linear equation [96]:

$$TS_1 = a * TS_2 + b \quad (5.4)$$

or described per moment in time, i :

$$TS_{1,i} = a * TS_{2,i} + b \quad (5.5)$$

The interpretation is that all points in a domain (TS_1, TS_2) lie exactly on a straight line for which TS_1 increases as TS_2 increases. The opposite holds for a fully negative correlation ($\rho = -1$): all points in a domain (TS_1, TS_2) are exactly located on a straight line for which TS_1 increases as TS_2 decreases. When there is no correlation ($\rho = 0$) there is no linear relation between both time series.

CROSS-CORRELATION AND WAVES

The above theory is translated to waves. The surface height (η) represented by Sentinel-2 imagery is defined over the dimensions (x, y, t), in which x and y form the spatial dimensions and t forms the time series, e.g. 4.5 s, defined over 10 snapshots in the case of the illustrating sinusoidal wave. That means, in every pixel (x, y) a time series of 4.5 s is defined. Figure 5.4a shows a cross-section of the first snapshot ($t = 0$ s) of the illustrating sinusoidal wave. In this cross-section the markers indicate a certain location on the x-axis, ranging from $X = 450$ m to $X = 550$ m for every 10 m. Each of these markers indicates the start of a time series that represents the surface height over the upcoming 4.5 s. These time series are provided in Figure 5.4b, using corresponding colours.

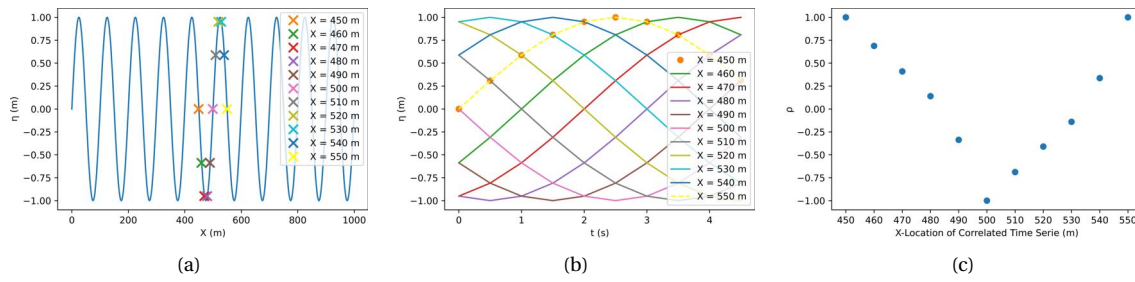


Figure 5.4: A cross-section of the first snapshot ($t = 0$ s) of the illustrating sinusoidal wave (a). The markers indicate the starting points of the time series in (b). In (c) the Pearson correlation coefficients (ρ) for correlations of the time series at $X = 450$ m and the time series indicated at the x-axis is presented.

Correlating the time series of $X = 450$ m with itself and with the other 10 time series ($X = 460$ m to $X = 550$ m), leads to 11 values of ρ . These values are shown in Figure 5.4c. A clear variation in the value of ρ is observed. A self-correlation, or auto-correlation, leads to $\rho = 1$. This corresponds with theory, since both time series are exactly equal. Looking at the correlation of the time series at $X = 450$ m and the time series at $X = 500$ m, a value of $\rho = -1$ is obtained. That indicates a fully negative correlation, which is logical since both time series are exactly opposite. Another interesting correlation is obtained between the time series starting at $X = 450$ m and $X = 550$ m. Since these two time series are exactly equal, the correlation value is $\rho = 1$. An important note here is that the value of ρ would be 1 as well, if both time series are not equal in absolute sense but only their gradient is the same. An example of that is shown in Figure 5.5a where a value of $\eta = 2$ m is added to the time series at $X = 450$ m. The correlation of those two time series amounts to exactly 1. These examples show the power of correlating time series in order to determine locations in space where the gradient, or form, of time series are similar.

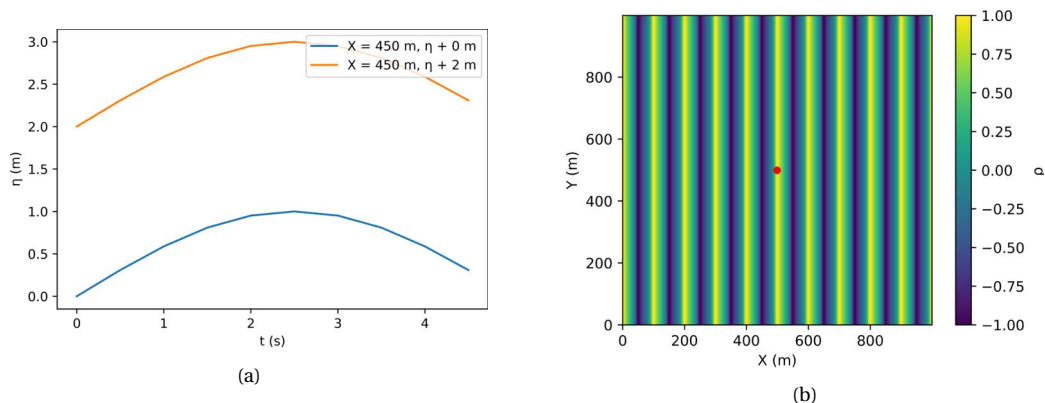


Figure 5.5: (a) Shows two time series of the illustrating sinusoidal wave. Both are time series at $X = 450$ m, while to one of them a value of $\eta = 2$ m is added. The correlation between both time series is $\rho = 1$. In (b) the time series in $X = 500$ m, $Y = 500$ m (red marker) is correlated with the time series of all other pixels in the domain of the illustrating sinusoidal wave.

The same principle is used to determine locations that show wave similarities. In Figure 5.5b the

concept is applied to a 3D domain (x, y, η) . The figure shows the result of a correlation of the time serie at $X = 500$ m, $Y = 500$ m and the time series at all other pixels in the domain of the illustrating sinusoidal wave. At every location where $\rho = 1$ the wave form is exactly equal to the wave form at $X = 500$ m, $Y = 500$ m. Note thereby that the result of these correlations forms a wave pattern by itself. Figure 5.5b shows that the correlation of time series can be used to reproduce a wave pattern showing similarities with the original wave pattern of the illustrating sinusoidal wave (see Figure 5.2a). This principle is used in various ways in the model.

The main mathematical principle that is used in the model is cross-correlation. A cross-correlation is the correlation of time series in spatial sense. The principle of cross-correlation can be used to observe the propagation of waves since maximum correlation values between time series are obtained for locations showing similar wave forms.

5.4. MODEL PART 0: PRE-PROCESSING

The aim of model part 0 is to pre-process raw Sentinel-2 data. A set of operations is performed to manipulate the data in order to enable the recognition of wave propagation.

5.4.1. MANUAL SELECTION OF THE AREA OF INTEREST

Sentinel-2 imagery comes in the form of tiles. Since the purpose of the model is to derive nearshore bathymetry, they contain land as well as sea areas. The automatic recognition of these areas is beyond the scope of this thesis. A nearshore sea area is therefore manually selected. Moreover, it is made sure that the area of interest does not contain cloud coverage.

5.4.2. SELECTION OF USABLE IMAGERY

Sentinel-2 imagery is provided in 13 spectral bands. In principle, enabling the usage of more temporal information leads to a more accurate wave characteristics estimation [64]. However, two complications lead to the use of only 8 bands: B02, B08, B03, B04, B05, B06, B07, B8A. These two complications include the impossibility to sufficiently increase the resolution of the 60 m resolution bands as well as the small time lag between B11 and B06 and between B8A and B12. Therefore, the use of B10, B01, B09, B11 and B12 is avoided.

5.4.3. EQUALISATION OF THE TIME LAG BETWEEN SPECTRAL BANDS

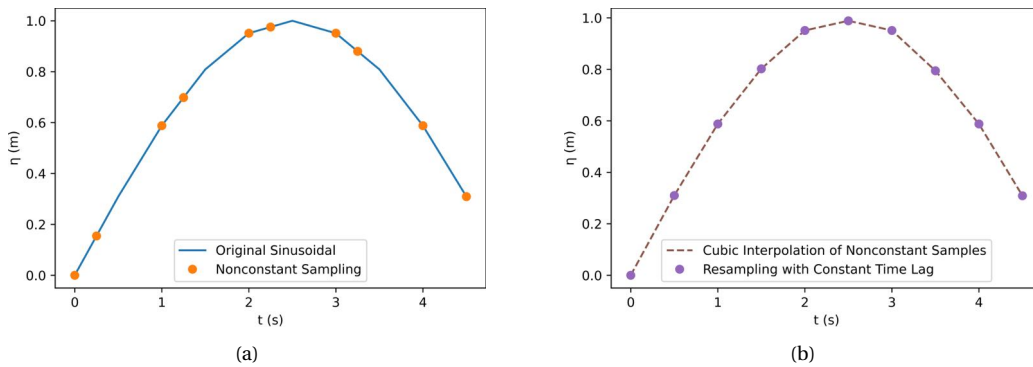


Figure 5.6: Interpolation of a time serie from an irregular time vector (a) to a regular time vector (b), using cubic spline interpolation.

As can be observed in Table 2.1, the time lag between each spectral band of the Sentinel-2 imagery is fluctuating. It varies in a range of 0.030 s to 0.324 s. In the model, time serie correlations are applied frequently. These correlations are not only performed between time series as a whole, but also between parts of time series or between shifted time series. That declares the need to equalise the time lag between each time step of the time series. Cubic spline interpolation is used for that operation: the time series of the satellite imagery are interpolated and resampled over a time vector

with constant time lag, which is the average time lag over 8 bands: 0.298 s. An example, using the illustrating sinusoidal wave, is provided in Figure 5.6. In this example, a time serie of the original wave is resampled over an irregular time vector (Figure 5.6a). Subsequently, the irregular time vector is interpolated. The resulting values of η in the resampled snapshot are indicated by the markers in Figure 5.6b. It is decided to use spline interpolation instead of some other interpolation methods, since spline interpolation ensures that the interpolation matches the known values of the provided snapshots, contradictory to e.g. trigonometric interpolation.

5.4.4. DETERMINATION OF THE ORDER OF SPECTRAL BANDS

Due to the placing of the 12 detectors of the Sentinel-2 satellites, the sequence of band detection switches approximately every 10 kms. For standard users, these locations of switching order are not known. Therefore the band order at the area of interest is assessed manually by looking at the raw satellite data. This is accomplished by observing the wave propagation in figures like Figure 2.4b.

5.4.5. DETRENDING AND NORMALISING

The satellite imagery is detrended: a linear trend in the surface height is removed in x- and y-direction, per spectral band. A normalising protocol is applied afterwards. In the context of this thesis, normalising defines the resampling between values of 1 and -1. The purpose is to equalise the information of all 13 spectral bands, which are not necessarily defined by the same ranges of pixel intensities. Both operations are only performed after manually selecting a nearshore sea area, since otherwise they are affected by the pixel intensities of land areas. An example of real satellite imagery, clarifying the need for detrending and normalising, as well as the need to be aware of sea and land areas is shown in Figure 5.7. In Figure 5.7b the pixel intensities corresponding to the cross-section indicated by the red line in Figure 5.7a are presented. It is obvious that a distinction between sea and land area exists (around $X = 35$ km) and furthermore a linear trend in the data containing sea area ($X = 0$ km to $X = 35$ km) is observed.

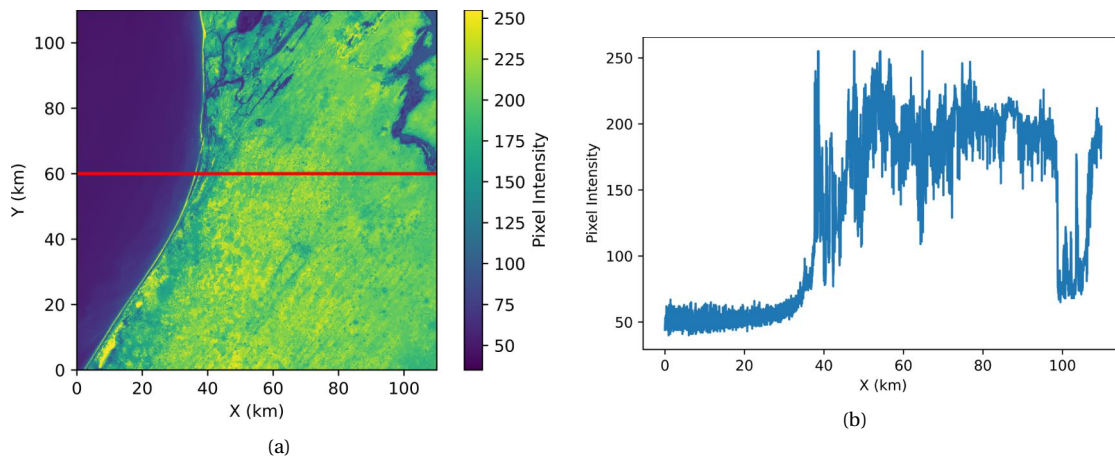


Figure 5.7: Example of Satellite Imagery in Saint-Louis, Senegal. In (b), showing the cross-section indicated by the red line in (a), a linear trend and clear distinction between sea and land area can be observed.

5.4.6. FILTERING THE IMAGERY USING A 2D FOURIER TRANSFORM

A 2D Fourier Transform [97] filter is applied in spatial sense and repeated for every spectral band of the satellite imagery. The surface height represented by the imagery is described by a variance-density spectrum, or energy-density spectrum. Both form a description of the surface height in a statistical sense by providing the distribution of the total variance, or total energy of the sea surface elevation over a range of frequencies, or wave periods ($T = 1/f$) [65]. The 2D Fourier transform filter is applied to remove a certain range of frequencies of the variance-density spectrum.

The variance-density spectrum is normally obtained by transforming the surface height data from

the temporal domain to the frequency, or spectral domain. A sufficient range of temporal information is needed to do so, a range that is not existent when Sentinel-2 imagery is regarded. Therefore, the filtering is based on offshore wave periods/frequencies. When waves are in offshore water ($d > L/2$) the temporal wave parameter T can be explicitly converted to the spatial wave parameter L using Equation 5.6 [65]:

$$L_0 = \frac{gT^2}{2\pi} \quad (5.6)$$

in which L_0 is the offshore wavelength and g represents the gravitational acceleration constant. In this way a range of wave periods can be defined and converted to a range of offshore wavelengths, which is then converted to a range of offshore wave numbers ($k = \frac{2\pi}{L_0}$). Subsequently a Fourier transform in the spatial domain - of which sufficient information is available - is then applied per satellite image, after which a spatial bandpass filter [98] is used to remove the wave numbers outside the defined range.

DESIGN CHOICE: REDUCING NOISE AND FINDING THE PEAK SWELL WAVE PERIOD

There are two possible main grounds to filter out a range of wave numbers, and thereby frequencies. First of all, some high frequency noise can be filtered out. A second possible reason is found in the need to find the peak swell wave period. Wave spectra are often characterised by two distinct peaks, indicating waves from two different sources. The wind sea waves are waves that are created locally and are therefore relatively less uni-directional (more short-crested) and defined over a broader range of wave periods [65]. In comparison, swell waves are created in a distant storm and due to frequency and direction dispersion they are relatively uni-directional. It is expected that these latter kind of waves are more easy to analyse due to three effects. First, wave parameters such as the (peak) wave period and wave direction are more clearly defined. Secondly, the swell waves are probably better visible on satellite imagery, due to the relatively coarse resolution of the imagery; longer wave patterns are thus better visible. And lastly, swell waves are relatively more affected by depth and less affected by external effects, such as wind [65]. It is therefore the peak swell wave period that is searched for when filtering based on the second ground is applied.

It has been chosen to use a filter that isolates the peak swell wave period as well as reduces noise. This corresponds with Almar *et al.* [64]. The typical filtering range that is required can be found in wave periods ranging from 6/7/8 s to 15 s. The filtering range is indicated when presenting related results.

Model part 0 includes six separately performed operations. First, the area of interest is manually selected from the raw imagery. The second operation consists of the selection of 8 - of a total of 13 - bands. This selection is based on two considerations: 1) the impossibility to sufficiently increase the resolution of 60 m resolution bands to 10 m and 2) the small time lag between some of the bands. In the third operation, the specific order of the bands is manually determined, after which the fourth operation aims to equalise the time lag between the bands. Fifthly, the imagery is detrended and normalised. The sixth and last operation applies a 2D Fourier filter based on offshore wave characteristics to the imagery. The 2D Fourier filter is meant to reduce noise and isolate the peak swell wave period. The specific filtering range acts as a design choice.

5.5. MODEL PART 1: IMAGE RESOLUTION AUGMENTATION

Model part 1 aims to augment, or increase, the resolution of the lower resolution spectral bands. An increase from 20 m resolution towards 10 m resolution is performed. The operation only includes the 20 m resolution bands, since the use of 60 m bands is avoided. A cubic spline interpolation in the Radon domain is introduced to augment the resolutions, since it is expected that a Radon transform enhances dominant wave features [5, 64]. It is therefore the favourable method for the aim of this thesis.

RADON TRANSFORM AND WAVES

The Radon transform [99] is a technique that is used commonly in order to find and enhance linear patterns in imagery [5]. It is already used in several applications regarding wave analyses [100], although it is mainly known from medical purposes [101]. There is a potential of the Radon transform for the purpose of image resolution augmentation. Bergsma *et al.* [5] already proved that augmenting the 20 m resolution bands of Sentinel-2 imagery to 10 m resolution, using a Radon transform, resolves the wave patterns remarkably well for longer wave features.

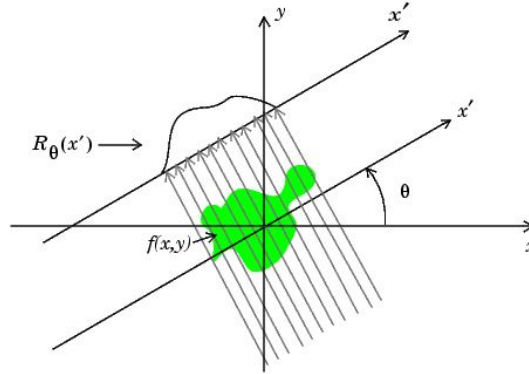


Figure 5.8: Schematic of Radon transform [2].

CONCEPT OF THE RADON TRANSFORM

The Radon transform is a way of transforming images from a standard spatial domain (x, y) to polar coordinates (θ, ρ) . When θ is defined over a range from 0° to 360° , or from -180° to $+180^\circ$ as in this thesis, for every θ a line through the origin of the image can be defined. The origin is commonly taken as the center of the image. θ then represents the angle between the particular line and the line of 0° through the origin. At those lines, ρ indicates the distance between a particular location and the origin. Now, for every combination of θ and ρ a line integral of the pixel intensities $(I(x, y))$ of the image is taken, perpendicular to the earlier defined line. An example of that is shown in Figure 5.8, in which x' defines a line, related to a certain θ , $f(x, y)$ represents the pixel intensity, the arrows specify the line integrals and R_θ is the result of the Radon transform for the particular θ . Note that the abbreviations as provided in the text above, and not as in the figure, are used in the context of this thesis. The Radon transform is mathematically notated as:

$$R_I(\theta, \rho) = \iint_D I(x, y) \delta(\rho - x \cos(\theta) - y \sin(\theta)) dy dx \quad (5.7)$$

When an image is transformed using Radon, a so-called sinogram is created. In the sinogram, per combination θ and ρ , the pixel intensity is shown. Figure 5.9 presents an example containing the illustrating sinusoidal wave. As can be seen in Figure 5.9b the highest absolute values of the pixel intensity are observed at $\theta = 0^\circ$ and $\theta = +/ -180^\circ$. This corresponds with the pattern of the sinusoidal wave. Furthermore, the signal at those angles varies from a pixel intensity of $+1000$ to -1000 , which corresponds to the values of an integral over $\eta = 1$ m and $\eta = -1$ m: $y = 1000$ m * $\eta = 1$ m = 1000 .

UPSAMPLING OF AN IMAGE USING A RADON TRANSFORM

The upsampling of an image is obtained by interpolating over ρ in the sinogram: the ρ -vector is resampled to 10 m resolution. After upsampling, the image is again transformed using an inverse Radon transform, leading to an image of higher resolution. It is expected that this method works quite well for the resolution augmentation of images containing waves. This is because the interpolation is performed per θ , which results in the isolation of the wave signal in one direction. The interpolation is therefore more focused on the wave signal itself; it interpolates an actual wave signal instead of other cross-wave-direction signals. Bergsma *et al.* [5] even suggested to solely perform an

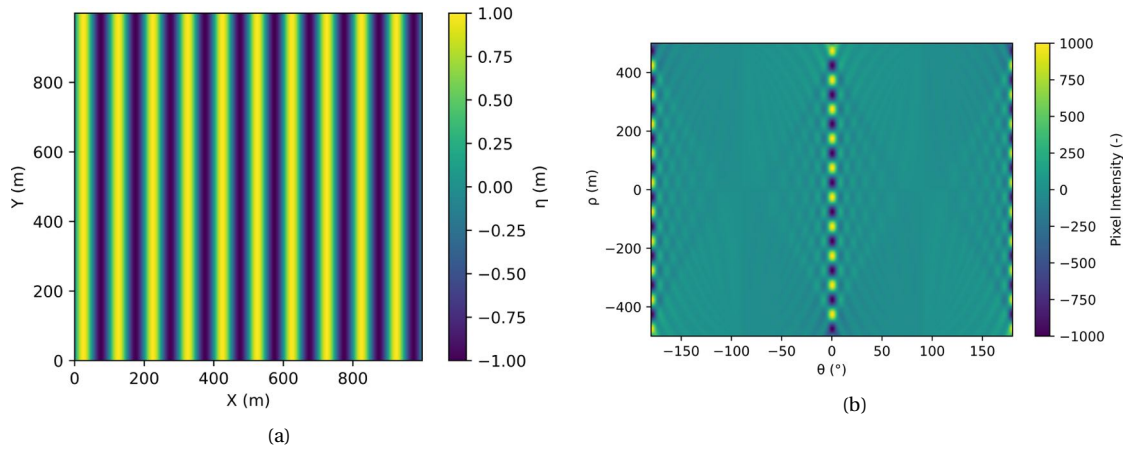


Figure 5.9: Example of a Radon transform in (a), the resulting sinogram is shown in (b). θ is defined from -180° to $+180^\circ$.

inverse Radon transform to the θ showing maximum pixel intensity variance. This is in fact a filter that isolates the dominant wave direction in the signal. Although very efficient, it is not needed within this part of the model, since a similar wave isolation is performed during the estimation of wave characteristics in model part 3. The interpolation of the ρ -vectors is performed using a cubic spline interpolation.

In model part 1 the resolution of lower resolution bands is augmented. This is done by means of a cubic spline interpolation in Radon space. Upsampling in Radon space is beneficial since the wave signal in dominant wave direction is isolated; the interpolation is thus performed over the isolated wave signal instead of over other cross-wave-direction signals.

5.6. MODEL PART 2: WAVE CHARACTERISTICS ESTIMATION

The aim of model part 2 is to estimate wave characteristics. Three separate wave characteristics are obtained: dominant wave direction, wavelength and wave celerity. Each of these wave characteristics is estimated per pixel of the domain (10 m resolution).

5.6.1. ESTIMATION OF DOMINANT WAVE DIRECTION

The estimation of the dominant wave direction consists of two operations: a cross-correlation and a Radon transformation.

CROSS-CORRELATION

In Section 5.3 the concept of cross-correlation is explained. This idea is exploited in order to estimate the dominant wave direction. For a certain pixel ($x = X, y = Y$) a time series consisting of 8 time steps is provided by the selected spectral bands of the Sentinel-2 imagery. By correlating the time series in ($x = X, y = Y$) with time series of surrounding pixels, the similarity of the temporal signal in those pixels with the signal in pixel ($x = X, y = Y$) can be assessed: a high, positive correlation indicates a lot of similarity, while a low, negative correlation indicates the opposite. For the purpose of wave characteristics estimation, a second feature is added to the correlation protocol. The time series of the surrounding pixels are purposely shifted with respect to the time series in the pixel of interest. The imposed shift is 0.298 s, the average time lag of the selected spectral bands. The shifted correlation leads to insights regarding the propagation of the wave in the pixel of interest: a maximum correlation in a surrounding pixel indicates that the wave has propagated in that direction; the wave is in the pixel of interest at $t = 0$ s and is near the pixel with maximum correlation at $t = 0.298$ s. An example of a shifted correlation, or cross-correlation, between the pixel of interest and surrounding pixels is shown in Figure 5.10a. The pixel of interest in the figure is ($x = 500$ m, $y = 500$ m). Note in Figure 5.10a the pixel of maximum correlation, which is slightly to the right of the pixel of interest. This is the effect of the imposed time shift.

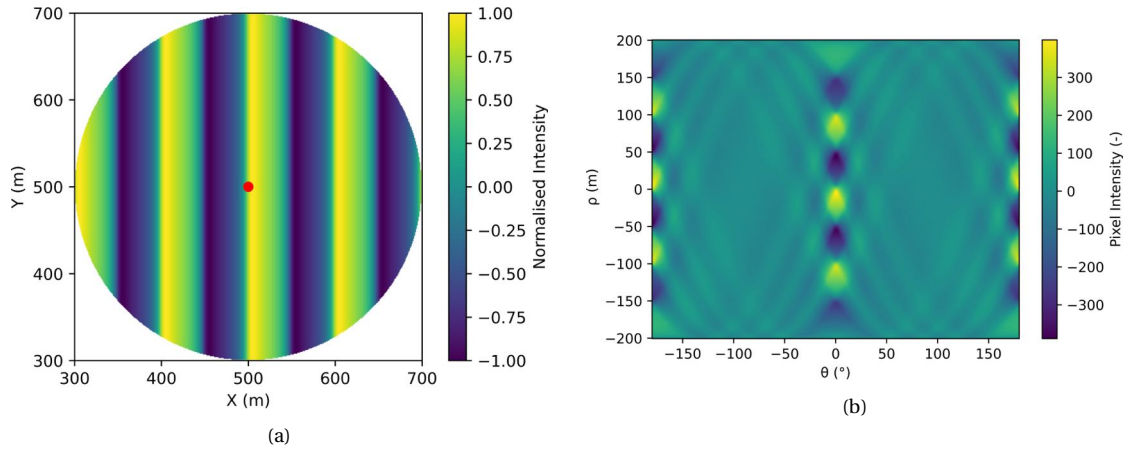


Figure 5.10: Cross-correlation for a pixel of interest. The resulting correlation is shown in (a). A sinogram, obtained by a Radon transform is provided in (b). The pixel of maximum correlation in (a) is slightly to the right of the pixel of interest, which is an effect of the imposed time shift.

RADON TRANSFORM TO ESTIMATE DOMINANT WAVE DIRECTION

The cross-correlation in Figure 5.10a is used to derive the dominant wave direction in the pixel of interest. A Radon transform is applied for that purpose, creating a sinogram of the cross-correlation image. It is shown in Figure 5.10b. The sinogram represents the pixel intensity, or energy per θ in an image. By calculating the variance per θ in the sinogram, the dominant wave direction is provided by the θ that shows maximum variance. As can be seen in Figure 5.10b there are two directions that show maximum variance: $\pm 180^\circ$ and 0° . The proposed method is unable to make a distinction between the propagating direction and the direction of which the waves come from. This should be assessed manually, which is straightforward, since the evaluation regards nearshore areas; the waves propagate into the direction of the shore. It is emphasised that the dominant wave direction is estimated separately for each pixel of the domain on the 10 m resolution grid. Figure 5.11 shows the result for a range of pixels of the illustrating sinusoidal wave. In this particular example it is chosen to provide the wave direction for a pixel every 100 m.

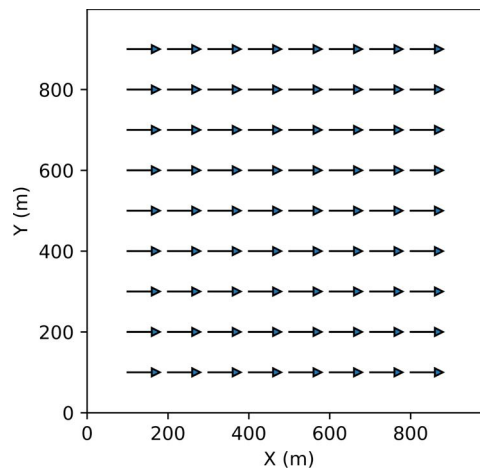


Figure 5.11: Overview of estimated wave direction for a range of pixels of the illustrating sinusoidal wave.

DESIGN CHOICE: DOMAIN RADIUS

The domain radius defines the size of the domain in which the surrounding points are located; no cross-correlations outside the domain are performed for a certain pixel of interest. The choice for a certain domain radius acts as a design choice. One could imagine a certain minimum domain size in order to observe the correct wave propagation. On the other side, a maximum domain size exists as well. Since the wave characteristics in satellite imagery are not constant over the domain

- wave direction, celerity and wavelength are varying values - a too large domain size would imply accounting for information of waves that are not of influence to the pixel of interest. The domain radius is defined as the distance between the point of interest and the most far away point in which a cross-correlation is performed.

5.6.2. ESTIMATION OF WAVELENGTH

The second wave characteristic that is estimated pixel-wise is the wavelength (L). Since it is estimated based on a filtered wave signal it should be interpreted as the wavelength corresponding to the peak of the wave spectrum, the peak wave period (T_p). The basis for the method is the cross-correlation image in Figure 5.10a, of which a sinogram is created in Figure 5.10b. The wave signal in dominant wave direction is isolated by taking the column in the sinogram corresponding to θ with maximum variance, which is a reconstruction of the wave signal. The wavelength is defined by using four typical locations on the isolated signal: the zero down-crossings, the zero up-crossings, the wave crests and the wave troughs [65]. It is proposed to calculate four separate wavelengths, based on those four wave locations. The resulting wavelength is the average of these four calculations. In this way, the errors per separate calculation are averaged out, e.g. the error that is induced by the skewness of the reconstructed signal in Figure 5.12. The proposed method is chosen above some other methods, e.g. a wavelength estimation based on a correlation of the reconstructed signal and a mirror of the reconstructed signal, resulting in half of the wavelength. The main reason for this is the expectation that the proposed method, based on locations on the wave, better handles vertically asymmetric wave forms.

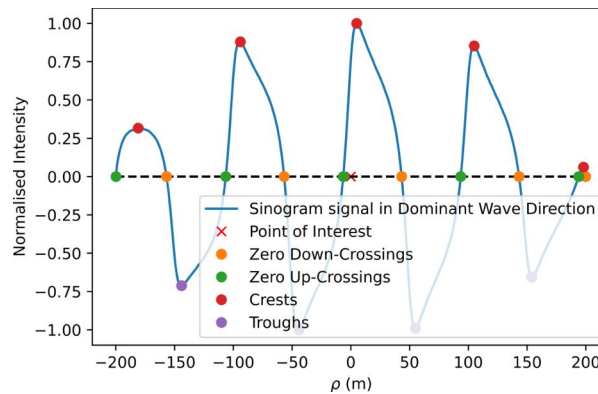


Figure 5.12: Estimation of wavelength for a pixel of the hypothetical sinusoidal.

DESIGN CHOICE: DOMAIN RADIUS

The domain radius of the performed cross-correlation for the purpose of wavelength estimation is again a design choice.

5.6.3. ESTIMATION OF WAVE CELERITY

The wave celerity forms the third and last wave characteristic that is estimated pixel-wise. Analogous to the estimation of wavelength, the estimated wave celerity can be seen as the celerity corresponding to the peak wave period. It is chosen to estimate wave celerity based on a correlation of two separated signals.

The method is explained using the illustrating sinusoidal wave. For a certain pixel of the sinusoidal wave, e.g. ($x = 500$ m, $y = 500$ m), a cross-correlation image with imposed time shift, likewise Figure 5.10a, is created. Figure 5.13a shows the resulting image. By taking the dominant wave direction in the pixel and performing a Radon transform to the correlation image, the wave signal in dominant wave direction is isolated and obtained from the sinogram. Figure 5.13b shows a normalised form of that signal. Now, a slightly different correlation is applied using the same point of interest and surrounding pixels. Instead of correlating the time series with an imposed time shift, the time series

are correlated without a time shift. This leads to a correlation image (Figure 5.13c) that shows maxima at the exact location of interest and at locations where the wave form is similar to that location; it is in fact a reconstruction of the raw wave signal. This correlation image is Radon transformed and normalised as well. By using the dominant wave direction, the isolated signal in Figure 5.13d is obtained. Note the subtle spatial shift between both wave signals.

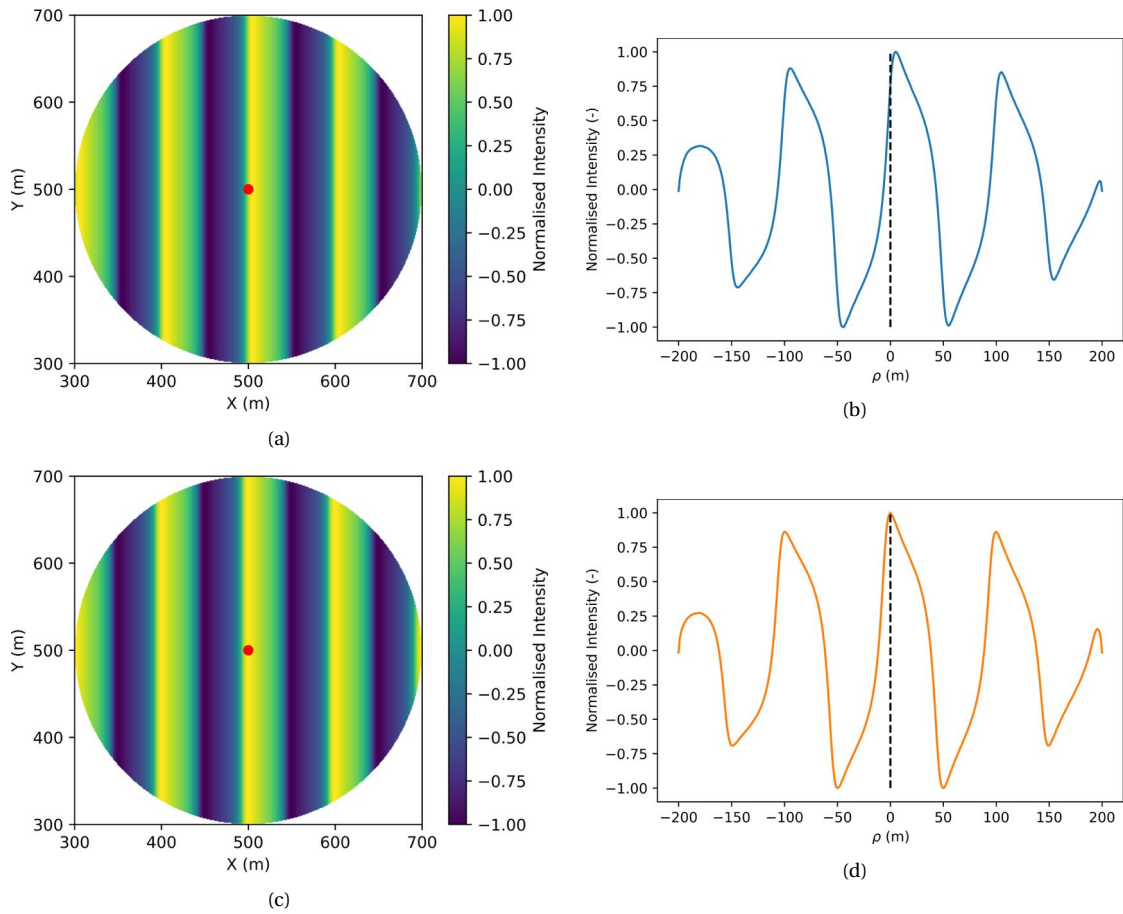


Figure 5.13: Correlation images and corresponding isolated signals. In (a) the cross-correlation that is obtained by cross-correlating a shifted signal is shown, the corresponding isolated signal is provided in (b). (c) Shows a correlation image that results from a correlation without a time shift. The corresponding isolated signal is shown in (d).

The existing spatial shift between both signals provides essential information, since it is the direct result of the imposed time shift. Therefore, by knowing the spatial shift, it is possible to estimate a celerity, which is defined as the spatial phase shift divided by the temporal phase shift. The spatial shift is obtained by applying a correlation. The signal in Figure 5.13b is shifted over small spatial steps, until a maximum correlation between both isolated wave signals (Figures 5.13b and 5.13d) shows up. The point of maximum correlation indicates the spatial phase shift between the signals. To obtain higher precision, both signals are linearly interpolated upfront on a grid of 0.1 m resolution. The estimated spatial phase shift is then divided by the imposed temporal shift, leading to an indication of the wave celerity in the pixel of interest. It should be noted that the window in which a maximum correlation is searched for is bound. Given the irregular nature of the satellite imagery, there is a possibility that a maximum correlation of the isolated signals is obtained some wavelengths away from the pixel of interest. This leads to unrealistic estimations of the celerity. Therefore, the maximum correlation has to be found in a pre-set window, corresponding to realistic estimations of the celerity. Figure 5.14 shows the way in which the celerity estimation is performed. The pre-set window is indicated by the green and red line.

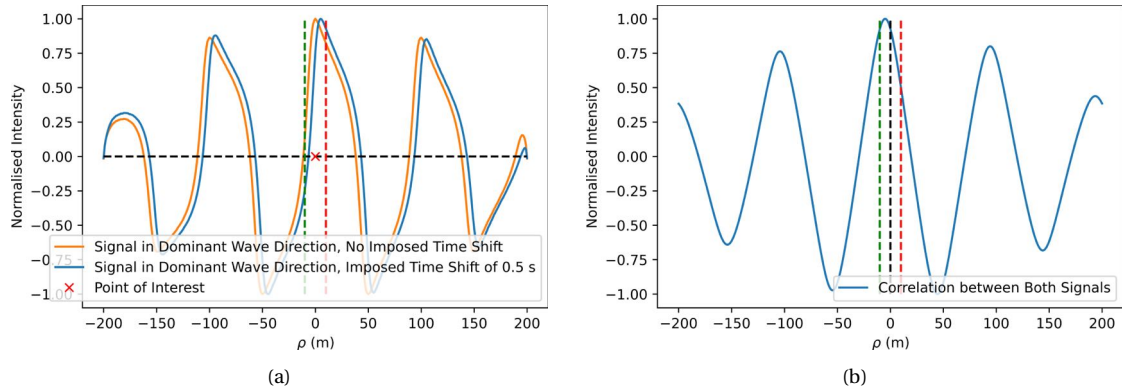


Figure 5.14: Celerity estimation of a certain pixel of the illustrating sinusoidal wave. (a) presents the two isolated wave signals. In (b) the location of maximum correlation between both signals is shown.

DESIGN CHOICE: DOMAIN RADIUS

The domain radius of the performed cross-correlation for the purpose of wave celerity estimation is a design choice.

Model part 2 includes the pixel-wise estimations of three distinct wave characteristics: 1) dominant wave direction, 2) wavelength and 3) wave celerity. All three estimations are obtained by performing a cross-correlation using shifted time series, leading to a cross-correlation image. To assess the dominant wave direction, the cross-correlation image is Radon transformed after which the variance over each direction in the resulting sinogram is calculated. Maximum variance indicates the dominant wave direction. The isolated signal in dominant wave direction is subsequently used to estimate the wavelength per pixel. A relatively plain protocol, using zero-crossings, crests and troughs, is used for that purpose. At last, wave celerity is estimated by assessing the spatial shift between two isolated wave signals. The first isolated wave signal is the one resulting from a shifted cross-correlation, while the second signal is obtained by a non-shifted cross-correlation. In each of the three distinct estimations, the domain radius that is used to construct the correlation images acts as a design choice.

5.7. MODEL PART 3: VIDEO CONSTRUCTION

The purpose of model part 3 is to construct a longer duration, wave-representing video. The wave characteristics estimation of model part 2 is used as basis.

5.7.1. MEDIAN FILTERING OF ESTIMATED WAVE CHARACTERISTICS

The wave characteristics 'dominant wave direction', 'wavelength' and 'wave celerity' are estimated per pixel. Concerning the irregularity of satellite imagery, it is expected that errors are induced when these parameters are estimated over the entire domain. A post-processing step is therefore added. The induced errors, or outliers, should be removed to ensure the quality of the resulting video. A median filter applied in spatial sense is proposed for that purpose. Per pixel, a square domain is defined, after which the median of the wave parameters in that domain is taken. This median value is applied as substitute for the wave parameter in the particular pixel. The operation is repeated for each pixel and each wave characteristic (direction, wavelength and celerity).

DESIGN CHOICE: SIZE OF THE MEDIAN FILTER DOMAIN

The size of the median filter domain is a design choice, indicated when presenting related results.

5.7.2. CREATION OF TIME VECTORS AND VIDEO CONSTRUCTION

The last part of the model consists of the actual video construction. For the entire area of interest a video showing the propagation of waves over the domain is created. The video is created using the following two steps:

1. The estimation of time vectors per pixel;
2. The combination of all time vectors to create a video.

STEP 1: THE ESTIMATION OF TIME VECTORS PER PIXEL

The time vector in a pixel, say pixel ($x = X$ m, $y = Y$ m) of the illustrating sinusoidal wave, forms a representation of surface height variation over a certain range of time. It is in fact the variation of surface height that is noticed by an observer at the particular pixel. The explanation of the method concerns the creation of one single time vector, for one specific pixel of the domain. For the purpose of illustration, the pixel ($x = 500$ m, $y = 500$ m) from the illustrating sinusoidal wave is taken. In reality, the creation of a time vector is repeated for every pixel of the entire domain. The estimation of a time vector consists of the following steps:

1. Estimating the perpendicular distance between surrounding pixels and the wave crest through the pixel of interest;
2. Estimating the travel time from surrounding pixels to the wave crest through the pixel of interest;
3. Creating temporal bins;
4. Estimating surface height per temporal bin and creating time vector for the pixel of interest.

ESTIMATING THE PERPENDICULAR DISTANCE BETWEEN SURROUNDING PIXELS AND THE WAVE CREST THROUGH THE PIXEL OF INTEREST

The celerity and dominant wave direction are known per pixel of interest. The wave direction makes an angle of 90° with the wave crest; when the wave direction is 0° with respect to the positive x-axis, the wave crest makes an angle of 90° with the positive x-axis. For all surrounding pixels in the domain, the perpendicular distance between the particular pixel and the wave crest through the pixel of interest, is estimated. This perpendicular distance represents the distance that information in a surrounding pixel has to travel until it reaches the pixel of interest. It is thereby assumed that the information over a wave crest is constant, which is true for infinitely long-crested waves: the surface height in a certain pixel on an infinitely long wave crest is equal to the surface height of all other points on the same wave crest. An example representing the introduced perpendicular distance is provided in Figure 5.15. Another sinusoidal wave propagating with an angle of -45° with respect to the positive x-axis is added to visualise how the perpendicular distance changes with changing wave direction. Note that the surface height over these infinitely long-crested wave crests is constant.

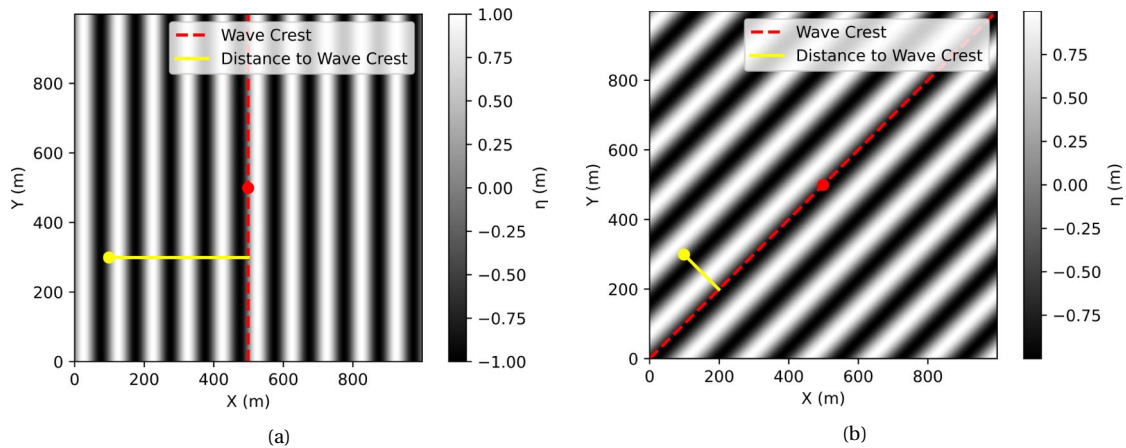


Figure 5.15: Perpendicular distance from a surrounding point (yellow marker) to the wave crest in the point of interest (red marker). The wave crest is indicated by a dashed red line and the perpendicular distance by a solid yellow line. In (a) the waves are propagating at an angle of 0° with respect to the positive x-axis, while in (b) the wave propagates with an angle of -45° with respect to the positive x-axis.

ESTIMATING THE TRAVEL TIME FROM SURROUNDING PIXELS TO THE WAVE CREST THROUGH THE PIXEL OF INTEREST

The travel time is the time it takes to travel from a surrounding point to the wave crest through the pixel of interest. It is the time it takes for information in the surrounding points to reach the pixel of interest. Information that travels from a surrounding point to the pixel of interest follows a certain path: the perpendicular distance between the surrounding point and the wave crest through the pixel of interest. During the defined travel, the information 'experiences' several celerities. It is in fact forced by each celerity that it comes across. Information could ideally be forced by all celerities (and wave directions) that it meets: a full 'langrangian' method would be created. It appears that such a method is computationally expensive. Therefore, a compromise is introduced: the travel time that corresponds to a certain surrounding point is determined by the celerity in the pixel of interest and the celerity in the surrounding point. The travel time is then obtained by first taking the integral of the celerities over the perpendicular distance - from surrounding point to wave crest - and secondly dividing the perpendicular distance by the integrated celerity. In this way a method is created in which not only the celerity of the pixel of interest is relevant, but also the celerity of surrounding points.

CREATING TEMPORAL BINS

The next step is to gather all travel times in temporal bins. These temporal bins are of pre-defined size and depend on the required resolution of the video. As standard, a video of two frames per second is taken. This leads to a temporal bin size of 0.5 s. Each bin now contains a set of travel times that are related to a certain surrounding location. The surface height in these surrounding locations is known at $t = 0$ s, since it is provided by the (resampled) satellite imagery. The satellite image in the middle of the 8 spectral bands is taken to provide the surface height at $t = 0$ s. Each bin now contains a set of (nearly equal) travel times, corresponding to a surrounding point and to a surface height at $t = 0$ s.

ESTIMATING SURFACE HEIGHT PER TEMPORAL BIN AND CREATING TIME VECTOR FOR THE PIXEL OF INTEREST

The last step is to take the surface heights per temporal bin and estimate one resulting surface height per bin from that. The resulting time vector for the pixel of interest is represented by the combining of resulting surface heights in all temporal bins. It has been chosen to obtain the resulting surface height in a temporal bin by taking a weighted average. The weights are based on the perpendicular distance from the surrounding points to the wave ray, or line of wave propagation, through the pixel of interest. Note that this implies a different concept than the perpendicular distance to the wave crest. The difference is shown in Figure 5.16. The weights are applied in a linear way. The surrounding points that are located exactly on the wave ray get a full, 100% weight, while the points of the domain that are located most far away of the wave ray get a 0% weight. The gradient between those points is linear. The weights are multiplied with the particular surface heights in the surrounding points.

In summary, the main point is that surrounding points located closer to the wave ray through the pixel of interest are made more important. It is expected that this approach is more realistic when real waves are evaluated, since they are not infinitely long-crested. Therefore, the information lying on the wave ray is more likely to influence the wave propagation in the pixel of interest than information that comes from a location far away of the propagation line.

NOTE: ESTIMATING WAVELENGTH FOR THE PURPOSE OF VIDEO CONSTRUCTION

In the Introduction (Chapter 1) it is explained that the linear dispersion relationship (Equation 1.1) can only be solved when two wave parameters are known. As can be read in above variants only one is used to construct the time vectors: the wave celerity. However, a second wave characteristic is hidden in the data that is used for it. The satellite image that is utilised to define the surface height at $t = 0$ s contains information regarding the wavelength; it forms a surface profile. In this way, the

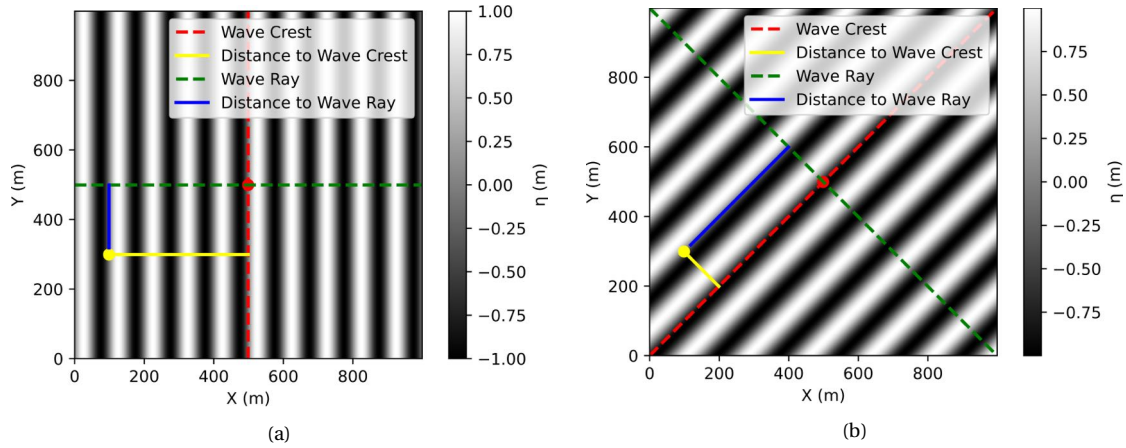


Figure 5.16: Example showing the difference between the perpendicular distance from a surrounding point to the wave crest in the pixel of interest and the perpendicular distance from a surrounding point to the wave ray in the pixel of interest. In (a) the waves are propagating at an angle of 0° with respect to the positive x-axis, while in (b) the wave propagate with an angle of -45° with respect to the positive x-axis.

time vectors contain information regarding the wavelength as well. If a time vector would be plotted over time and divided by the celerity in the pixel of interest, the wavelength would become visible.

STEP 2: COMBINATION OF ALL TIME VECTORS TO CREATE A VIDEO

In all pixels of the domain a time vector is created. The video emerges by aligning these time vectors, making sure that they include the same temporal range. The maximum duration of the video depends on the estimated celerities and the size of the overall chosen domain. Note that this is not the same concept as the duration of wave visibility.

In model part 3, the estimated wave characteristics of model part 2 are converted to a resulting video. Two distinct operations are performed for that purpose. At first, a post-processing step is added: the application of a median filter. The median filter replaces the value of an estimated wave characteristic by the median value of the surrounding pixels. The size of the median filter is a design choice. The second operation is the video construction itself. To that end, a time vector is created per pixel of interest; the video results from the combination and alignment of time vectors corresponding to each pixel of the domain. For a certain pixel of interest, the time vector is created following a set of steps. The first step includes calculating the distance from each surrounding point to the wave crest through the pixel of interest. This distance is thereafter converted to a travel time by using the celerities in the pixel of interest as well as the celerities in the surrounding pixels. The surface heights in surrounding points corresponding to (nearly) equal travel times are gathered in temporal bins. The resulting surface height in a temporal bin is then calculated by a linearly weighted average protocol, providing larger weights to pixels relatively closer to the line of wave propagation. The time vector in a pixel of interest is created afterwards by combining the resulting surface heights of all temporal bins. Repeating these steps for each pixel of the domain and combining the time vectors leads to the resulting video.

5.8. SUMMARY CHAPTER 5: SPATIO-TEMPORAL CROSS-CORRELATION MODEL

A spatio-temporal cross-correlation model is developed to construct a longer duration video from FUNWAVE / Sentinel-2 imagery. It consists of four model parts:

0. Pre-processing;
1. Image resolution augmentation;
2. Wave characteristics estimation;
3. Video construction.

An overview of the model is provided in Figure 5.1. Each of the model parts includes a set of operations. Moreover, several design choices corresponding to the model are introduced. These design choices are case-dependent parameter settings corresponding to a particular operation.

AIM OF THE MODEL PARTS

The four model parts relate to the research sub-objectives that are introduced in Chapter 1. The development of the entire model is based on and structured in these parts. The model is designed to handle raw Sentinel-2 user products. It is therefore first needed to **pre-process** the products in model part 0. The second step results from the essence of the model: the aim to enlarge the range of temporal information, from a short burst of Sentinel-2 imagery to a longer duration video. Therefore, model part 1, **image resolution augmentation**, is required to increase the amount of available temporal information upfront. Model part 2 is introduced as a result of the aim to construct a video that represents the propagation of waves; a **wave characteristics estimation** in the space-time domain acts as basis for the video. Model part 3 eventually performs the last part: **the video construction** itself.

CROSS-CORRELATION

The main mathematical principle that is used in the model is cross-correlation. A cross-correlation is the correlation of time series in spatial sense. The principle of cross-correlation can be used to observe the propagation of waves since maximum correlation values between time series are obtained for locations showing similar wave forms. Each of the four model parts makes use of or contributes to the cross-correlation. In model part 2, time series per pixel are cross-correlated with each other in order to estimate wave characteristics. The other three model parts consist of steps that improve or prepare the cross-correlation or make use of the estimated wave characteristics.

MODEL PART 0: PRE-PROCESSING

Model part 0 includes six separately performed operations. First, the area of interest is manually selected from the raw imagery. The second operation consists of the selection of 8 - of a total of 13 - bands. This selection is based on two considerations: 1) the impossibility to sufficiently increase the resolution of 60 m resolution bands to 10 m and 2) the small time lag between some of the bands. In the third operation, the specific order of the bands is manually determined, after which the fourth operation aims to equalise the time lag between the bands. The fifth operation includes the detrending and normalising of the imagery. The sixth and last operation applies a 2D Fourier filter based on offshore wave characteristics to the imagery. The 2D Fourier filter is meant to reduce noise and isolate the peak swell wave period. The specific filtering range acts as a design choice.

MODEL PART 1: IMAGE RESOLUTION AUGMENTATION

In model part 1 the resolution of lower resolution bands is augmented. This is done by means of a cubic spline interpolation in Radon space. Upsampling in Radon space is beneficial since the wave signal in dominant wave direction is isolated; the interpolation is thus performed over the isolated wave signal instead of over other cross-wave-direction signals.

MODEL PART 2: WAVE CHARACTERISTICS ESTIMATION

Model part 2 includes the pixel-wise estimations of three distinct wave characteristics: dominant wave direction, wavelength and wave celerity. All three estimations are obtained by performing a cross-correlation using shifted time series, leading to a cross-correlation image. To assess the dominant wave direction, the cross-correlation image is Radon transformed after which the variance over each direction in the resulting sinogram is calculated. Maximum variance indicates the dominant wave direction. The isolated signal in dominant wave direction is subsequently used to estimate the wavelength per pixel. A relatively plain protocol, using zero-crossings, crests and troughs, is used for that purpose. Finally, wave celerity is estimated by assessing the spatial shift between two isolated wave signals. The first isolated wave signal is the one resulting from a shifted cross-correlation, while the second signal is obtained by a non-shifted cross-correlation. In each of the three distinct estimations, the domain radius that is used to construct the correlation images acts as a design choice.

MODEL PART 3: VIDEO CONSTRUCTION

In model part 3, the estimated wave characteristics of model part 2 are converted to a resulting video. Two distinct operations are performed for that purpose. The first operation includes a post-processing step: the application of a median filter. The median filter replaces the value of an estimated wave characteristic by the median value of the surrounding pixels. The size of the median filter is a design choice. The second operation is the video construction itself. To that end, a time vector is created per pixel of interest; the video results from the combination and alignment of time vectors corresponding to each pixel of the domain. For a certain pixel of interest, the time vector is created following a set of steps. The first step includes calculating the distance from each surrounding point to the wave crest through the pixel of interest. This distance is thereafter converted to a travel time by using the celerities in the pixel of interest as well as the celerities in the surrounding pixels. The surface heights in surrounding points corresponding to (nearly) equal travel times are gathered in temporal bins. The resulting surface height in a temporal bin is then calculated by a linearly weighted average protocol, providing larger weights to pixels relatively closer to the line of wave propagation. The time vector in a pixel of interest is created afterwards by combining the resulting surface heights of all temporal bins. Repeating these steps for each pixel of the domain and combining the time vectors leads to the resulting video.

6

DATASET ANALYSIS

The spatio-temporal cross-correlation model has been applied to two different datasets: Dataset 1, a synthetic FUNWAVE dataset and Dataset 2, Sentinel-2 imagery. The results of the analyses are discussed per dataset based on the structure as provided by the model requirements (see Table 6.1). First, results corresponding to the wave direction estimations, the wavelength estimations and the wave celerity estimations are presented. These results relate to the first qualitative criterium of model requirement 1: a pixel-wise wave characteristics assessment. The results are followed by the wave spectra that are obtained from the video construction, which are related to the second criterium of model requirement 1: a wave spectra assessment. Next, an indication of the video duration is provided: the temporal range of visible wave propagation in the constructed video. These results are used to evaluate model requirement 2. The last results correspond to the use of the model in order to estimate bathymetry: model requirement 3. Relevant design choices are provided in the description of each particular result. These include the domain radius, the 2D Fourier filtering range and the size of the median filter that have been applied.

Table 6.1: Model requirements, together with quantitative evaluation criteria (quant. criteria) and qualitative evaluation criteria (qual. criteria).

Model Requirement	Quant. Criteria	Qual. Criteria
1. Wave propagation in video	- -	1) Pixel-wise wave char. assessment 2) Wave spectra assessment
2. Visible wave duration in video	Visible wave duration [s]	-
3. Accuracy of depth estimation	ρ [-] & RMSE [m]	Visual assessment

Section 6.1 provides the results related to the analysis of the synthetic FUNWAVE dataset. In Section 6.2 thereafter the results of the analysis of Sentinel-2 imagery in Saint-Louis are shown. The third section, Section 6.3, discusses the analysis of Sentinel-2 imagery in Capbreton. A concluding overview and interpretation of the results is provided in Section 6.4, making an attempt to point out the most important aspects that could be observed in the presented results. These observations are based on the research objective and model requirements. The research objective has been stated as:

The explicit aim of this research is to construct a one-minute video from a short burst of Sentinel-2 imagery (2.586 s), a video that accurately represents the propagation of waves. In addition, the potential of the video to estimate wave-derived nearshore bathymetry is shown. A DMD-based DIA is exploited for that purpose. The video is constructed by developing a spatio-temporal cross-correlation model.

6.1. RESULTS: SYNTHETIC FUNWAVE DATASET

No 2D Fourier filtering protocols have been applied during the analysis of the synthetic FUNWAVE dataset. The applied median filter is indicated where relevant.

6.1.1. WAVE DIRECTION ESTIMATIONS

Wave direction estimations have been obtained for every pixel of the synthetic FUNWAVE domain. The results are shown in Figure 6.1b. A domain radius of 100 m has been used for each single estimation. An overview of the synthetic FUNWAVE domain is provided in Figure 6.1a.

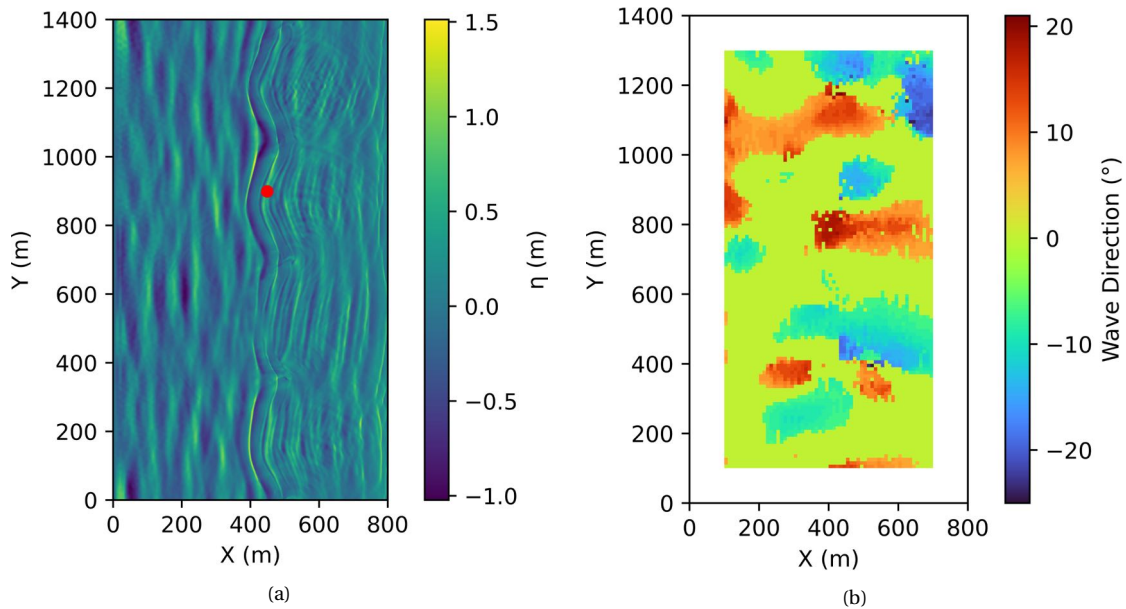


Figure 6.1: Wave direction estimations for the entire domain of the synthetic FUNWAVE dataset (b). A domain radius of 100 m has been used. In (a) an overview of the domain is provided. The red marker in (a) corresponds to the red markers in Figure 6.2.

The cross-correlation image that corresponds to the red pixel in Figure 6.1a is presented in Figure 6.2. A domain radius of 100 m has been used.

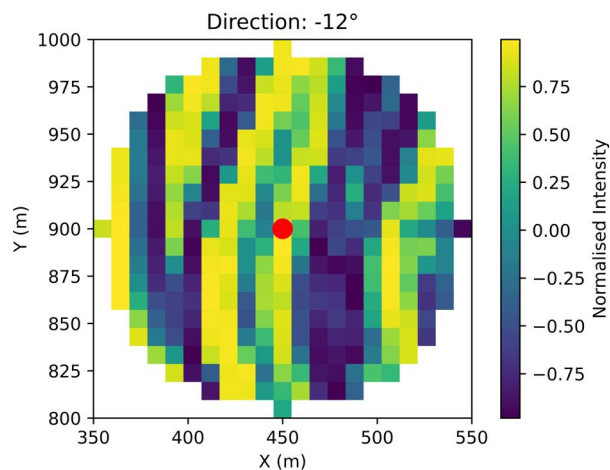


Figure 6.2: Cross-correlation images corresponding to a wave direction estimation for pixel ($X = 450$ m, $Y = 900$ m) of the synthetic FUNWAVE dataset. A domain radius of 100 m has been used.

6.1.2. WAVELENGTH ESTIMATIONS

The wavelength has been estimated for every single pixel of the synthetic FUNWAVE domain. Results are shown in Figure 6.3b. A domain radius of 100 m has been used.

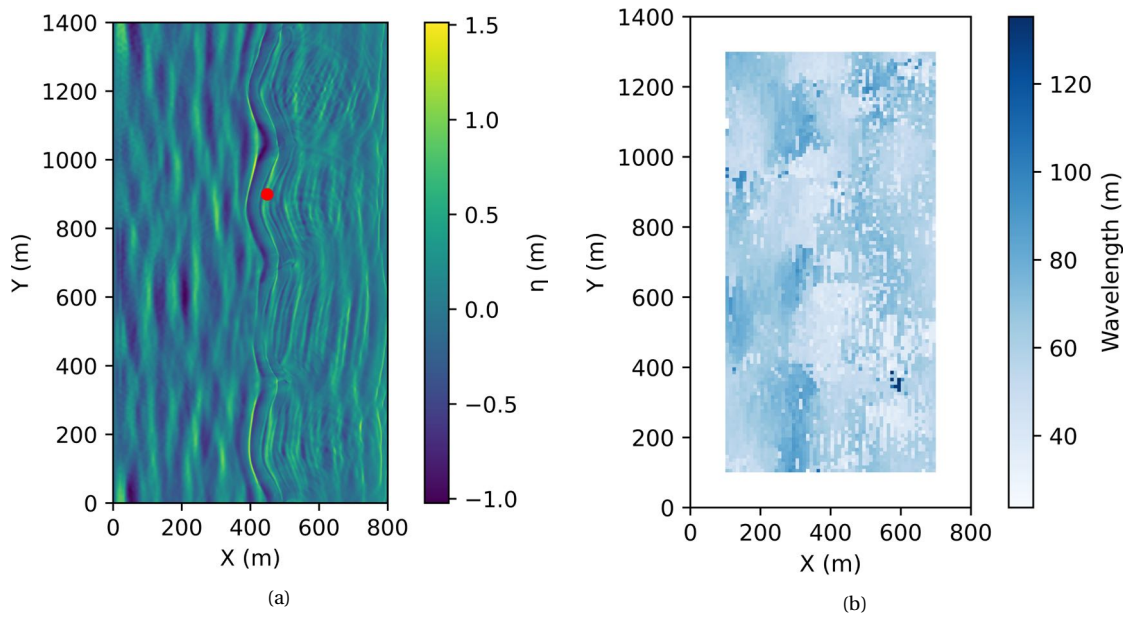


Figure 6.3: Wavelength estimations for the entire domain of the synthetic FUNWAVE dataset (b). In (a) an overview of the domain is provided. A domain radius of 100 m has been used.

A wavelength has been estimated for the same pixel as above: the red pixel in Figure 6.3a. Figure 6.4 shows the results for a domain radius of 100 m.

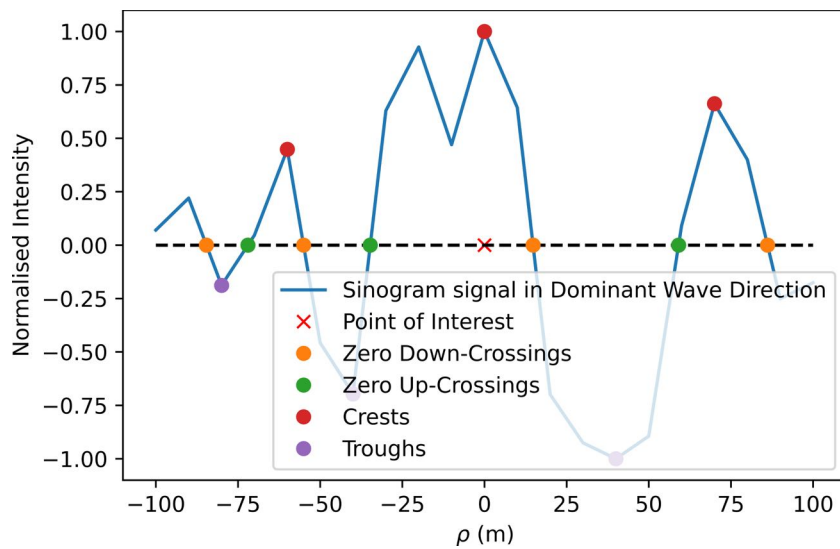


Figure 6.4: Wavelength estimation for pixel ($X = 450$ m, $Y = 900$ m) of the synthetic FUNWAVE dataset. A domain radius of 100 m has been used.

6.1.3. CELERITY ESTIMATIONS

Celerity estimations have been performed for every pixel of the entire synthetic FUNWAVE domain. It is provided in Figure 6.5.

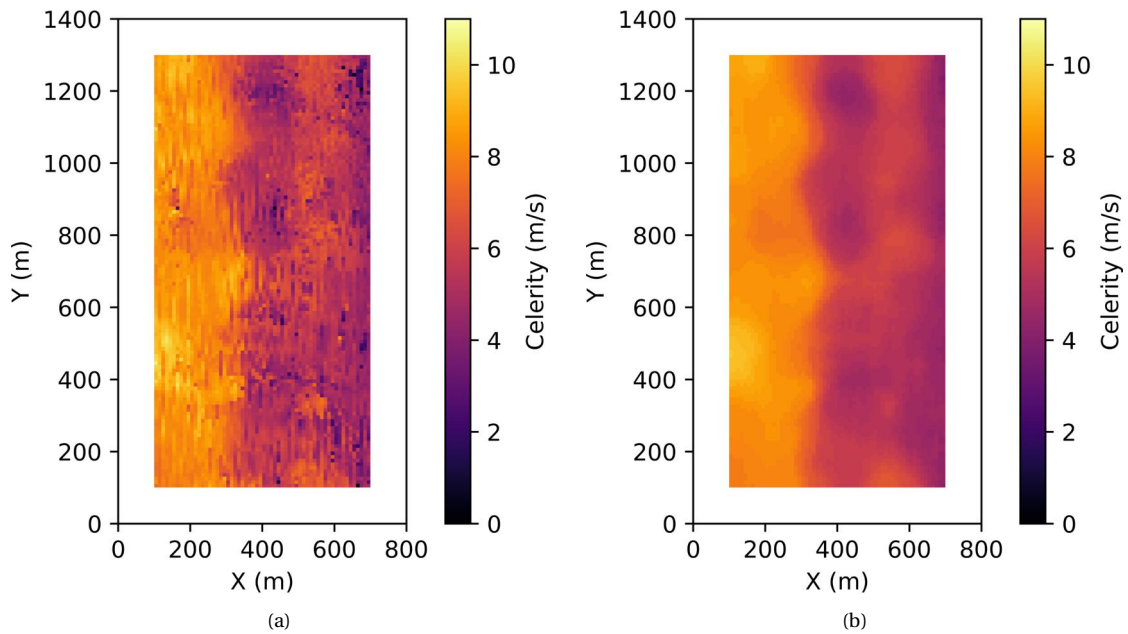


Figure 6.5: Celerity estimations for the entire domain of the synthetic FUNWAVE dataset. In (a) an overview of the celerity field without median filtering is provided. The domain in (b) shows the field with median filtering, the size of the applied median filter is 100 m. A domain radius of 100 m has been used.

A celerity has been estimated for the red pixel in Figure 6.5a. A domain radius of 100 m has been used. It is provided in Figure 6.6.

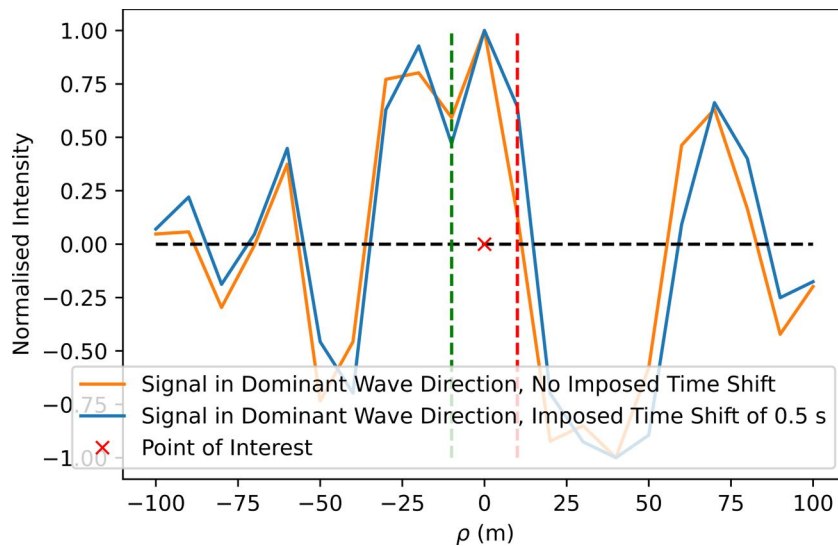


Figure 6.6: Celerity estimation for pixel ($X = 450$ m, $Y = 900$ m) of the synthetic FUNWAVE dataset. A domain radius of 100 m has been used.

6.1.4. WAVE SPECTRA

Wave spectra have been obtained from the video that is constructed based on the synthetic FUNWAVE dataset. The 2D variance-density spectrum and the frequency-direction spectrum are presented in Figure 6.7. The size of the applied median filter is 100 m.

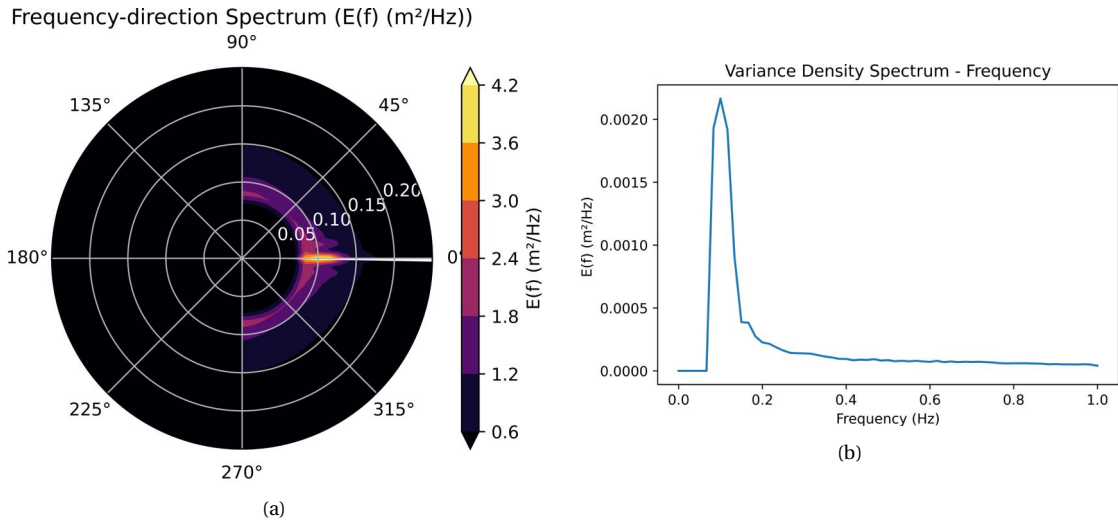


Figure 6.7: Frequency-direction spectrum (a) and 2D variance-density spectrum (b). Both have been obtained from the constructed video that is related to the synthetic FUNWAVE dataset. The size of the applied median filter is 100 m.

6.1.5. VIDEO DURATION

Figure 6.8 shows two snapshots of the constructed video that is related to the synthetic FUNWAVE dataset. The first snapshot is of $t = -30$ s while the second snapshot is of $t = 29.5$ s. In both figures waves are visible: the duration of the video is at least one minute. The size of the applied median filter is 100 m.

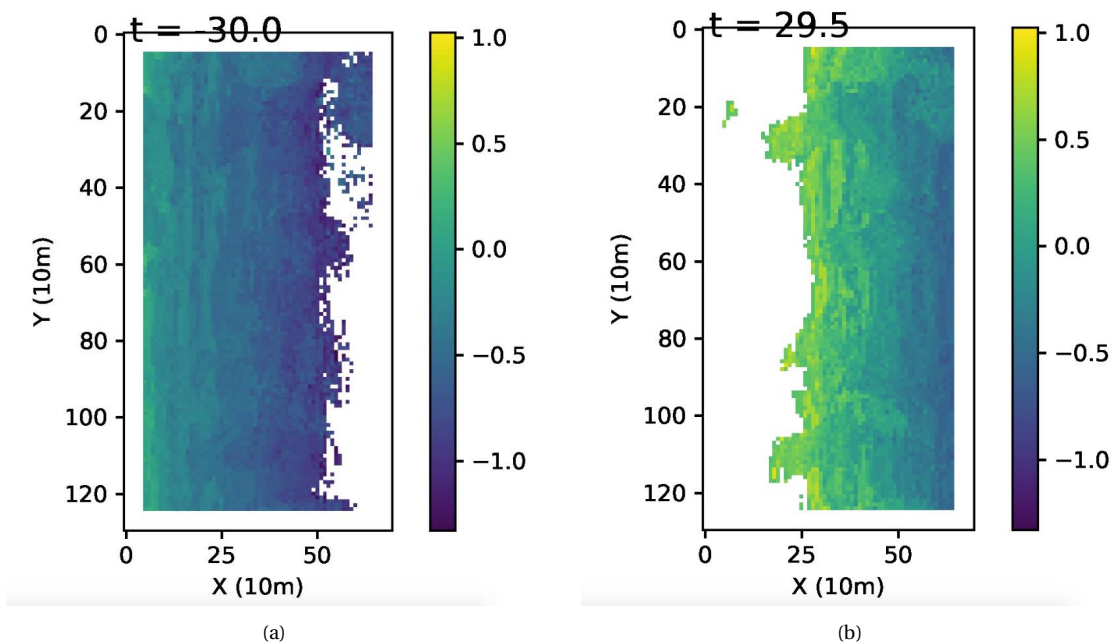


Figure 6.8: Snapshots of the constructed video that relates to the synthetic FUNWAVE dataset. (a) Is the snapshot at $t = -30$ s and (b) is the snapshot at $t = 29.5$ s.

6.1.6. BATHYMETRY ESTIMATIONS

A bathymetry has been derived from the constructed video related to the synthetic FUNWAVE dataset. Two methods have been applied to obtain a bathymetry estimation. In Figure 6.9b, the DMD-based DIA [82] has been used to estimate a depth profile. The third figure, Figure 6.9c shows the obtained bathymetry when the linear dispersion relation is used pixel-wise. The ground truth, including arhythmic sandbar, is shown in Figure 6.9a. The size of the applied median filter is 100 m in both bathymetry estimations.

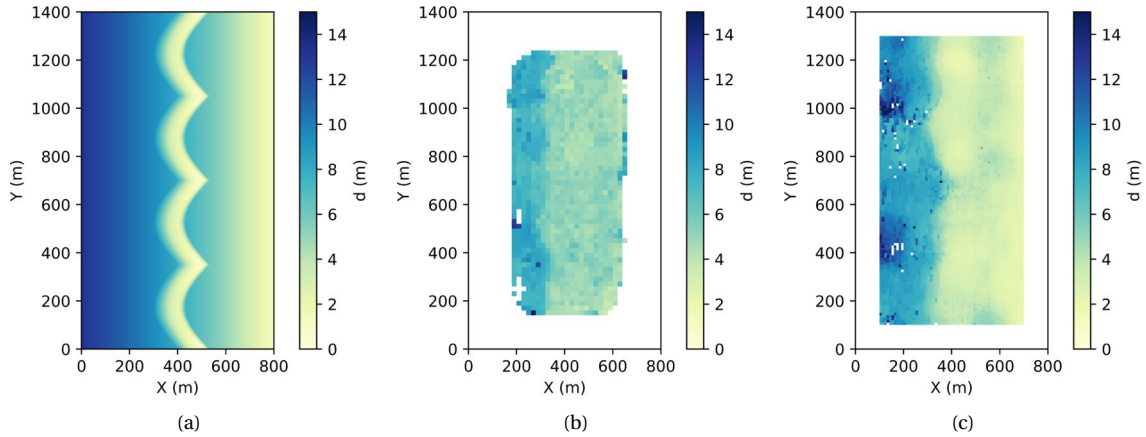


Figure 6.9: Bathymetry estimation for the domain of the synthetic FUNWAVE dataset. In (a), the ground-truth input bathymetry of the FUNWAVE simulation is shown. (b) Presents the bathymetry estimation obtained by a DMD-based DIA, while (c) shows the bathymetry estimation based on explicitly solving the linear dispersion relation. The size of the median filter is 100 m.

Figure 6.10a shows the difference between the DMD-based DIA bathymetry estimation and the ground truth. In Figure 6.10b a similar figure is presented related to the difference between the bathymetry estimation based on pixel-wise solving the linear dispersion relation and the ground-truth. The DMD-based DIA bathymetry estimation shows a correlation of 0.218 between the estimated and ground-truth bathymetry. This corresponds to a RMSE of 6.44 m over the entire domain. The estimation based on a plain, explicit solution of the dispersion relation presents a correlation of 0.221. The RMSE of this estimation is 6.80 m over the entire domain.

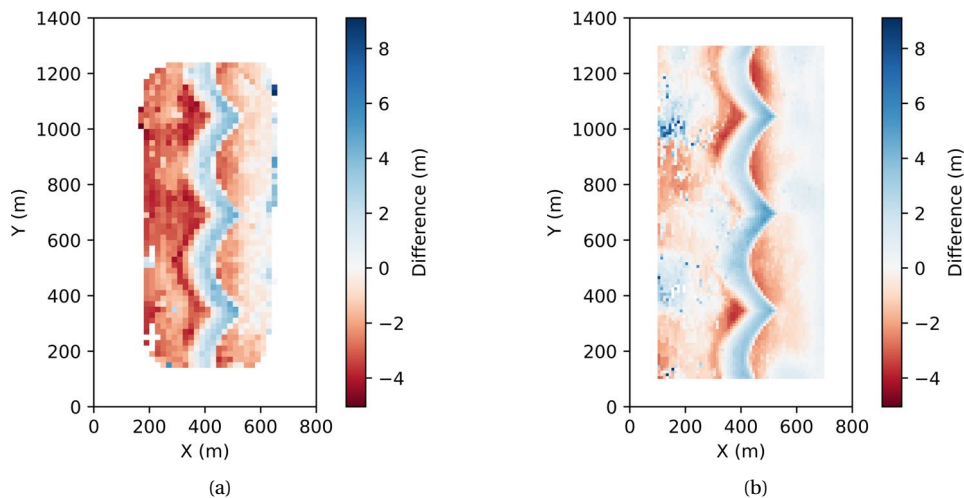


Figure 6.10: Comparison of a bathymetry estimated by a DMD-based DIA and the FUNWAVE ground-truth (a), as well as a comparison between bathymetry estimated by explicitly solving the linear dispersion relation and the ground-truth (b). The difference in both figures is calculated as: 'bathymetry estimation' - 'ground-truth'.

6.2. RESULTS: SENTINEL-2 IMAGERY IN SAINT-LOUIS

The results related to the application of the model to Sentinel-2 imagery in Saint-Louis are presented analogously to those in Section 6.1. The results regard the site of Saint-Louis at 04/03/2019. The applied (Fourier and median) filter range is provided where necessary.

6.2.1. WAVE DIRECTION ESTIMATIONS

The dominant wave direction has been estimated pixel-wise using a domain radius of 450 m. An overview is provided in Figure 6.11b. A narrow 2D Fourier filter ranging from $T = 7$ s to $T = 15$ s for offshore wave conditions has been applied upfront. A raw Sentinel-2 image is provided in Figure 6.11a.

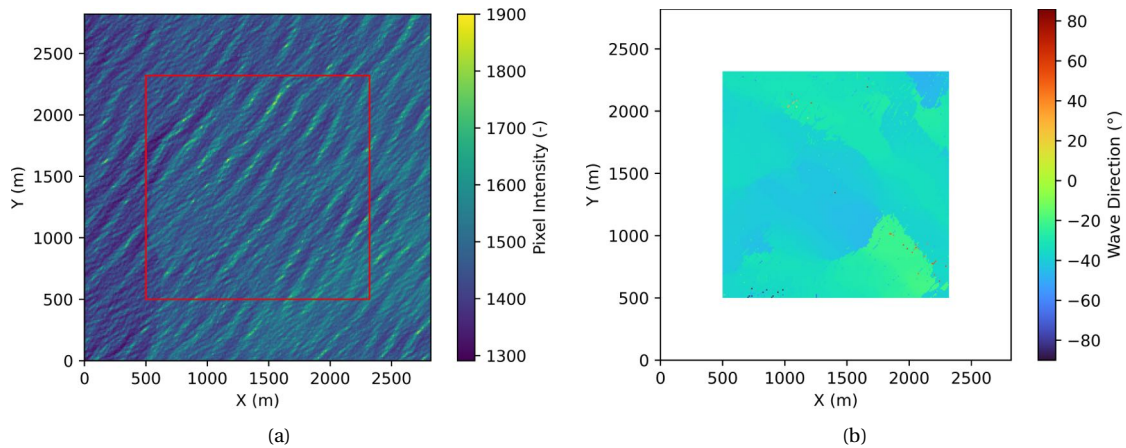


Figure 6.11: Estimations of wave direction applied to the domain of the research site off the coast of Saint-Louis (b). A 2D Fourier filter ranging from $T = 7$ s to $T = 15$ s for offshore wave conditions has been applied upfront. (a) Shows the raw Sentinel-2 image. The red square corresponds to the domain in which the directions are estimated.

6.2.2. WAVELENGTH ESTIMATIONS

The wavelength has been estimated pixel-wise using a domain radius of 450 m. An overview is provided in Figure 6.12b. A narrow 2D Fourier filter ranging from $T = 7$ s to $T = 15$ s for offshore wave conditions has been applied upfront.

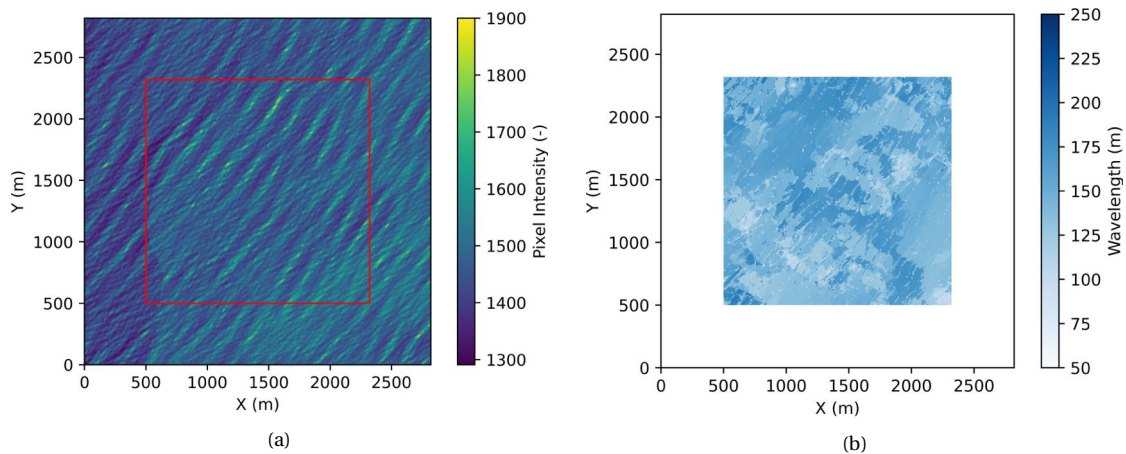


Figure 6.12: Estimations of wavelength applied to the domain of the research site off the coast of Saint-Louis (b). A 2D Fourier filter ranging from $T = 7$ s to $T = 15$ s for offshore wave conditions has been applied upfront. (a) Shows the raw Sentinel-2 image. The red square corresponds to the domain in which the wavelengths are estimated.

6.2.3. WAVE CELERITY ESTIMATIONS

Figures 6.13a and 6.13b show the pixel-wise celerity estimations for the domain of Saint-Louis. In Figure 6.13a a narrow 2D Fourier filtering is applied: $T = 7$ s to $T = 15$ s for offshore wave conditions. In Figures 6.13b a median filter has been applied afterwards to the celerity domain. The median filter has a size of 500 m.

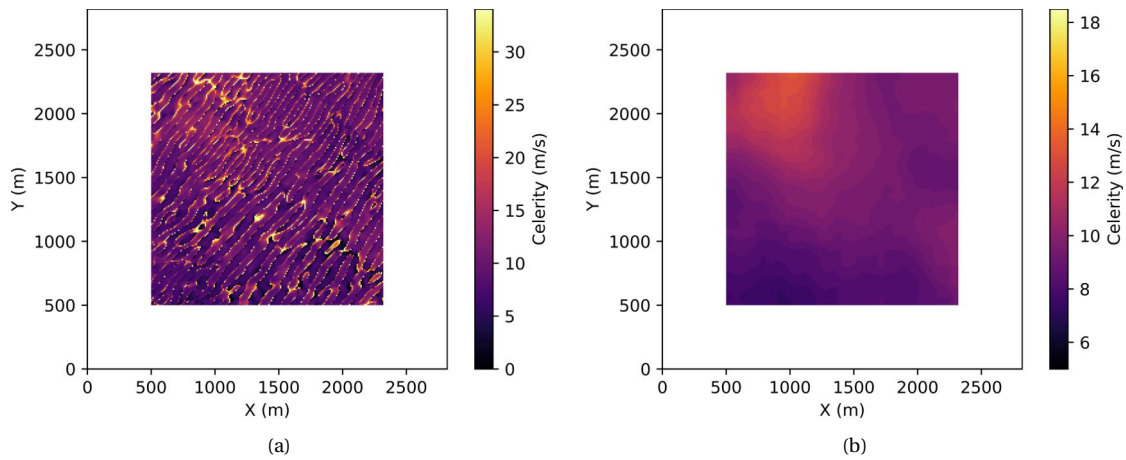


Figure 6.13: Celerity estimations for the domain of Saint-Louis. A narrow 2D Fourier filter has been applied to (a): $T = 7$ s to $T = 15$ s. In (b) a median filter has subsequently been added to the domain of (a). The size of the median filter is 500 m. Note that the colourbars do not match by purpose, otherwise characteristic variability would disappear.

6.2.4. WAVE SPECTRA

In Figure 6.14 a 2D variance-density spectrum and a frequency-direction spectrum obtained from the video related to the Sentinel-2 imagery in Saint-Louis are shown. Both spectra relate to a video that has been constructed using a narrow 2D Fourier filter: $T = 7$ s to $T = 15$ s. The median filter that has been applied to the video has a size of 500 m.

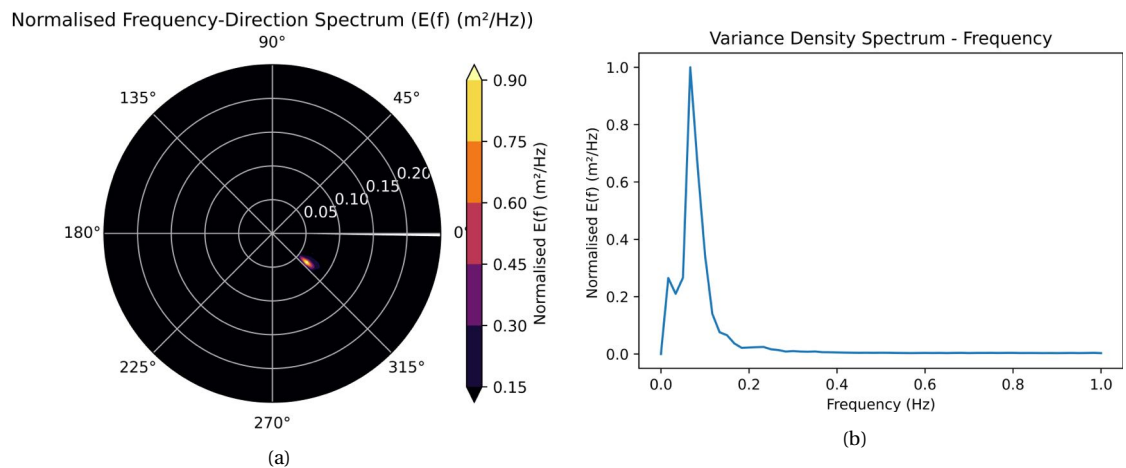


Figure 6.14: Frequency-direction spectrum (a) and 2D variance-density spectrum (b) corresponding to the video that represents wave propagation in the domain of Saint-Louis. A narrow 2D Fourier filter has been applied: $T = 7$ s to $T = 15$ s. A median filter of size 500 m is used.

6.2.5. VIDEO DURATION

Figure 6.15 shows two snapshots of the constructed video that is related to the Sentinel-2 imagery in Saint-Louis. The first snapshot is of $t = -30$ s while the second snapshot is of $t = 29.5$ s. In both figures waves are visible: the duration of the video is at least one minute. The applied 2D Fourier filter ranges from $T = 7$ s to $T = 15$ s, the median filter has a size of 500 m.

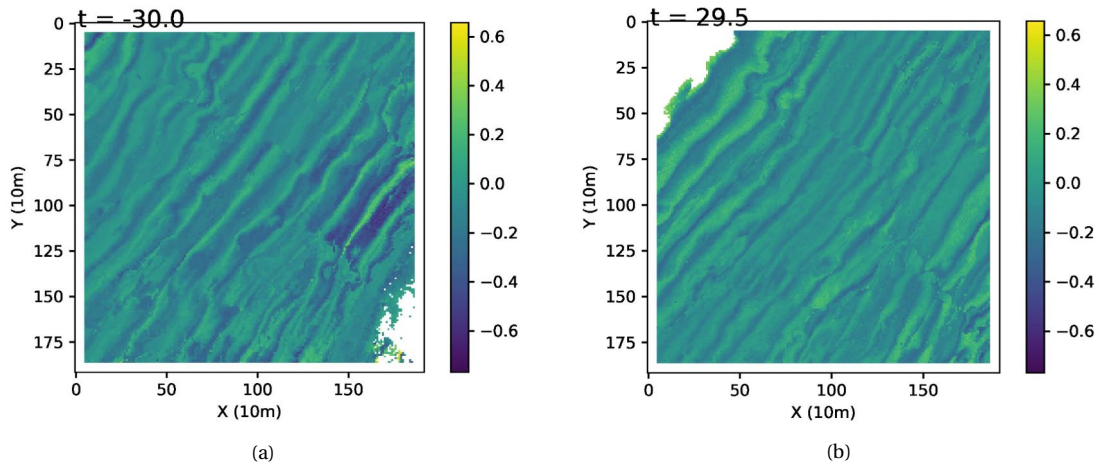


Figure 6.15: Snapshots of the constructed video that relates to the Sentinel-2 imagery in Saint-Louis. (a) Is the snapshot at $t = -30$ s and (b) is the snapshot at $t = 29.5$ s.

6.2.6. BATHYMETRY ESTIMATIONS

Figure 6.16a presents the EMODnet ground-truth bathymetry for Saint-Louis. The red square indicates the area of which the bathymetry is estimated. In Figure 6.16b a bathymetry estimation for the same location has been performed using a filtered signal. The 2D Fourier filter ranges from $T = 7$ s to $T = 15$ s. A median filter of size 500 m has been applied. The bathymetry has been estimated using a DMD-based DIA. Figure 6.16c provides a bathymetry estimation that has exploited a pixel-wise solving of the linear dispersion relation. The same filtering ranges have been applied. Table 6.2 provides the correlation coefficients and root-mean-square errors that correspond to the estimation.

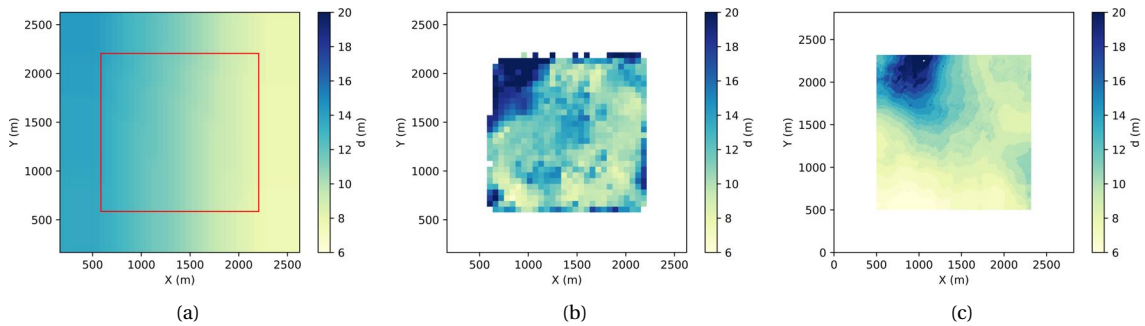


Figure 6.16: EMODnet ground-truth bathymetry (a) and a bathymetry estimations in Saint-Louis (b,c). (b) Represents a bathymetry estimation using a DMD-based DIA, (c) shows the bathymetry estimation when a pixel-wise solving of the linear dispersion relation is exploited. In (b) and (c) a 2D Fourier filter ranging from $T = 7$ s to $T = 15$ s and median filter of 500 m have been applied.

Table 6.2: Overview of Pearson correlation coefficients (ρ) and RMSE between estimated bathymetry and ground-truth in Saint-Louis.

Filtering	ρ	RMSE
Fourier: $T = 2$ s to $T = 25$ s, Median: 50 m	0.070	8.87 m

6.3. RESULTS: SENTINEL-2 IMAGERY IN CAPBRETON

The results related to the application of the model to Sentinel-2 imagery in Capbreton are presented analogously to those in Section 6.1 and Section 6.2. The results refer to the site of Capbreton at 30/03/2018. The applied (Fourier and median) filter range is provided where necessary.

6.3.1. WAVE DIRECTION ESTIMATIONS

The dominant wave direction has been estimated pixel-wise using a domain radius of 450 m. An overview is provided in Figure 6.17b. A narrow 2D Fourier filter ranging from $T = 6$ s to $T = 15$ s for offshore wave conditions has been applied upfront. A raw Sentinel-2 image is provided in Figure 6.17a.

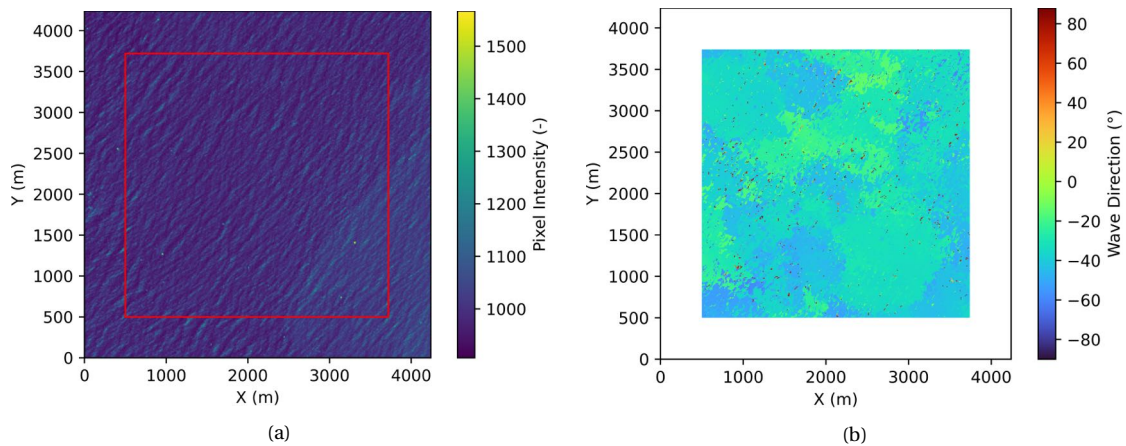


Figure 6.17: Estimations of wave direction applied to the domain of the research site off the coast of Capbreton (b). A 2D Fourier filter ranging from $T = 6$ s to $T = 15$ s for offshore wave conditions has been applied upfront. (a) Shows the raw Sentinel-2 image. The red square corresponds to the domain in which the directions are estimated.

6.3.2. WAVELENGTH ESTIMATIONS

The wavelength has been estimated pixel-wise using a domain radius of 450 m. An overview is provided in Figure 6.18b. A narrow 2D Fourier filter ranging from $T = 6$ s to $T = 15$ s for offshore wave conditions has been applied upfront.

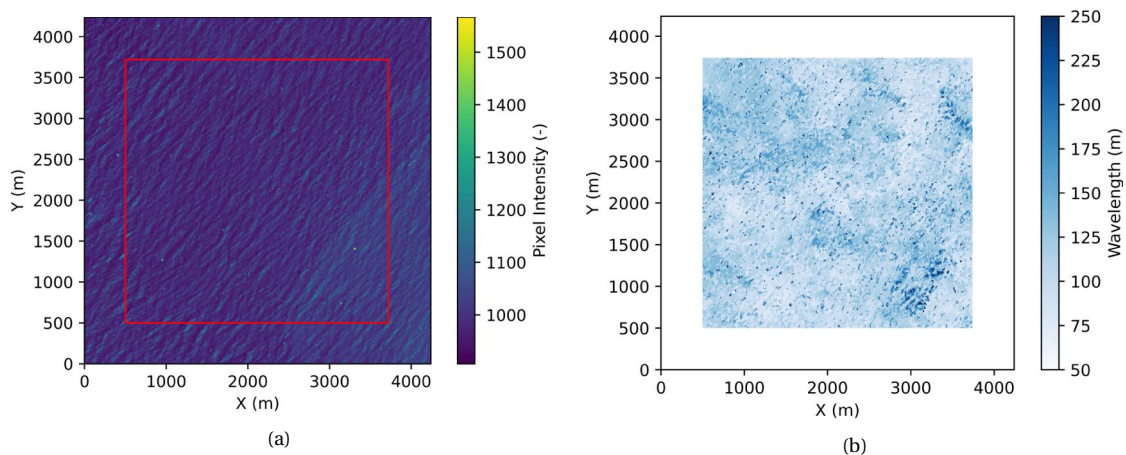


Figure 6.18: Estimations of wavelength applied to the domain of the research site off the coast of Capbreton (b). A 2D Fourier filter ranging from $T = 6$ s to $T = 15$ s for offshore wave conditions has been applied upfront. (a) Shows the raw Sentinel-2 image. The red square corresponds to the domain in which the directions are estimated.

6.3.3. WAVE CELERITY ESTIMATIONS

Figures 6.19a and 6.19b show the pixel-wise celerity estimations for the domain of Capbreton. In Figure 6.19a a narrow 2D Fourier filtering is applied: $T = 6$ s to $T = 15$ s for offshore wave conditions. In Figures 6.19b a median filter has been applied afterwards to the celerity domain. The median filter has a size of 100 m.

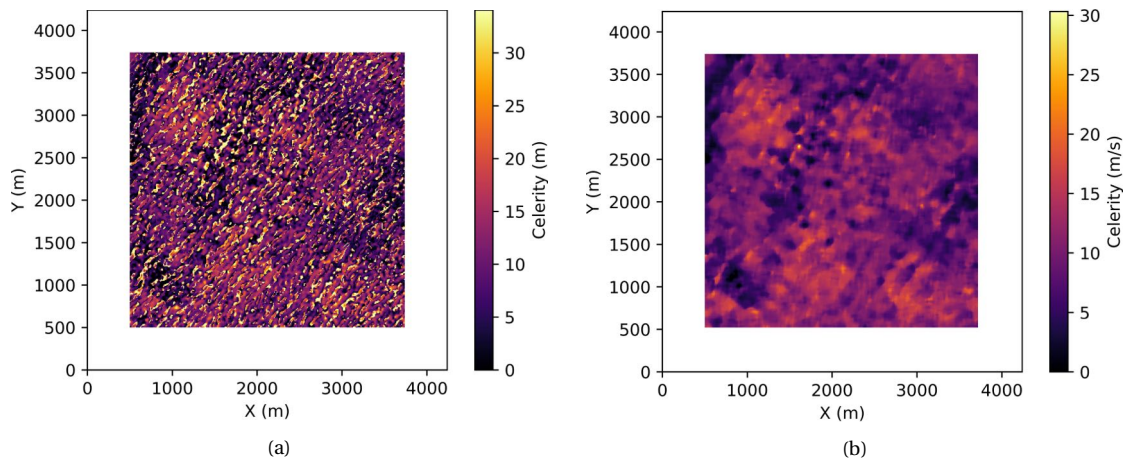


Figure 6.19: Celerity estimations for the domain of Capbreton. A narrow 2D Fourier filter has been applied to (a): $T = 6$ s to $T = 15$ s. In (b) a median filter has subsequently been added to the domain of (a). The size of the median filter is 100 m. Note that the colourbars do not match by purpose, otherwise characteristic variability would disappear.

6.3.4. WAVE SPECTRA

In Figure 6.20 a 2D variance-density spectrum and a frequency-direction spectrum obtained from the video that is related to the Sentinel-2 imagery in Capbreton is shown. The figure relates to a video that has been constructed using a narrow 2D Fourier filter: $T = 6$ s to $T = 15$ s. The median filter that has been applied to the video has a size of 100 m.

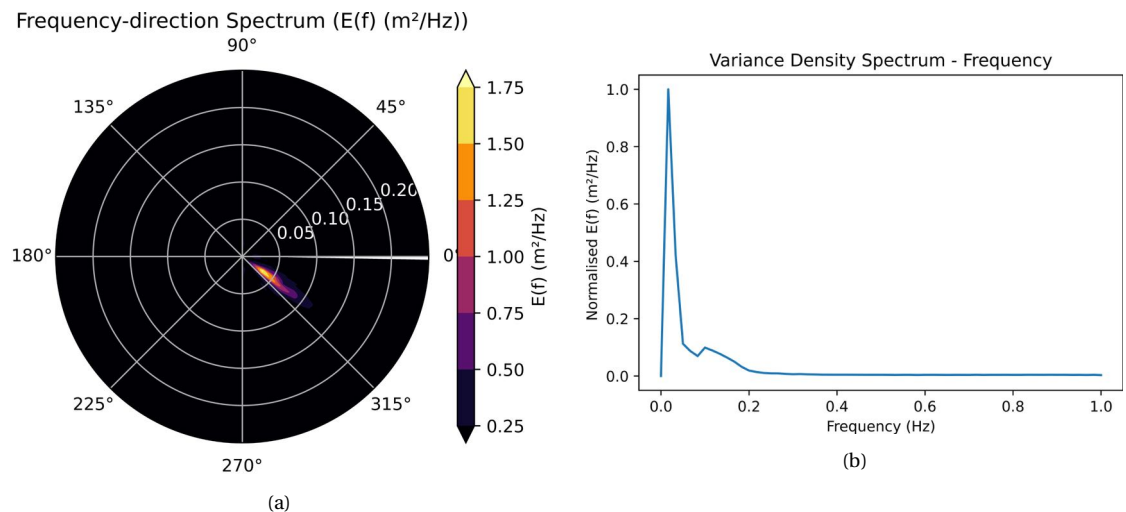


Figure 6.20: Frequency-direction spectrum (a) and variance-density spectrum (b) corresponding to the video that represents wave propagation in the domain of Capbreton. Narrow 2D Fourier filter has been applied: $T = 6$ s to $T = 15$ s. The median filter has a size of 100 m.

6.3.5. VIDEO DURATION

Figure 6.21 shows two snapshots of the constructed video that is related to the Sentinel-2 imagery in Capbreton. The first snapshot is of $t = -10$ s while the second snapshot is of $t = 12$ s. In both figures waves are visible: the duration of the wave-representing video is 22 s. The waves disappear outside this range. The applied 2D Fourier filter ranges from $T = 6$ s to $T = 15$ s, the median filter has a size of 100 m.

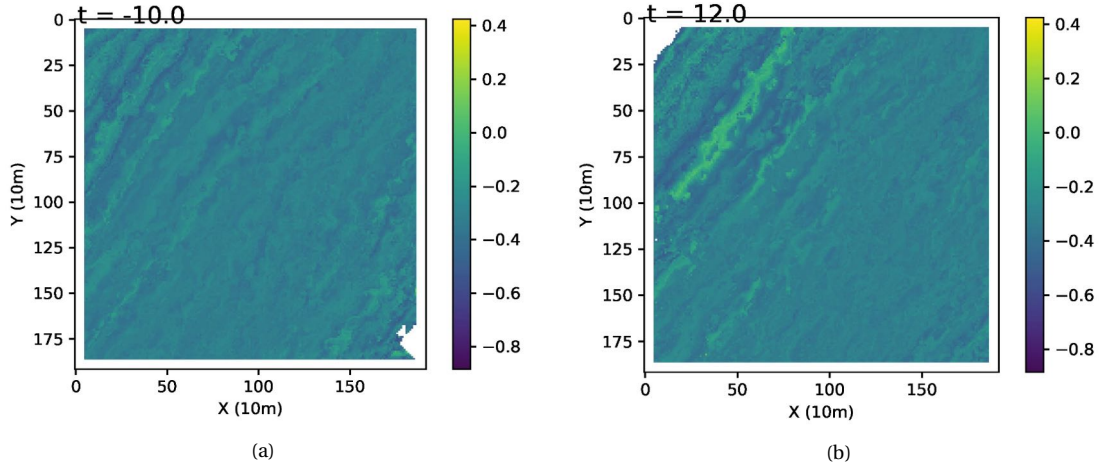


Figure 6.21: Snapshots of the constructed video that relates to the Sentinel-2 imagery Cepbreton. (a) Is the snapshot at $t = -10$ s and (b) is the snapshot at $t = 12$ s.

6.3.6. BATHYMETRY ESTIMATIONS

Figure 6.22a presents the EMODnet ground-truth bathymetry for Capbreton. The red square indicates the area of which the bathymetry is estimated. In Figures 6.22b and 6.22c a bathymetry estimation for the same location is performed using a signal that is filtered upfront by a narrow 2D Fourier filter: $T = 6$ s to $T = 15$ s. The result is also filtered afterwards using a median filter of size 100 m. Table 6.3 provides the correlations and root-mean-square errors that correspond to the estimations.

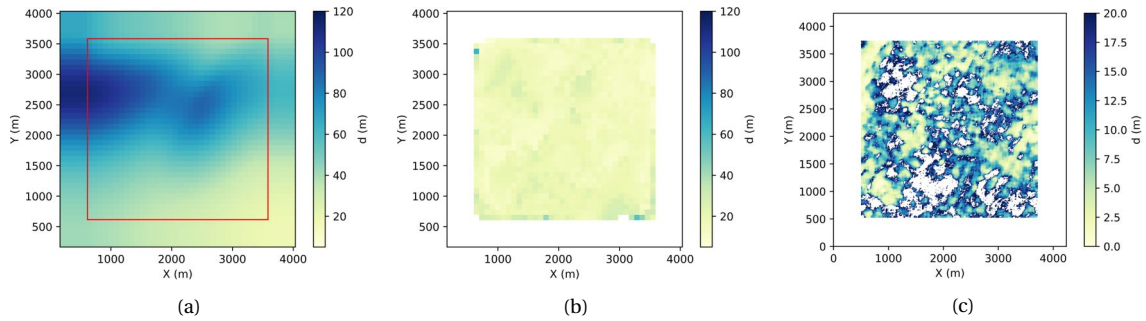


Figure 6.22: EMODnet ground-truth bathymetry (a) and a bathymetry estimation in Capbreton. 2D Fourier filter: $T = 6$ s to $T = 15$ s, median filter: 100 m. (b) Shows the bathymetry estimation that is produced using a DMD-based DIA, in (c) the bathymetry is estimated by pixel-wise solving of the linear dispersion relation.

Table 6.3: Overview of pearson correlation coefficients (ρ) and RMSE between estimated bathymetry and ground-truth in Capbreton.

Filtering	ρ	RMSE
Fourier: $T = 6$ s to $T = 15$ s, Median: 50 m	0.068	54.05 m

6.4. INTERPRETATION OF DATASET ANALYSIS

The most important observations to make in the presented results are provided below. These observations are based on the model requirements and research (sub-)objectives.

6.4.1. INTERPRETATION OF SYNTHETIC FUNWAVE DATASET ANALYSIS

Figure 6.1 The dominant wave direction estimations correspond to the observed refraction patterns in the raw imagery. A domain radius of 100 m leads to sufficient similarity.

Figure 6.2 The cross-correlation image visually represents the raw imagery. A domain radius of 100 m leads to a wave direction estimation that corresponds to the raw imagery in Figure 6.1.

Figures 6.3 and 6.4 The estimated wavelengths (domain radius 100 m) range between 30 m and 130 m, which corresponds to the raw imagery.

Figures 6.5 and 6.6 The estimated celerity (domain radius 100 m) shows a decreasing gradient towards the shore, together with a sudden decrease at the input sandbar (middle of the domain). Both observations correspond with the expectations since celerity is expected to decrease for smaller depths. (b) Shows that a small median filter (100 m) removes the wavy variability of (a). Furthermore, both figures slightly resemble the pattern of the arrhythmic input sandbar.

Figure 6.7 The wave spectra corresponding to the video show a peak at circa 0 degrees and at circa 0.1 Hz. The spectra are compared to the input wave statistics in Chapter 7.

Figure 6.8 Both snapshots of the resulting video show wave propagation - a wavy pattern is visible. This means the video is able to represent wave propagation for at least one minute.

Figures 6.9 and 6.10 Both bathymetry estimations show a decreasing gradient towards the shore. This gradient is similar to the input bathymetry. The typical bathymetric features of the arrhythmic sandbar have mostly disappeared. The corresponding value of ρ is relatively low, while the RMSE is relatively high.

6.4.2. INTERPRETATION OF SENTINEL-2 IMAGERY ANALYSIS IN SAINT-LOUIS

Figure 6.11 The estimated wave direction (domain radius 450 m) resembles the wave propagation in the raw imagery.

Figure 6.12 The wavelength estimations are in the range of 150 m to 200 m. This resembles the wavelengths as observed in the raw imagery.

Figure 6.13 The celerity field without median filtering shows wavy variations. The estimated celerity varies between realistic and unrealistic values. When the field is median filtered (size 500 m), the wavy variations disappear.

Figure 6.14 The wave spectra corresponding to the video show a peak at circa 315 or -45 degrees and at circa 0.1 Hz. The spectra are compared to the in-situ measurements in Chapter 7.

Figure 6.15 Both snapshots of the resulting video show wave propagation - a wavy pattern is visible. That means the video is able to represent wave propagation for at least one minute.

Figure 6.16 Both bathymetry estimations show a recognisable gradient, although it is not similar to the input bathymetry. The corresponding value of ρ is relatively low, while the RMSE is relatively high.

6.4.3. INTERPRETATION OF SENTINEL-2 IMAGERY ANALYSIS IN CAPBRETON

Figure 6.17 The estimated wave direction (domain radius 450 m) resembles the wave propagation in the raw imagery. The field is messier than the field in Saint-Louis, which corresponds to the more short-crested waves.

Figure 6.18 The wavelength estimations are in the range of 50 m to 100 m. This resembles the wavelengths as observed in the raw imagery. The waves are shorter than those in Saint-Louis, which corresponds to the expectations.

Figure 6.19 The celerity field without median filtering shows wavy variations. The estimated celerity varies between realistic and unrealistic values. When the field is median filtered using a median filter of 100 m, the wavy variations slightly disappear, although they are still recognisable.

Figure 6.20 The wave spectra corresponding to the video show a peak at circa 315 or -45 degrees and at circa 0.025 Hz.

Figure 6.21 Both snapshots of the resulting video show wave propagation - a wavy pattern is visible. However, the snapshots are at -10 s and + 12 s. That means the video is not able to represent wave propagation for at least one minute.

Figure 6.22 Both bathymetry estimations do not show a recognisable gradient. The corresponding value of ρ is relatively low, while the RMSE is relatively high.

III

REFLECTION

7

DISCUSSION

The results of this work are discussed and put in perspective. First, the main results in relation to the research objective are elaborated upon in Section 7.1. Section 7.2 thereafter provides the most important delimitations and assumptions. These form the boundaries of the work. In Section 7.3 a retrospection to the thesis is provided, followed by a specific discussion of the added value of the work in Section 7.4.

7.1. INTERPRETATION OF RESULTS

The structure as provided by the research objective and corresponding model requirements is roughly followed to give an interpretation of the results. The research objective has been stated as:

The explicit aim of this research is to construct a one-minute video from a short burst of Sentinel-2 imagery (2.586 s), a video that accurately represents the propagation of waves. In addition, the potential of the video to estimate wave-derived nearshore bathymetry is shown. A DMD-based DIA is exploited for that purpose. The video is constructed by developing a spatio-temporal cross-correlation model.

The four sub-objectives that together define the research objective are presented in Chapter 1. The research objective has led to three model requirements which indicate the most important demands of the developed model.

- Requirement 1: An accurate representation of wave propagation in the constructed video;
- Requirement 2: A one minute duration of wave visibility in the constructed video;
- Requirement 3: An accurate bathymetry estimation as consequence of the constructed video.

7.1.1. WAVE PROPAGATION IN THE CONSTRUCTED VIDEOS

Waves are observed for at least one minute in the FUNWAVE-related video construction (Figure 6.8). The corresponding wave spectra also show good alignment with the input wave characteristics (Figure 6.7). The peak of the obtained wave spectrum is found at 0.1 Hz while the dominant wave direction appears at 0 degrees. Both values correspond to the input values being $T_p = 10 \text{ s} = 1/f$ and $\text{Dir} = 15 \text{ degrees}$. These results indicate a proper representation of average wave propagation in the constructed video.

The results related to the Sentinel-2 imagery in Saint-Louis provide for similar observations. It appears to be possible to construct a video that shows wave propagation for at least a minute (Figure 6.15). A comparison between the in-situ measured 2D variance-density spectrum in Saint-Louis and the video-obtained spectrum reveals that the video on average represents wave propagation quite well (Figure 7.1). The video that results from the analysis in Capbreton shows less satisfactory results (Figure 6.21). The total duration of wave visibility in this video is 22 s. There is no wave spectrum available to compare the results in Capbreton.

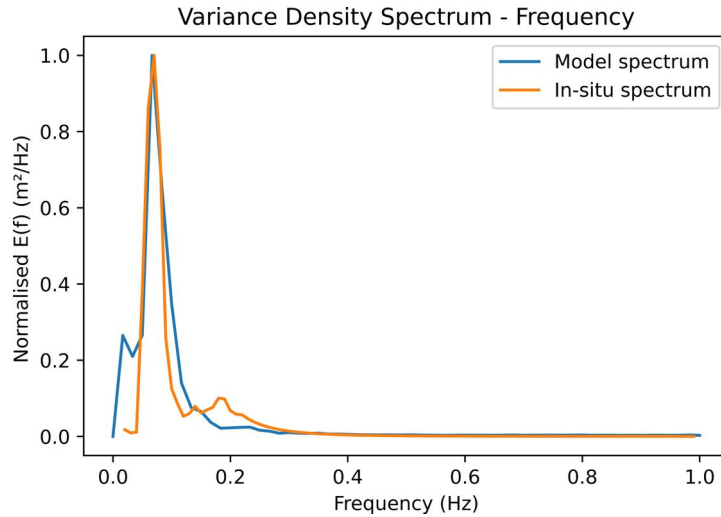


Figure 7.1: Comparison of in-situ measured and video-obtained 2D variance-density spectrum in Saint-Louis.

7.1.2. BATHYMETRY ESTIMATIONS

The bathymetry estimations corresponding to the synthetic FUNWAVE dataset, as well as to both research sites of the Sentinel-2 imagery, show (almost) no quantitative correlation with the ground-truth. The obtained RMSE's are significant compared to other literature (e.g. Almar *et al.* [64]). A visual inspection of the results related to the synthetic FUNWAVE dataset leads to more insights. The existing gradient in the bathymetry - from offshore to onshore - is recognisable in the estimated bathymetries (Figures 6.9b and 6.9c). This trend is also observed in Figure 7.2, which shows a cross-section of the ground-truth FUNWAVE bathymetry and corresponding estimated bathymetries. The bathymetries estimated by the DMD-based DIA as well as by pixel-wise solving the linear dispersion relationship¹ are included. Pixel-wise solving of the linear dispersion relationship generally shows an underestimation of the existing bathymetry while a correct linear trend towards the shore is apparent. This result is also visible in Figure 6.10b. The DMD-based DIA bathymetry estimation performs worse: the linear trend is barely recognisable. Furthermore, it is interesting to observe a slightly wavy pattern in the bathymetry estimation following from pixel-wise solving of the linear dispersion relationship. The particular bathymetry (orange line) follows the structure of the sandbar as well.

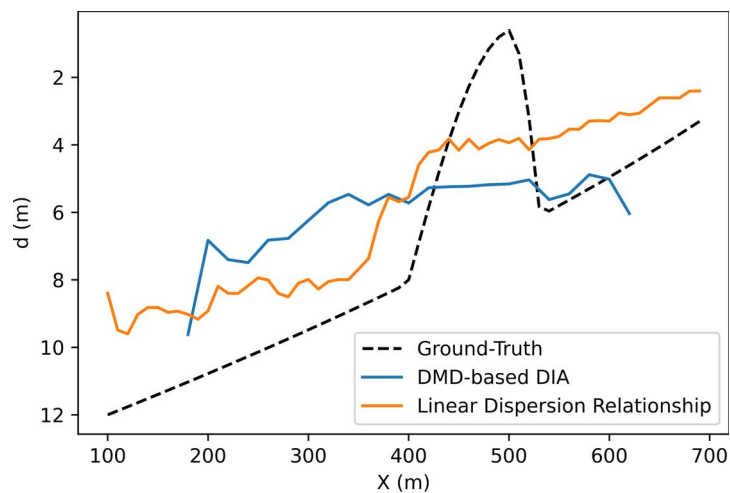


Figure 7.2: Cross-section of ground-truth bathymetry and estimated bathymetries related to the synthetic FUNWAVE dataset. The cross-section is at $Y = 700$ m.

¹By 'pixel-wise solving of the linear dispersion relationship' the benchmark method introduced in Chapter 4 is meant. In this method wave characteristics are directly converted to depth, avoiding the use of a video.

The bathymetry estimations in Saint-Louis provide for other observations (Figure 6.16). Both estimations show a gradient from the upper left part of the image to the lower right. This gradient does not correspond to the gradient in the ground-truth, which is fully orientated from left to right. The case in Capbreton (Figure 6.22) does not show any visible correspondence between the ground-truth and estimated bathymetries. Based on the above observations some initial conclusions are made. These conclusions are used as a starting point to analyse the performance of the model in more detail.

There is a distinct difference in performance between the video constructions and the bathymetry estimations. The videos generally represent average wave propagation in good order, while the bathymetry estimations are less accurate. The video constructions related to the synthetic FUNWAVE dataset and the Sentinel-2 imagery in Saint-Louis show correct wave propagation for sufficient duration. The video construction in Capbreton shows waves for less temporal range. Regarding bathymetry, a correct linear trend is observed in the estimations related to the FUNWAVE dataset, although the model underestimates the local depth. An interesting gradient is visible in the bathymetry estimations related to Saint-Louis. The bathymetry estimations in Capbreton do not show any correspondence with the ground-truth.

7.1.3. ESTIMATION OF WAVE CHARACTERISTICS IN THE FUNWAVE DOMAIN

An accurate bathymetry estimation or correct wave-representing video is largely determined by the estimation of wave characteristics. It is therefore interesting to evaluate the accuracy of the model's three different wave characteristics estimations in the FUNWAVE domain.

DOMINANT WAVE DIRECTION ESTIMATIONS IN THE FUNWAVE DOMAIN

The dominant wave direction is estimated first in the model, hence the accuracy of the other wave characteristics depends on it: the isolated wave signal in the dominant wave direction is used pixel-wise for the estimation of wavelength and wave celerity. The dominant wave direction estimations have appeared to be stable and to be of good quality in the case of the FUNWAVE domain: for instance, the estimations follow the expected refraction patterns around the sandbar (Figure 6.1b). It is noted that a proper choice of domain radius is essential for accurate estimations. As is shown in Figure 7.3 a small domain radius results in the loss of detail and thereby the loss of wave visibility, while a large domain radius results in accounting for waves that are too far away from the pixel of interest. A domain radius in the order one wavelength has appeared to be the most robust for the purpose of dominant wave direction estimation.

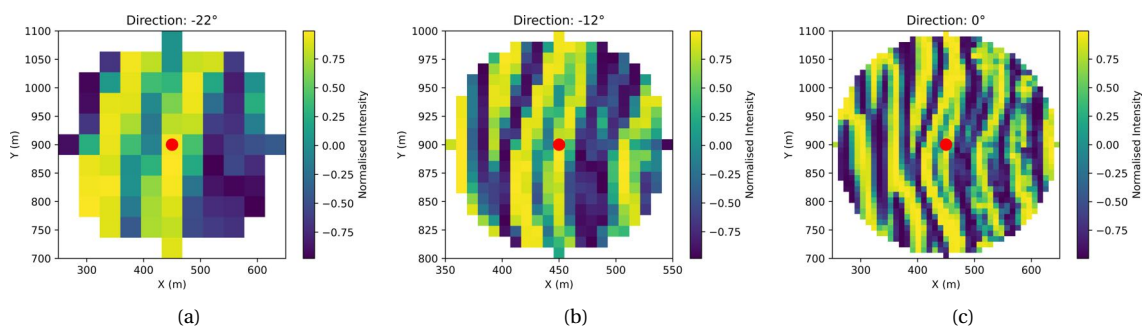


Figure 7.3: Cross-correlation images corresponding to a wave direction estimation for pixel ($X = 450$ m, $Y = 900$ m) of the synthetic FUNWAVE dataset (Figure 6.1a). In (a) a domain radius of 50 m has been applied, in (b) a domain radius of 100 m and in (c) a domain radius of 200 m.

DISCREPANCY BETWEEN WAVELENGTH AND CELERITY ESTIMATIONS FOR LARGER DEPTHS

In Figure 7.4 wavelength and celerity estimations are presented for the same cross-section of the synthetic FUNWAVE domain. In Figure 7.4a the orange line represents the wavelength estimation as performed by the model. The black dashed line indicates the wavelength as a result of solving the linear dispersion relationship, in which the ground truth bathymetry and the estimated celerity

act as input values. The opposite holds true for Figure 7.4b: the blue line represents the celerity estimation of the model, while the black dashed line shows the celerity as a result of the linear dispersion relationship, in which the ground-truth bathymetry and the wavelength estimation act as input values. It is observed that the coloured and black dashed lines in both figures are relatively close to each other in the nearshore areas ($X = 650\text{m}$ to $X = 800\text{ m}$), while they deviate in larger depths. This indicates a discrepancy between the estimated wavelengths and estimated celerities in larger depths, which is probably induced by either an error in wavelength estimations, an error in celerity estimations or an error in both.

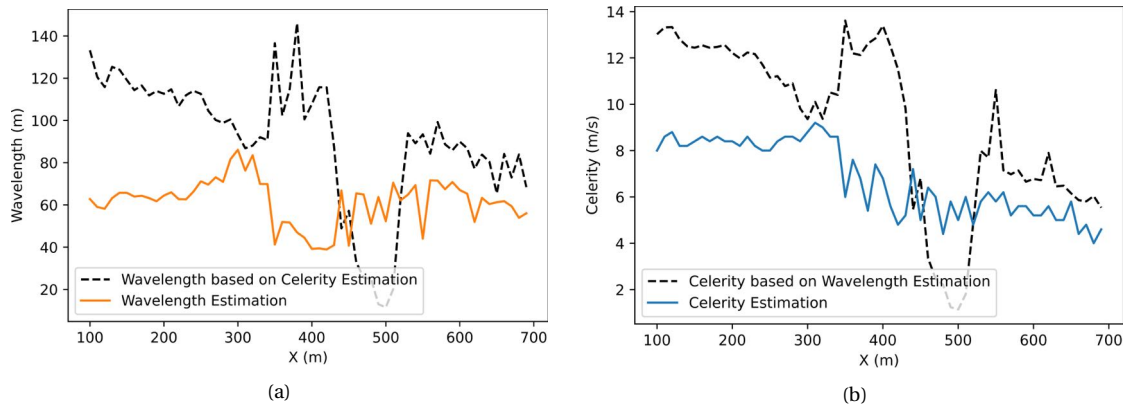


Figure 7.4: Cross-sections of the synthetic FUNWAVE domain at $Y = 700\text{ m}$, presenting celerity and wavelength estimations. (a) represents the wavelength estimation, while (b) shows the celerity estimation.

The observed discrepancy between wavelength estimations and celerity estimations for larger depths in the FUNWAVE domain is explained by the analyses in Figure 7.5. This figure provides an overview of the theoretical application range of the developed model.

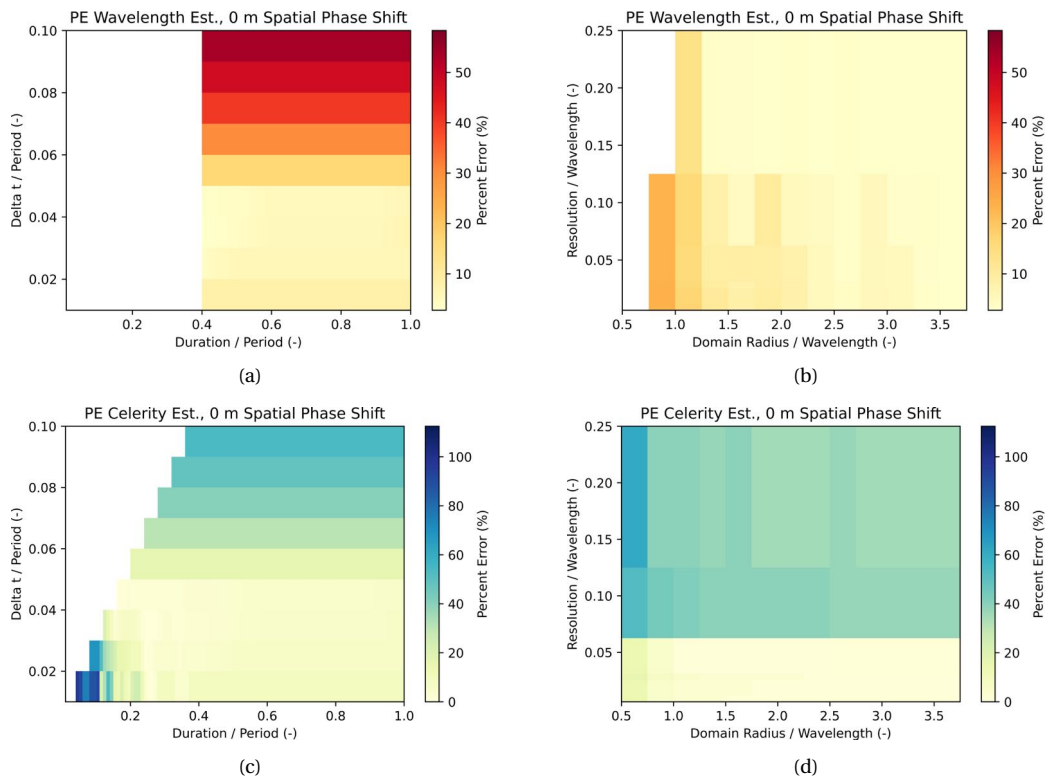


Figure 7.5: Theoretical application range of the model. (a) and (b) show the temporal and spatial wavelength estimation errors. (c) and (d) represent the temporal and spatial celerity estimation errors. All for 0 m spatial wave phase shift.

THEORETICAL APPLICATION RANGE

The results in Figure 7.5 represent the theoretical application range of the model. In Figure 7.5a, the theoretical Percent Error (PE) related to the estimation of wavelength as performed by the model is presented for combinations of two temporal dimensionless values: "Time Lag / Wave Period" ($\Delta t/T$) and "Burst Duration / Wave Period" (Dur/T). On the other hand, Figure 7.5b shows the theoretical PE in relation to two spatial dimensionless values: "Spatial Resolution / Wavelength" (Res/L) and "Domain Radius / Wavelength" ($Radius/L$). Figures 7.5c and 7.5d analogously provide similar results regarding the theoretical celerity estimation errors. The theoretical application range of the model is defined by applying the model to a set of synthetic sinusoidal waves. The figures as provided show the PE for 0 m spatial wave phase shift. Please see Appendix C for an extensive explanation of these analyses.

ACCURACY OF WAVELENGTH ESTIMATIONS IN THE FUNWAVE DOMAIN

The typical wave period in the FUNWAVE analysis is $T_p = 10$ s. The wavelength related to this peak wave period and the largest depth in the domain ($d = 13$ m), calculated by using the linear dispersion relationship, is circa 100 m. Knowing the utilised domain radius of 100 m, the dimensionless value $Radius/L$ is circa 1 for the most offshore waves in the FUNWAVE domain. On the other hand, the dimensionless value Res/L is circa 0.1 for the same waves. Note that $Res = 10$ m. The corresponding PE is indicated by the black marker in Figure 7.6b. Both dimensionless values increase towards the shore because wavelengths typically decrease towards lower depths [65]. The black dashed square in Figure 7.6b indicates the area for $L < 50$ m in relation to the characteristics of the synthetic FUNWAVE dataset. The results show that the estimations of the most offshore wavelengths in the FUNWAVE domain correspond to the lower left of the figure and thus to relatively high percent errors. Estimations at the onshore side correspond to the relatively upper right of the figure since wavelengths have decreased. The percent errors therefore also decrease towards the shore². Furthermore, the wave period is also influencing the wavelength estimations in the FUNWAVE domain. The obtained PE for a Δt of 0.5 s and a burst duration of 4.5 s is represented by the black marker in Figure 7.6a. However, the typical wave period does not decrease towards the shore: the PE related to the wave period is constant over the domain. It is therefore concluded that the overall wavelength estimation error decreases towards lower depths, as a result of decreasing wavelengths.

The wavelength estimation errors in the FUNWAVE domain decrease for lower wavelengths and therefore towards lower depths. The wave period does not influence the error decrease.

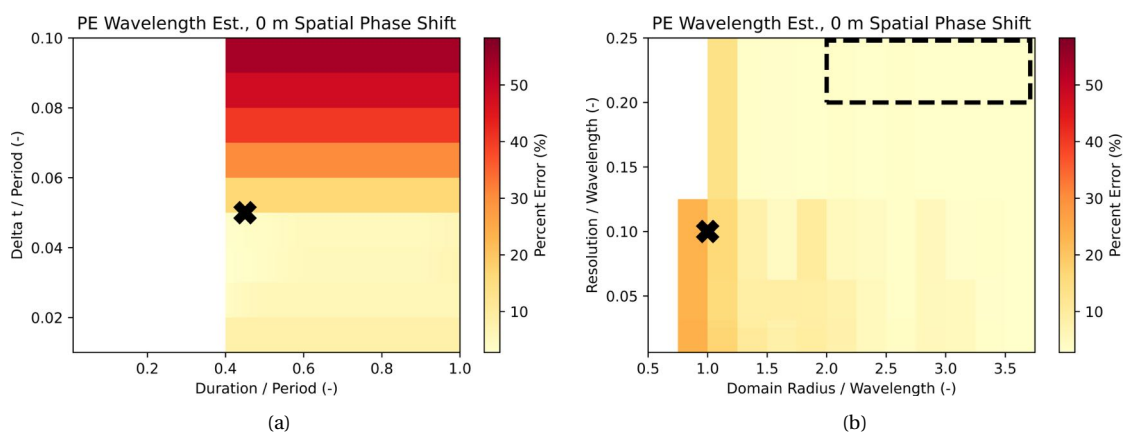


Figure 7.6: Theoretical application range of the model in relation to the estimation of wavelength. (a) Shows the temporal analysis, while (b) presents the spatial analysis. The black marker in (a) represents the PE for typical FUNWAVE characteristics and a wave period of $T_p = 10$ s. In (b), again for typical FUNWAVE characteristics, the black marker represents the PE for the most offshore wavelength, while the black dashed square shows the error for $L < 50$ m.

²There is of course a limit to these decreasing errors when shallow water depths are reached.

ACCURACY OF CELERITY ESTIMATIONS IN THE FUNWAVE DOMAIN

The celerity estimations in the FUNWAVE domain show a different pattern. Figure 7.7b indicates large errors for a typical value of $Res/L = 0.1$ at the offshore side of the FUNWAVE domain in relation to the characteristics of the synthetic FUNWAVE dataset: Radius = 100 m and Res 10 m. The corresponding PE is represented by the black marker. These errors increase or decrease for decreasing wavelength, depending of the pixel position with respect to the wave phase (see Appendix C). In Figure 7.7b, for instance, the results for 0 m spatial shift are provided. The black dashed square again indicates the area for $L < 50$ m in relation to typical FUNWAVE characteristics.

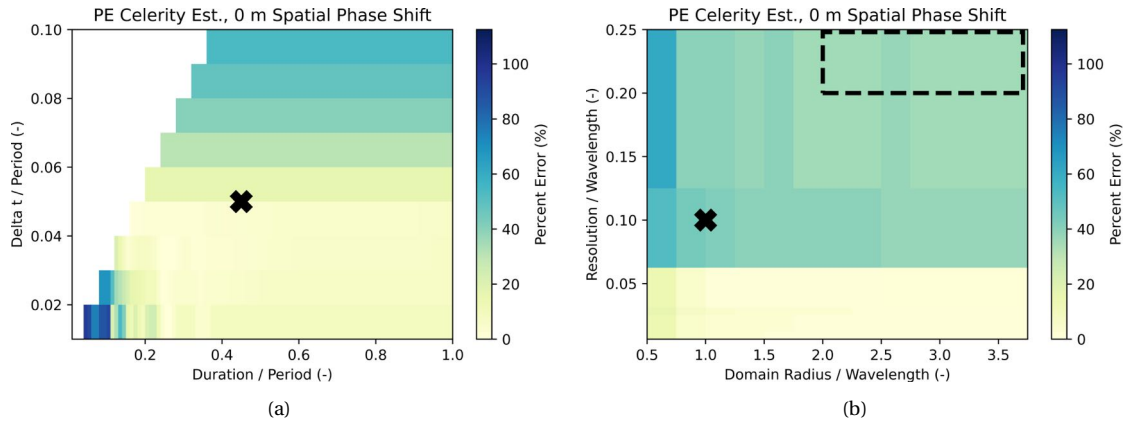


Figure 7.7: Theoretical application range of the model in relation to the estimation of celerity. (a) Shows the temporal analysis, while (b) presents the spatial analysis. The black marker in (a) represents the PE for typical FUNWAVE characteristics and a wave period of $T_p = 10$ s. In (b), again for typical FUNWAVE characteristics, the black marker represents the PE for the most offshore wavelength, while the black dashed square shows the error for $L < 50$ m.

Figure 7.8 shows the average celerity estimation errors for a range of wavelengths, averaged over the different pixel positions with respect to the wave phase. The domain radius and spatial resolution are kept constant: Radius = 100 m and Res = 10 m. It is observed that on average the absolute celerity estimation errors increase for decreasing wavelengths. Furthermore, a clear underestimation of celerities is observed for wavelength ranges corresponding to the FUNWAVE domain.

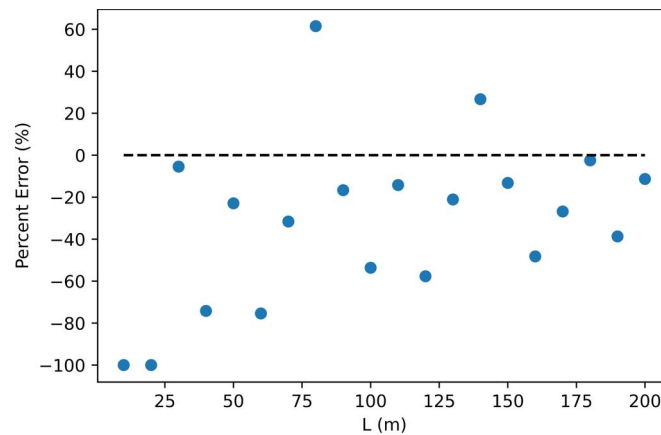


Figure 7.8: Celerity estimation errors for varying wavelength. The domain radius and spatial resolution are as used in the FUNWAVE analysis: 100 m and 10 m, respectively.

The wave period appears to be less relevant for the same reasons as above. The corresponding PE for $T_p = 10$ s, a Δt of 0.5 s and a burst duration of 4.5 s is indicated by the black marker in Figure 7.7a.

The celerity estimation errors in the FUNWAVE domain increase for decreasing wavelengths and therefore towards lower depths. The wave period does not influence the error increase.

CELERITY ESTIMATION ERRORS DOMINATE WAVELENGTH ESTIMATION ERRORS

The celerity estimation errors seem to be dominating the wavelength estimation errors with respect to the bathymetry estimation in the FUNWAVE domain. This is because the celerity estimation error mostly increases towards the shore, while the error in wavelength estimation decreases. Furthermore, typical celerity estimation errors are several factors larger than typical wavelength estimation errors, for example see Figures 7.6 and 7.7. Figure 7.8 also provides for an explanation of the underestimation of bathymetry in the FUNWAVE domain (Figure 7.2): following the linear dispersion relationship, an underestimation of celerity leads to an underestimation of depth, especially since the error in celerity is dominating the error in wavelength. The following is therefore concluded:

The celerity estimation errors appear to be a dominant influencing factor for the accuracy of bathymetry estimation and act as the main explanation for the underestimation of depth in the FUNWAVE domain. The celerity estimation errors are sensitive to the present wave characteristics while the Percent Errors are relatively large.

An explanation of the most probable reasoning behind the observed errors is provided later on. First, the results related to the Sentinel-2 imagery are discussed.

7.1.4. ESTIMATION OF WAVE CHARACTERISTICS IN SENTINEL-2 IMAGERY

The observations in the FUNWAVE domain are translated to the analysis of Sentinel-2 imagery. There is no ground to doubt the accuracy of the estimations of dominant wave direction. Figures 6.11b and 6.17b show results that seem reasonable. The results related to wavelength estimations are satisfactory as well (Figures 6.12b and 6.18b). This is supported by the observations in Figure 7.9, the theoretical application range of the model. Typical wavelengths at both research sites range from 100 m to 300 m, meaning that as long as the domain radius is large enough - larger than 1.5 times the wavelength - the results are expected to be accurate. This is the case if a domain radius of 450 m is used. The corresponding area is indicated by the black square in Figure 7.9b. The temporal analysis shows similar results. Assuming a wave period of at least 5 s, in relation to a Δt of 0.29... s and a burst duration of 2.055 s - both after pre-processing, no significant error is expected. The corresponding PE is indicated in Figure 7.9a.

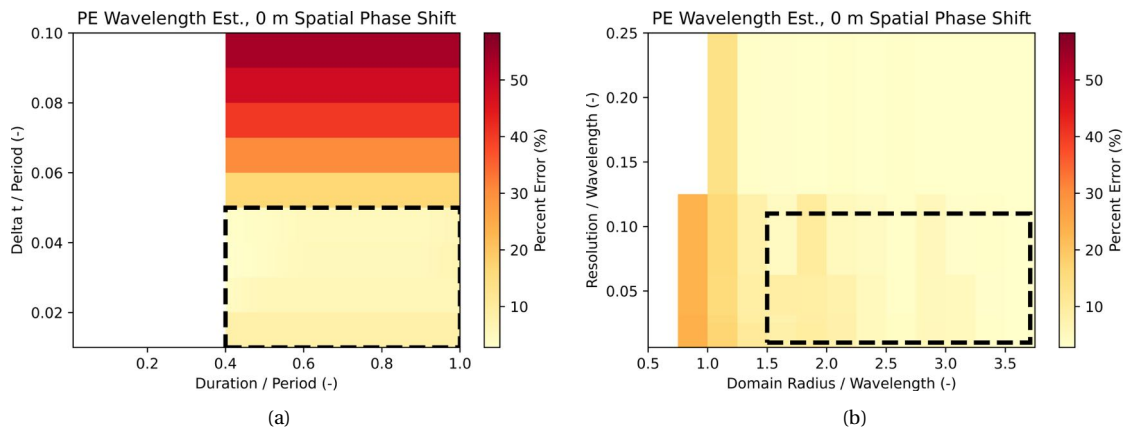


Figure 7.9: Theoretical application range of the model in relation to the estimation of wavelength for Sentinel-2 Imagery. (a) Shows the temporal analysis, while (b) presents the spatial analysis. The black dashed squares indicate the expected errors for present wave characteristics and typical characteristics of Sentinel-2 imagery.

ACCURACY OF CELERITY ESTIMATIONS IN THE SENTINEL-2 IMAGERY

The celerity estimations again tell a different story. Starting from the results in Figure 7.5 it is clear that the celerity estimation error is strongly influenced by the present wave characteristics. The Δt of Sentinel-2 imagery after pre-processing is 0.29... s, while the burst duration is 2.055 s. The area that corresponds with the typical Sentinel-2 characteristics and a wave period ranging from 5 s to 25 s is projected by the black dashed square in Figure 7.10a. The dimensionless value of Dur / T shows

that the Percent Errors generally become larger than 10% for wave periods larger than circa 8 s: left of the orange dashed line. On the other hand, the Percent Errors also become larger than 10% for wave periods smaller than 5 s when the value of $\Delta t/T$ is analysed. The area above the red dashed line indicates this area. These observations mainly show that analysing Sentinel-2 imagery using the spatio-temporal cross-correlation model is on the edge of possibilities due to the characteristics of the Sentinel-2 constellation: a short burst of temporal information combined with a relatively small amount of snapshots.

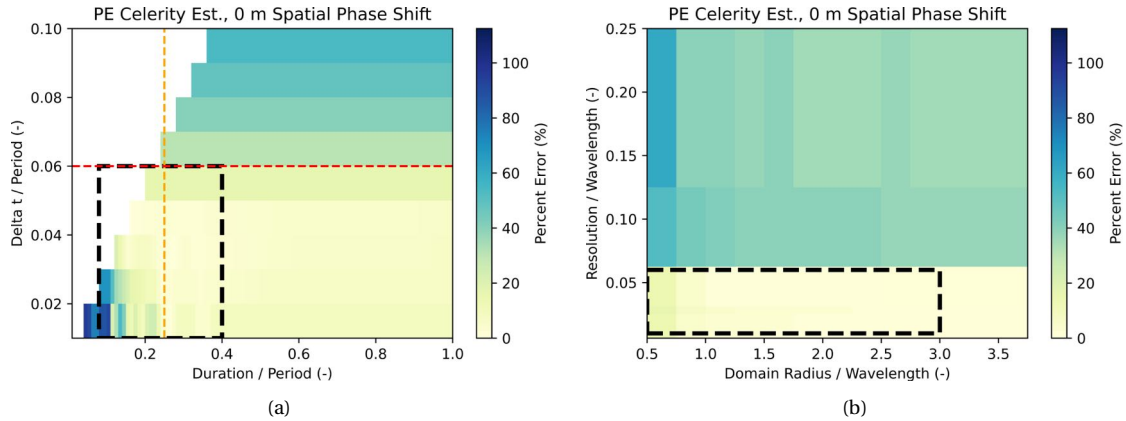


Figure 7.10: Theoretical application range of the model in relation to the estimation of celerity for Sentinel-2 Imagery. (a) Shows the temporal analysis while (b) shows the spatial analysis. In (a) the black dashed square indicates the expected errors for present wave characteristics and typical characteristics of Sentinel-2 imagery. The orange dashed line represents wave periods of 8 s, while the red dashed line represents wave periods of 5 s. In (b) the black dashed square represents wavelengths of at least 150 m. Both figures are in relation to Sentinel-2 imagery characteristics.

The celerity estimations in Saint-Louis and Capbreton show a clear difference. The estimations in Saint-Louis (Figure 6.13a) present a rather smooth celerity field, while the field in Capbreton is a lot messier (Figure 6.19a). An explanation is found in the theoretical application range in spatial sense. As Figure 7.10b shows, the error in estimated celerities is relatively low as long as the wavelength is larger than 150 m, taking into account a spatial resolution of 10 m. Both research sites are characterised by a different wave climate: typically the waves in Saint-Louis are longer and more long-crested than those in Capbreton [5, 64]. This result is also observed in Figures 6.12b and 6.18b. This difference in wave climate declares the difference in celerity estimations; due to shorter and short-crested waves, the waves in Capbreton are a lot harder to accurately analyse. The related Percent Errors in Capbreton are probably found above the black dashed square in Figure 7.10b.

The temporal application framework shows that estimating celerity from Sentinel-2 imagery by using the developed spatio-temporal cross-correlation model is at the edge of possibilities. For almost all wave periods, a significant error is expected. The difference between the rather smooth celerity field in Saint-Louis and the messy celerity field in Capbreton is explained by the difference in present wavelengths in relation to the spatial theoretical application range.

INFLUENCE OF WAVE PHASE TO THE CELERITY ESTIMATIONS

The celerity estimations in Saint-Louis show another interesting feature. As could be observed in Figure 6.13a, the estimations follow a wavy pattern: there is a clear correlation between remarkably high celerity estimations and the wave forms in raw satellite imagery (Figure 6.11a). These variations are probably explained by the way in which the celerity estimation protocol is defined.

The model estimates celerity by searching for maximum cross-correlation values in surrounding pixels: the locations that show maximum correlation with a shifted time series are the pixels to which the wave propagates. Dividing the obtained spatial shift by the imposed temporal shift leads to a celerity estimation. This celerity estimation protocol is sensitive for cross-correlation errors, especially for longer wave periods. When wave periods increase, the part of the wave that is observed

during a certain range of time - the burst duration - decreases. For increasing wave periods, eventually the observed part of the wave per pixel becomes rather small. This leads to the phenomenon that observed wave parts become similar to other observed wave parts, although both wave parts are in reality not the same.

For example, for shorter wave periods a cross-correlation of a time series that represents the part of the wave between the backface and the crest will show maximum correlations with time series that represent the same part: between backface and crest. That means the wave has propagated towards the location with maximum correlation during the imposed time shift. When wave periods increase, the part of the wave between backface and crest becomes similar to the part of the wave between trough and backface. When a cross-correlation is applied for the particular time series, there is a possibility that maximum correlation is obtained between the two different wave parts: the part between the backface and crest and the part between the trough and backface. This leads to an error in the estimation of the spatial shift; it is not the particular wave propagation that is observed, but the wave propagation plus, or minus a quarter of a wavelength. This ultimately leads to errors in the celerity estimations. The same principle is observed for cross-correlations between the parts of the wave between the crest and frontface and between the frontface and trough.

It is interesting to observe the different behaviour in the estimated celerity fields of the FUNWAVE domain, the domain in Saint-Louis and the domain in Capbreton. The field in Saint-Louis clearly shows the wavy pattern as explained above. A similar structure is recognised in the celerity field corresponding to the FUNWAVE domain, although less persistent. This is probably due to lower wave periods. The domain in Capbreton does not show a clear wavy pattern in the celerity field. That is because the error in these particular results is dominated by the short wavelength in combination with typical Sentinel-2 characteristics.

For longer wave periods the celerity estimation fields show variations following a wavy pattern, explained by cross-correlation errors that become more persistent when wave periods increase.

7.1.5. FILTERING

Two filtering methods have been applied in the model to reduce the obtained celerity estimation errors: 2D Fourier filtering and median filtering. The influence of both methods is discussed briefly.

2D FOURIER FILTERING

A 2D Fourier filtering has been applied upfront to the raw satellite imagery. The range of the filtering is such that it isolates the swell wave signal. The specific ranges have been determined empirically: $T = 7$ s to $T = 15$ s for the domain in Saint-Louis and $T = 6$ s to $T = 15$ s for the domain in Capbreton. Both filtering ranges correspond to offshore wave conditions. The result of the 2D Fourier filtering is significant: it improves the celerity field and the duration of the video. Figure 7.11 shows the celerity field in Saint-Louis, with and without 2D Fourier filtering. In both figures no median filter has been applied. As can be observed, the pixel-wise variations in Figure 7.11b are decreased compared to Figure 7.11a. This is explained by removing shorter wavelengths and wave periods of the spectrum, leading to the reduction of errors as shown in Figure 7.5. A smoother celerity field is favourable for the resulting duration of the video. It increases the wave visibility from 14 s to more than a minute in the case of Saint-Louis. A question that arises is whether the 2D Fourier filtering removes too much information from the wave signal, e.g. the DMD-based DIA solves the wave signal for multiple harmonics so a broad spectrum should be favourable. The constructed video certainly represents a more 'averaged' signal than without the 2D Fourier filtering. These effects are discussed later on.

2D FOURIER FILTERING BASED ON OFFSHORE WAVE PARAMETERS

A remark is made about the consequences that are induced by filtering based on offshore wave parameters. The wave periods and frequencies are actually filtered based on the filtering of wave numbers (k). Therefore, when regarding intermediate water depths, an error is induced to the range of

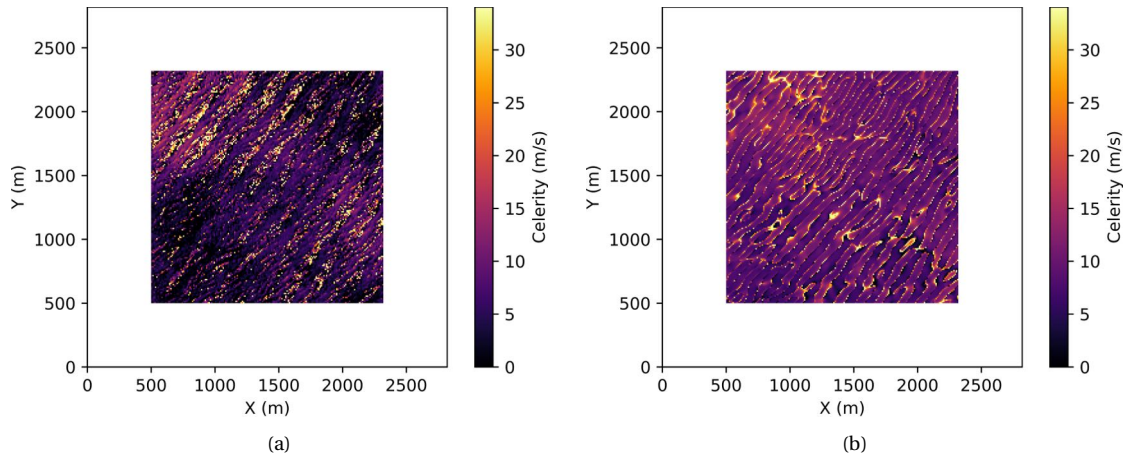


Figure 7.11: Celerity estimations for the domain of Saint-Louis. A narrow 2D Fourier filter has been applied to (b): $T = 7$ s to $T = 15$ s. In (a) no 2D Fourier filter has been applied. Both results are provided without a median filter.

wave periods that is filtered out. When waves enter intermediate water, their wavelengths decrease. As a result, when a certain wave number in intermediate water is related to a wave period using the offshore relation, the actual result is a wave period that is too low; e.g. when a wave period of 5 s is targeted, in reality the particular wave number relates to a wave period of 6 or 7 s. Therefore, the lower and upper limit of the range of filtered wave periods will be somewhat higher than intended when filtering in intermediate waters. The consequence is that there will be too many wave periods filtered out on the lower side of the range, while there are too few wave periods filtered out on the upper side.

MEDIAN FILTERING

After estimating the celerity field a median filter has been applied. The intention of the median filter is to smooth out the wavy variations in the celerity field. The consequences of a median filter are illustrated in Figure 7.12. Clearly, the median filter smooths out the variations. Assuming that wave characteristics are constant over a wavelength, the results of the median filter are favourable. A median filter larger than 500 m (Figure 7.12b) would lead to too much smoothing and removal of typical gradients in the case of Saint-Louis, e.g. in Figure 7.12c the effect of a 1000 m median filter is shown. In Appendix D the effect of a range of median filters to the celerity estimations is presented. Like the 2D Fourier filter, the median filter also extends the duration of wave visibility in the resulting videos while details are removed. The implications of that are discussed later on.

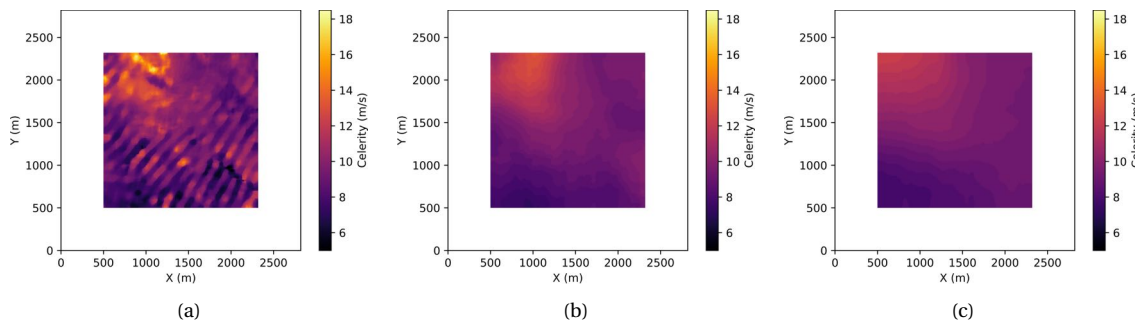


Figure 7.12: Celerity estimations for the domain in Saint-Louis. The median filter increases over the figures. In (a) a median filter of 100 m has been applied, in (b) a median filter of 500 m has been used and in (c) a median filter of 1000 m.

The application of a 2D Fourier filter as well as a median filter leads to smoothing of the resulting wave field. Both filters therefore extend the duration of wave visibility in the video while important details are probably lost.

7.1.6. AVERAGE REPRESENTATION OF WAVE CHARACTERISTICS IN THE VIDEO

The constructed videos appear to represent the wave spectra in good order. However, a discrepancy between the quality of the resulting bathymetries and the quality of the videos is observed. This is probably explained by the fact that the video represents wave characteristics in an average way, while it lacks detailed information per pixel. There are two distinct reasons for this: 1) the "averaging" filters that have been applied to reduce the celerity estimation errors and 2) the way in which the video is constructed leading to even more "averaging".

INFLUENCE OF FILTERS

As explained, the pixel-wise estimation of celerity is characterised by relatively large errors. In an attempt to reduce those errors two filtering methods have been applied: a 2D Fourier filter and a median filter. Both filters are used to remove the variations in the celerity field. As a consequence of the filters the resulting celerity field is averaged, leading to loss of pixel-wise detail. For example, an extreme variant of the median filter, one that is as large as the entire domain, would lead to a flat celerity field; the celerity over the domain would be uniform. A video construction based on such a celerity field would lead to a video that perfectly shows a propagating wave for sufficient duration, however the propagation would be incorrect. This example shows that applying filters leads to loss of detail per pixel, meaning that the resulting video lacks pixel-wise details as well.

INFLUENCE OF VIDEO CONSTRUCTION METHOD

The videos are constructed by combining time vectors per pixel. The way in which these time vectors are created is another source of averaging in the resulting video. There are two ways in which the information in the video is averaged. First, the time vectors are created by combining pixels in temporal bins. Each temporal bin, corresponding to a certain travel time to the pixel of interest, consists of number of surface heights. These surface heights are combined using a weighted average protocol, leading to loss of detailed information. The second source of averaging is due to the way travel times are calculated. Each travel time, from a surrounding pixel to the pixel of interest, is calculated by means of dividing the spatial distance by the average of the celerity in the pixel of interest and the surrounding pixel. This assumption is valid for pixels that are relatively close to each other, but becomes less true for pixels far away. As a consequence, details per pixel are lost.

The constructed videos represent wave characteristics quite well in average sense. This is due to the "averaging" effect of the applied filters and the video construction method.

7.1.7. VIDEO DURATION

One of the model requirements is the sufficient duration of wave visibility in the constructed videos. It has been observed that the videos related to the FUNWAVE domain and the domain in Saint-Louis are able to show waves for at least a minute. The video in Capbreton performs less: waves are only visible for 22 s. An explanation is found in the corresponding celerity fields. As explained, the celerity field in Capbreton is messier than the other two celerity fields. This is a result of the relatively small wavelengths in Capbreton in relation to typical Sentinel-2 characteristics, which leads to larger celerity estimation errors. The consequence of a messy celerity field is the loss of wave stochasticity. When celerity estimations in pixels close to each other differ more than they do in reality, the created time vectors in those pixels lose coherence for time steps far away from $t = 0$ s: the wave signals in neighbouring pixels become diverged. This effect explains the short duration of wave visibility in the video of Capbreton.

Above explanation also emphasises the need for a smooth celerity field and therefore the need for the application of a 2D Fourier filter and median filter. As explained, finding correct filter ranges is in fact an act of fine balance: too large of a filter removes important details, while too small of a filter reduces the duration of wave visibility in the resulting video. This holds true for the 2D Fourier filter as well as for the median filter.

7.1.8. CELERITY, VIDEO AND BATHYMETRY

In this thesis bathymetry has been estimated using two different methods. The first method makes use of a video construction and a DMD-based DIA. In the second method, the video is avoided and bathymetry is directly estimated by pixel-wise solving of the linear dispersion relationship. The resulting bathymetries of both methods have already been discussed in Section 7.1.2. The upcoming section elaborates upon the bathymetries in relation to the celerity estimations and video construction.

BATHYMETRY ESTIMATION USING A DMD-BASED DIA

Estimating bathymetry using a DMD-based DIA makes use of a video construction. The bathymetry estimations show almost no correspondence to the ground-truth in a qualitative and quantitative perspective, except for a correct linear trend in the bathymetry estimation related to the FUNWAVE domain (Figure 6.9b). The low correlations are explained by the "averaging" effect: several factors have resulted in a video that represents wave characteristics solely in average sense. A lot of details per pixel are lost due to the influence of the applied filters and the way in which the video is constructed. Although these measures extended the duration of wave visibility in the constructed videos, apparently they have removed a too large range of frequencies from the wave spectrum. The DMD-based DIA is a frequency-based algorithm, separating the provided signal in harmonics. The removing of a part of these harmonics clearly leads to too much loss of information.

BATHYMETRY ESTIMATION BY PIXEL-WISE SOLVING OF THE LINEAR DISPERSION RELATIONSHIP

The second method avoids the use of a video and thereby the use of a DMD-based DIA. It is interesting to observe the relation between celerity and bathymetry estimations. In both the FUNWAVE dataset (Figures 6.5b and 6.9c) and the case in Saint-Louis (Figures 6.13b and 6.16c) the bathymetry estimations seem to follow the pattern of celerity estimations: similar gradients are observed in the celerity fields and bathymetry fields. In Appendix E a range of bathymetry estimations in Saint-Louis is provided.

Especially in the case of Saint-Louis these results lead to questions regarding the validity of the ground-truth bathymetry. Assuming that the celerity estimations are characterised by similar errors per pixel, the resulting celerity field in Saint-Louis probably shows errors in an absolute sense while the gradient of the estimations can be trusted. This assumption is supported by the results in Figure 7.8. Furthermore, the resulting bathymetry (Figure 6.16c) shows a quite natural pattern. On the other hand, the ground-truth bathymetry is obtained from a rough bathymetric chart created in 2018 while the estimated bathymetry relates to March 2019. It is therefore not a bold assumption to state that the bathymetry estimation in Saint-Louis probably performs better than can be proven by comparing to the ground-truth. The main takeaway from these last observations is that the celerity estimation errors are the most dominating factor in the context of this thesis: reducing those errors would certainly lead to better bathymetry estimations.

When the construction of a video is avoided, the resulting bathymetry estimations seem to follow the pattern of the celerity estimations. Moreover, there are reasons to doubt the validity of the ground-truth in Saint-Louis. All together, this leads to the key message that the celerity estimation errors are probably the most important factor in the context of this thesis.

7.2. DELIMITATIONS AND ASSUMPTIONS

The delimitations and assumptions form the boundaries of this study. They consist of conscious decisions upfront about the subjects and methodologies that have been included during the research. Only the most important delimitations and assumptions are mentioned.

7.2.1. SCOPE OF THE THESIS

The research objective has been stated in the beginning of this section. The following delimitations follow from this research objective statement:

- The research has focused on the construction of a one-minute video in order to show the potential of Sentinel-2 imagery for bathymetry estimation using a DMD-based DIA. Bathymetry estimations are benchmarked by using a plain pixel-wise solving of the linear dispersion relationship, avoiding the use of a video construction. Other bathymetry estimation methods have been ignored;
- A *wave-derived* bathymetry estimation has been deployed instead of a bathymetry estimation based on other physical principles;
- The research has covered *nearshore* bathymetry, meaning that the focus is on intermediate to shallow water depths and the boundary between sea and shore is out of scope;
- A spatio-temporal cross-correlation model has been developed for the purpose of a video construction. Other mathematical approaches have been ignored.

7.2.2. DATASETS

Three distinct datasets have been used during the research. The first of these, a set of synthetic sinusoidal waves, has been used to define the theoretical application range in Appendix C. This implies that the theoretical application range is based on the analysis of linear wave forms instead of non-linear wave forms such as Sentinel-2 data. The wave characteristics of this dataset are uniform as well. The other two datasets, a synthetic FUNWAVE dataset and Sentinel-2 imagery, have been used to perform the dataset analyses. The lack of typical satellite noise in the FUNWAVE dataset compared to Sentinel-2 data influences the particular analysis. The FUNWAVE simulation is forced by $H_s = 1.4$ m and $T_p = 10$ s, indicating typical swell wave conditions. The input bathymetry ranges between depths of 13 m and 0 m, which corresponds to intermediate to shallow water depths when typical estimated wavelengths of 40 to 100 m are taken into account (Figure 6.3b). The wave solving capabilities of the FUNWAVE simulation are not seen as delimitation, since literature shows that a FUNWAVE simulation performs well in intermediate to shallow water [89, 102, 103].

The Sentinel-2 imagery focuses on two research sites: one in Saint-Louis and one in Capbreton. The imagery of 4 March 2019 in Saint-Louis and of 30 March 2018 in Capbreton has been analysed. The selection of both sites and dates has been based on a range of arguments: cloud coverage, preferable wave conditions and available wave measurements. Furthermore, both research datasets are characterised by a persistent swell wave climate and probably range from deep to intermediate and shallow water depths.

7.2.3. GROUND-TRUTH WAVE SPECTRUM

The wave spectrum that has been used to compare the result of the Sentinel-2 imagery analysis in Saint-Louis is provided by the Saint-Louis 2019 experiment. The obtained in-situ wave spectrum is the result of measurements provided by an ADCP. It is assumed that these measurements represent the present wave spectrum at 11:33h, 04/03/2019, which is the sensing date of the Sentinel-2 imagery. The ADCP measurements are conducted at 11:30h, 04/03/2019.

7.2.4. GROUND-TRUTH BATHYMETRIC DATA

The ground-truth bathymetry data of the Sentinel-2 imagery analysis is formed by EMODnet bathymetric data [93, 94]. For both locations, the EMODnet dataset of 2018 is used. It is assumed that this

dataset is representative of the bathymetric situation at the sensing moments of the Sentinel-2 imagery: 30/03/2018 in Capbreton and 04/03/2019 in Saint-Louis. As explained in Section 7.1 there are reasons to doubt this assumption.

7.2.5. CURRENTS AND WIND

Currents and wind have not been taken into account in the research. Both effects influence the propagation of waves and thereby directly influence wave characteristics.

7.3. RETROSPECTION

The following four aspects of the research could have been executed differently, only the most important aspects are mentioned:

- **Choice of research sites.** The area in Capbreton is known as a challenging area [64]. The bathymetry is characterised by a high gradient and the typical waves are relatively short. In hindsight, it would have been better to base the model on a set locations that are known for more easy conditions such as Saint-Louis.
- **Wave spectrum in Capbreton.** For the research site in Capbreton no in-situ wave spectra corresponding to the date of interest was available. This was a conscious choice: the dates of which in-situ wave spectra for the site in Capbreton exist did not provide for reliable Sentinel-2 imagery due to large cloud coverage and/or low wave heights.
- **Reliability of ground-truth bathymetry.** The accuracy of the ground-truth bathymetries in Saint-Louis and Capbreton should be doubted. Both ground-truths are provided by a rough bathymetric chart. Detailed in-situ measurements would have been better data to compare with.
- **Synthetic FUNWAVE dataset.** The analysis based on the FUNWAVE simulation has provided for the most valuable results. Since the input data of such a synthetic dataset is known, the performance of the model could accurately be assessed. It would have been interesting to evaluate more datasets like the synthetic FUNWAVE dataset, for example FUNWAVE simulations with different input wave characteristics or different bathymetry. These simulations would have provided for valuable insights.

7.4. ADDED VALUE OF THE RESEARCH

The research is put in perspective. The added value of the research is discussed based on the retrospection, the assumptions and delimitations and the interpretation of the results.

A distinct difference in performance between the video construction and the bathymetry estimations is observed. The video construction represents average wave propagation in good order. The resulting bathymetry estimations are of lesser quality. The bathymetry estimations based on pixel-wise solving of the linear dispersion relationship, avoiding the use of a video construction, show that the celerity estimation errors are a dominant aspect in the context of the developed spatio-temporal cross-correlation model. The dominant wave direction estimations and wavelength estimations performed by the model are generally accurate.

As main product of the model, the video construction is not suitable to estimate bathymetry using a DMD-based DIA. However, the video construction and corresponding model may be used for some other applications:

- The video as constructed by the model represents average wave propagation in a decent way. It can therefore be used to obtain the wave spectrum from Sentinel-2 imagery for a certain date and location of interest;
- In general, the video offers a way to enlarge the range of temporal information based on Sentinel-2 imagery. It is therefore a useful tool to combine Sentinel-2 imagery with a set of other applications that need more temporal information;

- The model is able to estimate dominant wave direction per pixel from Sentinel-2 imagery for a certain date and location of interest. The dominant wave direction provides valuable information such as refraction and diffraction patterns which can be used to indicate typical bathymetric features, e.g. the sandbar in Figure 6.1b;
- The model can also be used to determine a partial wave climate for a certain location on Earth. By estimating dominant wave direction and wavelength over the duration of a year, an indication of a wave climate is obtained.

Besides applications of the video construction related to Sentinel-2 imagery, the obtained knowledge can be translated to other fields of interest:

- The results of Figure 7.5 and Appendix C show that the accuracy of the model possibly increases for changing satellite characteristics. For example, increasing the burst duration leads to decreasing celerity estimation errors. The same holds for an increase of spatial resolution. That means the model should work well for satellites that provide a longer burst duration combined with higher resolution, such as Pleiades in persistent mode [64]. Even the analysis of shorter waves would then be enabled. An increase of burst duration is indicated by the red arrow in Figure 7.13a, a decrease of resolution by the red arrow in Figure 7.13b. The black dashed square in Figure 7.13a indicates typical Sentinel-2 characteristics in relation to a wave period of 5 to 25 s. The black marker in Figure 7.13b shows the PE for a wavelength of 100 m in relation to typical Sentinel-2 characteristics, indicating that an increase of resolution would enable the model to analyse shorter wavelengths from imagery, such as the waves in Capbreton;
- The model should also perform quite well for data with lower Δt such as standard video imagery. Typical Percent Errors corresponding to video imagery are projected by the red box in Figure 7.13a, combining a low Δt and a large burst duration.

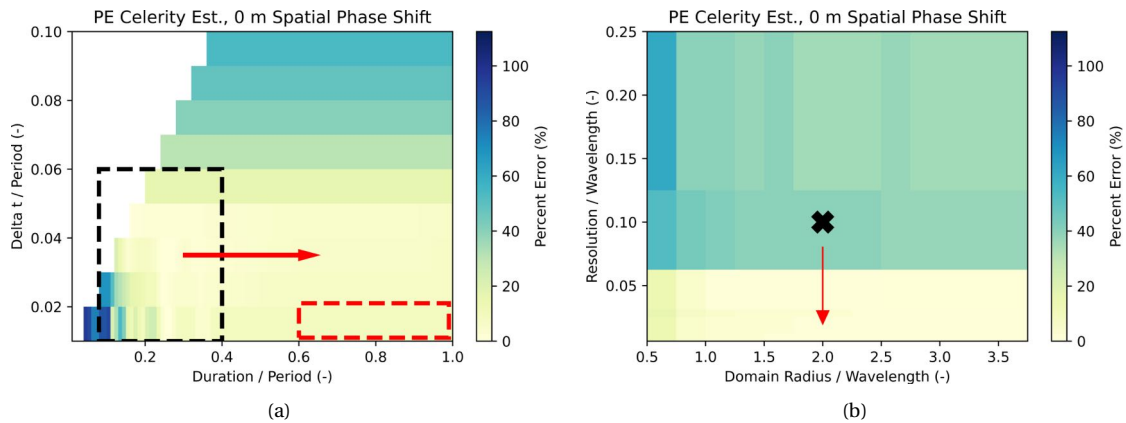


Figure 7.13: Theoretical application range corresponding to celerity estimation errors. In (a) the temporal analysis is presented, while (b) shows the spatial analysis. The black dashed square in (a) corresponds to typical Sentinel-2 characteristics and a wave period ranging from 5 s to 25 s. The red arrow in (a) shows the effect of an increasing burst duration, while the red dashed square in (a) indicates typical errors corresponding to video imagery: a low Δt and a large burst duration. In (b) the black marker shows the PE for a wavelength of 100 m in relation to Sentinel-2 characteristics, e.g. waves in Capbreton. The red arrow in (b) shows the effect of an increasing resolution, e.g. from 10 m to 1 m.

8

CONCLUSION

The results and discussion are used to provide answers to the main research question and the 10 underlying sub-questions. The main research question has been stated as:

Is it possible to construct a one-minute video that represents the propagation of waves, from a 2.586-second burst of Sentinel-2 satellite imagery, by developing a spatio-temporal cross-correlation model, in order to show the potential for the estimation of wave-derived nearshore bathymetry using a DMD-based DIA?

It is concluded that it is possible to construct a one-minute video representing wave propagation from Sentinel-2 imagery as long as wave conditions are preferable. The constructed videos have been used to estimate a wave-derived nearshore bathymetry by means of a DMD-based DIA. This has led to the conclusion that the videos as constructed lack the ability to estimate an accurate bathymetry using a DMD-based DIA. The arguments on which these conclusions are based are elaborated upon in more detail. The sub-questions that correspond to each section are indicated in the header of the particular section, e.g. SQ1 = sub-question 1. (see Chapter 1).

SPATIO-TEMPORAL CROSS-CORRELATION MODEL (SQ1, SQ2, SQ3)

A spatio-temporal cross-correlation model has been developed in this work to construct a wave-representing video. The model consists of four parts:

- **Model part 0:** Pre-processing;
- **Model part 1:** Image resolution augmentation;
- **Model part 2:** Wave characteristics estimation;
- **Model part 3:** Video construction.

In model part 1 the resolution of a set of 20 m resolution spectral bands has been augmented by means of a cubic spline interpolation in the Radon domain. Subsequently, in model part 2, three wave characteristics have been estimated separately per pixel: dominant wave direction, wavelength and celerity. A spatio-temporal cross-correlation method has been used for this purpose. The estimated wave characteristics have ultimately been used to construct a video in model part 3. The video construction method combines time vectors which are created by taking the weighted average of surface heights per predefined temporal bin.

WAVE PROPAGATION IN THE CONSTRUCTED VIDEOS (SQ4, SQ5)

It is concluded that the constructed videos are generally able to show wave propagation for at least one minute. The required video duration of one minute is not obtained in the case of Capbreton due to large errors in the corresponding celerity field. These large celerity estimation errors are the result of relatively short wavelengths. It appears furthermore that the constructed videos represent wave propagation accurately in an average sense. The wave spectra obtained from the videos show

good alignment with input wave characteristics and in-situ measurements. A pixel-wise and detailed description is lacking in the videos. This is a consequence of the "averaging" effects which are induced by three different sources: the 2D Fourier filtering, the median filtering and the way in which the videos are constructed.

BATHYMETRY ESTIMATION USING A VIDEO AND A DMD-BASED DIA (SQ6, SQ7)

Using the constructed videos to estimate bathymetry by means of a DMD-based DIA does not provide satisfactory results. The obtained errors are large in a quantitative and qualitative perspective, although a correct linear trend is recognised in the analysis of the synthetic FUNWAVE dataset. The large errors are explained by the "averaging" effects as mentioned. The DMD-based DIA is a frequency-based algorithm, inverting depth by separating the signal in harmonics. These harmonics have disappeared to a large extent by the "averaging" effects. The demands of the DMD-based DIA to the constructed videos appear to be contradictory in relation to the developed model: a long duration of wave visibility requires a large amount of filtering in order to reduce variations in the celerity field, while an accurate, detailed and pixel-wise representation of wave propagation asks for the reduction of filtering.

BATHYMETRY ESTIMATION USING PIXEL-WISE SOLVING OF THE LINEAR DISPERSION RELATIONSHIP (SQ8, SQ9)

Estimating bathymetry by pixel-wise solving of the linear dispersion relationship, avoiding the use of a video, provides for interesting insight. The bathymetry estimations follow the pattern of the estimated celerity fields. From the FUNWAVE analysis and the estimated theoretical application range the celerity estimation is concluded to be the other dominant source of errors, next to the applied filters and the way in which the videos are constructed. When the use of a video is avoided, reduction of the celerity estimation errors should therefore lead to an increasing accuracy of bathymetry estimation.

APPLICATION LIMITS OF THE MODEL IN RELATION TO SENTINEL-2 IMAGERY (SQ10)

A theoretical application range of the model has been defined. It shows that estimating wave characteristics from Sentinel-2 imagery by means of the developed model is in the realm of possibilities. In a temporal sense, relatively large celerity estimation errors are expected for wave periods lower than 5 s and higher than 8 s. The model is less sensitive for spatial parameters: as long as wavelengths are larger than circa 150 m the celerity estimation error is acceptable in relation to Sentinel-2 imagery characteristics.

ADDED VALUE OF THE SPATIO-TEMPORAL CROSS-CORRELATION MODEL

In conclusion, the developed model and related video constructions offer added value, although not for the purpose of a bathymetry estimation by means of a DMD-based DIA. The constructed videos represent wave propagation in an average sense and can therefore be exploited for wave-related purposes, e.g. obtaining wave spectra, estimating dominant wave direction and estimating wave climates. In general, the video offers a way to enlarge the temporal range of Sentinel-2 imagery. It is furthermore concluded that the model is probably more suitable for use in combination with other types of imagery, including satellite imagery with larger burst duration and increased spatial resolution as well as standard video imagery.

9

RECOMMENDATIONS

The discussion of recommendations is separated into three sections. First, an overview of suggested next research steps regarding the improvement of the model is provided in Section 9.1. Section 9.2 thereafter makes suggestions from a broader perspective. It focuses on recommendations about other applications of the developed model. The last section, Section 9.3, takes the broadest view. It elaborates upon recommendations regarding the use of Sentinel-2 imagery for bathymetry estimation purposes, thereby leaving the constraints of this thesis: a wave-derived nearshore bathymetry by using a spatio-temporal cross-correlation model. Section 9.3 is in fact an answer to the question: "What would I do if I had to repeat the research, solely taking Sentinel-2 imagery as input data and bathymetry estimation as aim?"

9.1. IMPROVING THE MODEL

A set of suggestions is made regarding the improvement of the developed spatio-temporal cross-correlation model. Each is discussed separately.

9.1.1. IN-DEPTH RESEARCH ON CELERITY ESTIMATION

From the discussion it appears that celerity estimation errors are one of the main bottlenecks in the model. An accurate celerity estimation is essential, either for representing correct wave propagation in the video or for the purpose of bathymetry estimation, with or without using a video construction. The decrease of celerity estimation errors would also lead to a decreasing need for filtering, which is beneficial to the accuracy of results. The celerity estimation errors are large and are generally underestimating. These results are supported by the theoretical application range (Figure 7.5, Appendix C). It is interesting to observe that even using the plainest type of dataset, a set of synthetic sinusoidal waves, the celerity estimation errors appear to be large. In this research some suggestions regarding the sources of these errors have been provided. It would be valuable to conduct research on the reasons for these errors and thereby develop methods to decrease them.

9.1.2. IN-DEPTH RESEARCH ON IMAGE RESOLUTION AUGMENTATION

The defined theoretical application range (Figure 7.5, Appendix C) shows that the spatial resolution of Sentinel-2 imagery is one of the limitations in this research (Figure 7.13b). A higher spatial resolution would lead to a decrease of celerity estimation errors by the model, especially for shorter wavelengths. In this research it has been decided to develop the model based on an interpolation in Radon space. It has appeared during the research that a resolution augmentation to higher resolutions, for example 5 m, does not lead to better results. Other upsampling methods have briefly been investigated as well. These methods include normal interpolation and interpolation based on deep learning algorithms. Further development of these methods would be a valuable next research step.

9.1.3. IN-DEPTH RESEARCH ON VIDEO CONSTRUCTION METHOD

Another significant bottleneck in the model is the way in which the video is constructed. The method results in loss of pixel-wise detail which is unfavourable for the use of a DMD-based DIA in order to invert depth. A different video construction method could possibly solve these problems. A 'full langrangian' method would be most promising from an idealistic point of view. In such a method the propagation of a certain wave part would be forced by every celerity and wave direction it experiences on its pathway. It is recognised that such a method is computationally expensive and leads to non-linearities. Research on finding a good compromise would be valuable.

9.1.4. RESEARCH USING DETAILED DATASETS

It appears that the synthetic FUNWAVE dataset has provided for valuable insights. The main advantage of this dataset has been the availability of detailed and structured ground-truths: knowing the ground-truths of separate model parts leads to precise insight and therefore knowledge regarding the performance of the model. It is therefore advised to conduct further research using more of these kinds of datasets. Two different types are suggested:

- Multiple variants of a synthetic dataset such as the FUNWAVE dataset. The synthetic FUNWAVE dataset could, for example, be reused with different input parameters, such as input bathymetry, input resolution and input wave characteristics;
- An actual Sentinel-2 dataset based on detailed in-situ experiments. Research using Sentinel-2 imagery of good quality (low cloud coverage, high and long waves) together with specific in-situ measurements would be very valuable. The in-situ measurement would ideally include bathymetry and wave characteristics (including celerity).

9.2. OTHER APPLICATIONS OF THE MODEL

In chapter 7 a discussion is provided about other applications of the model. Based on this discussion some suggestions for further research are provided.

9.2.1. RESEARCH ON OTHER TYPES OF IMAGERY

The model has appeared to be more accurate in relation to other temporal and spatial characteristics, mainly a higher spatial resolution, a longer burst duration and a shorter time lag (Figures 7.13a and 7.13b). It would be interesting to assess the value of the spatio-temporal cross-correlation model in relation to imagery that corresponds to these characteristics, e.g. higher quality satellite data or video imagery.

9.2.2. RESEARCH ON THE VALUE OF OTHER APPLICATIONS

The constructed videos are able to represent wave propagation in an average sense. It would be interesting to assess the value of these possibilities, for example in relation to coastal management strategies. Research that explores these possibilities is advised.

9.3. SENTINEL-2 IMAGERY AND BATHYMETRY ESTIMATION

It is interesting to reflect on the research from a wider point of view. The focus of this thesis has purposely been narrowed upfront: a *spatio-temporal cross-correlation* model has been developed to construct a *wave-representing video*, a video that initially has been meant to estimate a *wave-derived* nearshore bathymetry by using a *DMD-based DIA*.

Discarding these constraints leads to a different perspective. The only two starting points that remain are the use of Sentinel-2 imagery as input data and the ultimate aim of a bathymetry estimation. The question is: "What would I do if I had to repeat the research, solely taking Sentinel-2 imagery as input data and bathymetry estimation as aim?". This leads to the following recommendations. Note that these recommendations are written from the writer's perspective and are therefore subjective.

9.3.1. KEEP FOCUSING ON A WAVE-DERIVED BATHYMETRY

The *wave-derived* bathymetry is still very promising, mainly because it avoids the calibration complications of *colour-based* routines. This makes wave-derived methods significantly more useful in a generalist sense.

9.3.2. KEEP FOCUSING ON A CROSS-CORRELATION IN SPACE-TIME DOMAIN

A cross-correlation in space-time domain remains an interesting technique. Although it has not yet led to sufficiently accurate results in relation to Sentinel-2 imagery. The resulting cross-correlation images in this thesis resolve the existing wave pattern of the raw imagery remarkably well. That means, a cross-correlation is a very effective way to reproduce a wave signal from a short burst of temporal information. The question is: how to get accurate wave characteristics estimations from these cross-correlation images?

9.3.3. FOCUS ON CELERITY ESTIMATION BY IMPROVING RESOLUTION AUGMENTATION

The celerity estimation seems to be the key for an accurate bathymetry estimation. In this research it is not yet accomplished to reduce the celerity estimation errors significantly. However, it is interesting to observe some results. First of all, the wavy variability in the estimated celerity fields is remarkable (Figure 6.19). Apparently, there is a correlation between the part of the wave that is observed and the estimation error. Furthermore, increasing the resolution while still representing the actual wave, should lead to a reduction of these errors. This is probably because there is less risk of cross-correlation errors (see Section 7.1.4). Both aspects would have the writer's full attention when the research had to be repeated.

9.3.4. MAKE THE CELERITY ESTIMATION PERFECT FOR SINUSOIDAL WAVES

In this research the analysis of plain synthetic sinusoidal waves has been used to explain the obtained results. A suggestion would be to start the research by analysing these simple waves. A next research question - e.g. for a next thesis - could be: "How can the celerity estimation error for a linear sinusoidal wave be reduced to zero, while using a spatio-temporal cross-correlation method?".

9.3.5. AVOIDING VIDEO CONSTRUCTION FOR BATHYMETRY ESTIMATION PURPOSES

The discussion in Chapter 7 shows that constructing a video leads to a lot of 'averaging' complications. At the same time, the filtering methods that lead to the averaging are needed to provide a video of sufficient duration for the use of a DMD-based DIA. It should therefore be doubted if a video construction is a correct method to estimate bathymetry from Sentinel-2 imagery. Although the video is meant to enlarge the temporal information and therefore to convert spatial wave characteristics to temporal wave characteristics, it is also a source of more processing: wave characteristics are converted to a video, which is reconverted to wave characteristics and depth. Avoiding a video construction and translating wave characteristics directly to depth could probably be a more satisfactory method.

REFERENCES

- [1] K. Mangor, N. Dronen, K. H. Kaergard, and N. E. Kristensen, *Shoreline Management Guidelines* (DHI, 2017).
- [2] P. Toft, *The Radon Transform - Theory and Implementation*, Ph.D. thesis, Technical University of Denmark (1996).
- [3] *Windguru*, <https://www.windguru.cz>, accessed: 22-04-2021.
- [4] *Gfs-wave*, <https://polar.ncep.noaa.gov/waves/ensemble/>, accessed: 22-04-2021.
- [5] E. W. J. Bergsma, R. Almar, and P. Maisongrande, *Radon-augmented sentinel-2 satellite imagery to derive wave-patterns and regional bathymetry*, *Remote Sens.* **11**, 1918 (2019).
- [6] M. Gawehn, A. van Dongeren, S. de Vries, C. Swinkels, R. Hoekstra, S.G.J. Aarninkhof, and J. Friedman, *The application of a radar-based depth inversion method to monitor near-shore nourishments on an open sandy coast and an ebb-tidal delta*, *Coastal Engineering* **159** (2020).
- [7] B. Neumann, A. T. Vafeidis, J. Zimmermann, and R. J. Nicholls, *Future coastal population growth and exposure to sea-level rise and coastal flooding - a global assessment*, *PLoS One* **10** (2015).
- [8] S. Vitousek, P. L. Barnard, C. H. Fletcher, N. Frazer, L. Erikson, and C. D. Storlazzi, *Doubling of coastal flooding frequency within decades due to sea-level rise*, *Scientific Reports* **7**, 1399 (2017).
- [9] U. N. The Ocean Conference, *Factsheet: People and oceans*, (2017).
- [10] D. Balk, M. Montgomery, G. McGranahan, D. Kim, V. Mara, M. Todd, T. Buettner, and A. Dorelien, *Mapping urban settlements and the risks of climate change in africa, asia and south america*, (2009).
- [11] Climate Central, *Flooded future: Global vulnerability to sea level rise worse than previously understood*, (2019).
- [12] V. Klemas, *The role of remote sensing in predicting and determining coastal storm impacts*, *Journal of Coastal Research* **25**, 1264 (2009).
- [13] R. J. Klein, R. J. Nicholls, and N. Mimura, *Coastal adaption to climate change: can the ipcc technical guidelines be applied?* *Mitigation and adaption strategies for global change* **4**, 239 (1999).
- [14] H. F. Stockdon and R. A. Holman, *Estimation of wave phase speed and nearshore bathymetry from video imagery*, *Journal of Geophysical Research* **105**, 22,015 (2000).
- [15] P. S. Bell, *Shallow water bathymetry derived from an analysis of x-band marine radar images of waves*, *Coastal Engineering* **37**, 513 (1999).
- [16] P. Jagalingam, B. Akshaya, and A. V. Hegde, *Bathymetry mapping using landsat 8 satellite imagery*, *Procedia Engineering* **116**, 560 (2015).
- [17] H. M. Dierssen, *Bathymetry: Assessing methods*, *Encyclopedia of Natural Resources* (2014).

- [18] F. Madricardo, F. Fogliani, A. Kruss, C. Ferrarin, N. M. Pizzeghelo, C. Murri, M. Rossi, M. Bajo, D. Bellafiore, E. Campiani, S. Fogarin, V. Grande, L. Janowski, E. Keppel, E. Leidi, G. Lorenzetti, F. Maicu, V. Maselli, A. Mercorella, G. M. Gavazzi, T. Minuzzo, C. Pellegrini, A. Petrizio, M. Prampolini, A. Remia, F. Rizzeto, M. Rovere, A. Sarretta, M. Sigovini, L. Sinapi, G. Umgieser, and F. Trincardi, *High resolution multi beam and hydrodynamic datasets of tidal channels and inlets of the venice lagoon*, *Scientific Data* **4** (2017).
- [19] P. S. Bell and J. C. Osler, *Mapping bathymetry using x-band marine radar data recorded from a moving vessel*, *Ocean Dynamics* (2011).
- [20] W. Williams, *The determination of gradients on enemy-held beaches*, *The Geographical Journal* **109**, 76 (1947).
- [21] C. Hart and E. Miskin, *Developments in the method of determination of beach gradients by wave velocities*, (1945).
- [22] C.-K. Wang and W. D. Philpot, *Using airborne bathymetric lidar to detect bottom type variation in shallow waters*, *Remote Sensing of Environment* **106**, 123 (2007).
- [23] D. R. Robert C. Hilldale, *Assessing the ability of airborne lidar to map river bathymetry*, *Earth Surf. Process. Landforms* **33**, 773 (2008).
- [24] G. C. Guenther, *Airborne lidar bathymetry*, (2004).
- [25] E.W.J. Bergsma and R. Almar, *Video-based depth inversion techniques, a method comparison with synthetic case*, *Coastal Engineering* (2018).
- [26] E.W.J. Bergsma, D. C. Conley, M. A. Davidson, T. J. O'Hare, and R. Almar, *Storm event to seasonal evolution of nearshore bathymetry derived from shore-based video imagery*, *Remote Sensing* **11**, 519 (2019).
- [27] S.G.J. Aarninkhof, *Nearshore Bathymetry derived from video imagery*, Ph.D. thesis, University of Technology Delft (2003).
- [28] F. Ziemer, C. Brockmann, R. A. Vaughan, J. Seemann, and C. M. Senet, *Radar survey of near shore bathymetry within the oroma project*, *EARSel eProceedings* **3** (2004).
- [29] P. Chernyshov, T. Vrecica, M. Streber, R. Carrasco, and Y. Toledo, *Rapid wavelet-based bathymetry inversion method for nearshore x-band radars*, *Remote Sensing of Environment* **240** (2020).
- [30] P. Bell, J. Williams, S. Clark, B. Morris, and A. Vila-Concej, *Nested radar systems for remote coastal observations*, *Journal of Coastal Research* **I**, 483 (2006).
- [31] L. P. Almeida, R. Almar, E.W.J. Bergsma, E. Berthier, P. Baptista, E. Garel, O. A. Dada, and B. Alves, *Deriving high spatial-resolution coastal topography from sub-meter satellite stereo imagery*, *Remote Sensing* **11**, 590 (2019).
- [32] A. Chybicki, *Mapping south baltic near-shore bathymetry using sentinel-2 observations*, *Polish Maritime Research* **3** **24**, 15 (2017).
- [33] E. Salameh, F. Frappart, R. Almar, P. Baptista, G. Heygster, B. Lubac, D. Raucoules, L. Almeida, E.W.J. Bergsma, S. Capo, M. de Michele, D. Idier, Z. Li, V. Marieu, A. Poupardin, P. A. Silva, I. Turki, and B. Laignel, *Monitoring beach topography and nearshore bathymetry using space-borene remote sensing: A review*, *Remote Sensing* **11**, 2212 (2019).
- [34] A. Cazenave, G. L. Cozannet, J. Benveniste, P. Woodworth, and N. Champollion, *Monitoring coastal zone changes from space*, (2017).

- [35] J. P. Werdell, B. A. Franz, S. W. Bailey, L. W. Harding, and G. C. Feldman, *Approach for the long-term spatial and temporal evolution of ocean color satellite data products in a coastal environment*, (2007).
- [36] ESA, *Sentinel-2*, <https://sentinel.esa.int/web/sentinel/missions/sentinel-2> (2020), accessed: 06-08-2020.
- [37] J. Li and D. P. Roy, *A global analysis of sentinel-2a, sentinel-2b and landsat-8 data revisit intervals and implications for terrestrial monitoring*, *Remote Sens.* **9**, 902 (2017).
- [38] M. Drusch, U. D. Bello, S. Carlier, O. Colin, V. Fernandez, F. Gascon, B. Hoersch, C. Isola, P. Laberinti, P. Martimort, A. Meygret, F. Spoto, O. Sy, F. Marches, and P. Bargellini, *Sentinel-2: Esa's optical high-resolution mission for gmes operational services*, *Remote Sensing of Environment* **120**, 25.
- [39] J. D. Hedley, C. Roelfsma, V. Brando, C. Giardino, T. Kutser, S. Phinn, P. J. M. ad Omar Barriker, J. Laporte, and B. Koetz, *Coral reef applications of sentinel-2: Coverage, characteristics, bathymetry and benthic mapping with comparison to landsat 8*, *Remote Sensing of Environment* **216**, 598 (2018).
- [40] F. van der Meer, H. van der Werff, and F. van Ruitenbeek, *Potential of esa's sentinel-2 for geological applications*, *Remote Sensing of Environment* **148**, 124 (2014).
- [41] E.W.J. Bergsma and R. Almar, *Coastal coverage of esa' sentinel 2 mission*, *Advance in space research* **65**, 2636 (2020).
- [42] ESA, *Copernicus*, https://www.esa.int/Applications/Observing_the_Earth/Copernicus/Overview3 (2020), accessed: 06-08-2020.
- [43] *Sentinel hub*, <https://www.sentinel-hub.com/>, accessed: 14-08-2020.
- [44] ESA, *Msi instrument overview*, <https://earth.esa.int/web/sentinel/technical-guides/sentinel-2-msi/msi-instrument> (2020), accessed: 06-08-2020.
- [45] F. de Lucia Lobo, P. W. Souza-Filho, E. M. de Moraes Novo, F. M. Carlos, and C. C. Barbosa, *Mapping minig areas in the brazilian amazon using msi/sentinel-2 imagery*, *Remote Sens.* **10**, 1178 (2018).
- [46] A. Ansper and K. Alikas, *Retrieval of chlorophyll a from sentinel-2 msi data for the european union water framework directive reporting purposes*, *Remote Sens.* **11**, 64 (2019).
- [47] G. Kaplan and U. Avdan, *Mapping and monitoring wetlands using sentinel-2 satellite imagery*, *Remote Sensing and Spatial Information Sciences* **4** (2017).
- [48] K. Toming, T. Kutser, A. Laas, M. Sepp, B. Paavel, and T. Noges, *First experiences in mapping lake water quality parameters with sentinel-2 msi imagery*, *Remote Sens.* **8**, 640 (2016).
- [49] G. Piazzzi, C. M. Tanis, S. Kuter, B. Simsek, S. Puca, A. Toniazzo, M. Takala, Z. Akyurek, S. Gabelani, and A. N. Arslan, *Cross-country assessment of h-saf snow products by sentinel-2 imagery validated against in-situ observations and webcam photography*, *Geosciences* **9** (2019).
- [50] C. Atzberger and K. Richter, *Spatially constrained inversion of radiative transfer models for improved lai mapping from future sentinel-2 imagery*, *Remote Sensing of Environment* **120**, 208 (2012).
- [51] I. Chysafis, G. Mallinis, S. Siachalou, and P. Patias, *Assessing the relationships between growing stock volume and sentinel-2 imagery in a mediterranean forrest ecosystem*, *Remote Sensing Letters* **8**, 508 (2017).

- [52] M. Pesaresi, C. Corbane, A. Julea, A. J. Florczyk, V. Syrris, and P. Soille, *Assessment of the added-value of sentinel-2 for detecting built-up areas*, *Remote Sens.* **8**, 299 (2016).
- [53] A. M. Abdi, *Land cover and land use classification performance of machine learning algorithms in a boreal landscape using sentinel-2 data*, *GIScience Remote Sensing* **57**, 1.
- [54] A. P. Yunus, J. Dou, X. Song, and R. Avtar, *Improved bathymetric mapping of coastal and lake environments using sentinel-2 and landsat-8 images*, *Sensors* **19**, 2788 (2019).
- [55] G. Casal, X. Monteys, J. Hedley, P. Harris, C. Cahalane, and T. McCarthy, *Assessment of empirical algorithms for bathymetry extraction using sentinel-2 data*, *International Journal of Remote Sensing* **40**, 2855 (2019).
- [56] D. R. Lyzenga, *Passive remote sensing techniques for mapping water depth and bottom features*, (1978).
- [57] R. P. Stumpf, K. Holderied, and M. Sinclair, *Determination of water depth with high-resolution satellite imagery over variable bottom types*, *Limnology and Oceanography* **48**, 547 (2003).
- [58] S. Liu, Y. Gao, W. Zheng, and Z. Li, *Performance of two neural network models in bathymetry*, *Remote Sensing Letters* (2015).
- [59] T. Sagawa, Y. Yamashita, T. Okumura, and T. Yamanokuchi, *Satellite derived bathymetry using machine learning and multi-temporal satellite images*, *Remote Sens.* **11**, 1155 (2019).
- [60] L. Wang, H. Liu, H. Su, and J. Wang, *Bathymetry retrieval from optical images with spatially distributed support vector machines*, *GIScience Remote Sensing* **56**, 323 (2018).
- [61] A. Misra, Z. Vojinovic, B. Ramakrishnan, A. Luijendijk, and R. Ranasinghe, *Shallow water bathymetry mapping using support vector machine (svm) technique and multispectral imagery*, *International Journal of Remote Sensing* **39**, 4431 (2018).
- [62] K. Kabiri, *Discovering optimum method to extract depth information for nearshore coastal waters from sentinel-2a imagery- case study: Nayband bay, iran*, *Remote Sensing and Spatial Information Sciences* **XLII=4/W4** (2017).
- [63] D. Traganos, D. Poursanidis, B. Aggarwal, N. Chrysoulakis, and P. Reinartz, *Estimating satellite-derived bathymetry (sdb) with the google earth engine and sentinel-2*, *Remote Sens.* **10**, 859 (2018).
- [64] R. Almar, E.W.J. Bergsma, P. Maisongrande, and L. P. de Almeida, *Wave-derived coastal bathymetry from satellite video imagery: A showcase with pleiades persistent mode*, *Remote Sensing of Environment* **231** (2019).
- [65] L. H. Holthuijsen, *Waves in Oceanic and Coastal Waters*, Vol. 3 (Cambridge University Press, 2009).
- [66] A. Poupardin, D. Idier, M. de Michele, and D. Racoules, *Water depth inversion from a single spot-5 dataset*, *IEEE Transactions on Geoscience and Remote Sensing* **119**, 2329 (2016).
- [67] R. A. Holman, K. L. Brodie, and N. J. Spore, *Surf zone characterization using a small quadcopter: Technical issues and procedures*, *IEEE Transactions on Geoscience and Remote Sensing* **55**, 2017 (2017).
- [68] Y. Matsuba and S. Sato, *Nearshore bathymetry estimation using uav*, *Coastal Engineering Journal* **60**, 51 (2018).
- [69] ESA, *Pleiades-hr (high-resolution optical imaging constellation of cnes)*, <https://earth.esa.int/web/eoportal/satellite-missions/p/pleiades> (2020), accessed: 11-08-2020.

- [70] DigitalGlobe, *Worldview-2*, <https://gbdxdocs.digitalglobe.com/docs/worldview-2> (2020), accessed: 12-08-2020.
- [71] R. Almar, E.W.J. Bergsma, M. A. Gawehn, S.G.J. Aarninkhof, and R. Benshila, *High-frequency temporal wave-pattern reconstruction from a few satellite images: A new method towards estimating regional bathymetry*, *Journal of Coastal Research* **95**, 996 (2020).
- [72] C. Daly, W. Baba, E.W.J. Bergsma, R. Almar, and T. Garlan, *The new era of regional coastal bathymetry from space: A showcase for west africa using sentinel-2 imagery*, Preprint submitted to *Remote Sensing of Environment* (2020).
- [73] R. Almar, E.W.J. Bergsma, M. A. Gawehn, S.G.J. Aarninkhof, and R. Benshila, *High-frequency temporal wave-pattern reconstruction from a few satellite images: A new method towards estimating regional bathymetry*, *Journal of Coastal Research* **95**, 996 (2020).
- [74] E.W.J. Bergsma, D. Conley, M. Davidson, and T. O'Hare, *Video-based nearshore bathymetry estimation in macro-tidal environments*, *Marine Geology* **374**, 31 (2016).
- [75] R. A. Holman, N. Plant, and T. Holland, *Cbathy: A robust algorithm for estimating nearshore bathymetry*, *J. Geophys. Res. Oceans* **118**, 2595 (2013).
- [76] M. de Michele, S. Leprince, J. Thiebot, D. Raucouls, and R. Binet, *Direct measurement of ocean waves velocity field from a single spot-5 dataset*, *Remote Sensing of Environment* **119**, 266 (2012).
- [77] T. W. Korner, *Fourier Analysis* (Cambridge University Press, 1989).
- [78] Y. T. Chan, *Wavelet Basics* (Springer, 1994).
- [79] R. Almar, P. Bonneton, N. Senechal, and D. Roelvink, *Wave celerity from video imaging: A new method*, (2009).
- [80] E. W. J. Bergsma and R. Almar, *Video-based depth inversion techniques, a method comparison with synthetic cases*, *Coastal Engineering* **138**, 199 (2018).
- [81] J. Friedman, *Development of an x-band radar depth inversion model at the sand motor*, (2014).
- [82] M. Gawehn, S. de Vries, and S. Aarninkhof, *Depth and surface current inversion on the fly: A new video based approach using the dynamic mode decomposition*, *Coastal Sediments 2019 Proceedings of the 9th International Conference*, 2511 (2019).
- [83] J. H. Tu, C. W. Rowley, and D. M. Luchtenburg, *On dynamic mode decomposition: Theory and applications*, *Journal of Computation Dynamics* **1** (2013).
- [84] P. Schmid and J. Sestherhenn, *Dynamic mode decomposition of numerical and experimental data*, *Journal of Fluid Mechanics* **656**, 5 (2010).
- [85] Legos, <http://www.legos.obs-mip.fr/>.
- [86] V. Cazaubiel, V. Chorvalli, and C. Miesch, *The multispectral instrument of the sentinel2 program*, *Proc. of SPIE* **10566** (2008).
- [87] F. Gascon, C. Bouzinac, O. Thepaut, M. Jung, B. Francesconi, J. Louis, V. Lonjou, B. Lafrance, S. Massera, A. Gaudel-Vacaresse, F. Languille, B. Alhammoud, F. Viallefont, B. Pflug, J. Bieniarz, S. Clerc, L. Pessiot, T. Tremas, E. Cadau, R. de Bonis, C. Isola, P. Martimort, and C. Fernandez, *Copernicus sentinel-2a calibration and products validation status*, *Remote Sens.* **9**, 584 (2017).
- [88] *Sentinel-2 Product Specification Document*, Tech. Rep. (Copernicus/Sentinel-2, 2021).

- [89] J. T. Kirby, G. Wei, Q. Chen, A. B. Kennedy, and R. A. Dalrymple, *Funwave 1.0: Fully nonlinear boussinesq wave model - documentation and user's manual*, .
- [90] *Funwave-tvd*, <https://fengyanshi.github.io/build/html/index.html>, accessed: 14-08-2020.
- [91] M. Brochinni, *A reasoned overview on boussinesq-type models: the interplay between physics, mathematics and numerics*, Proceedings of the Royal Society **469**.
- [92] *Google maps*, <https://www.google.com/maps>, accessed: 22-04-2021.
- [93] *What is emodnet?* <https://emodnet.eu/en/what-emodnet> ().
- [94] *Emodnet: Bathymetry*, <https://emodnet.eu/en/bathymetry> ().
- [95] *Gebco: The general bathymetric chart of the oceans*, <https://www.gebco.net/>.
- [96] Statistics How To, *Correlation coefficient*, <https://www.statisticshowto.com/probability-and-statistics/correlation-coefficient-formula/>, accessed: 13-08-2020.
- [97] J. Stewart, *Calculus: Early Transcendental Functions*, Vol. 8 (Cengage Learning Inc., 2015).
- [98] J. M. Blackledge, *Digital Signal Processing*, Vol. 2 (Woodhead Publishing, 2006).
- [99] J. Radon, *Ufiber die bestimmung von funktionen durch ihre integral-werte langs gewisser mannigfaltigkeiten*, Sachs. Akad. Der Wiss. Leipz. Math-Phys **62**, 262 (1917).
- [100] R. Almar, H. Michallet, R. Cienfuegos, P. Bonneton, M. Tissier, and G. Ruessink, *On the use of the radon transform in studying nearshore wave dynamics*, Coast. Eng. **122**, 24 (2017).
- [101] P. Kuchment, *The Radon Transform and Medical Imaging* (Soc. Industr. Appl. Math, 2013).
- [102] F. Shi, B. Tehranirad, J. Kirby, J. Harris, and S. Grilli, *FUNWAVE-TVD: Fully nonlinear Boussinesq wave model with TVD solver documentation and user's manual*, Tech. Rep.
- [103] M. Malej and J. M. Smith, *Introduction to phase-resolving wave modeling with FUNWAVE*, Tech. Rep. (Engineer Research and Development Center - U.S. Army, 2015).
- [104] *Nyquist frequency*, <https://www-sciencedirect-com.tudelft.idm.oclc.org/topics/earth-and-planetary-sciences/nyquist-frequency> (2013), accessed: 20-04-2021.
- [105] *How to calculate percent error*, (2020), accessed: 18-04-2021.

Appendices



WAVE CLIMATE CAPBRETON, FRANCE, MARCH 2018

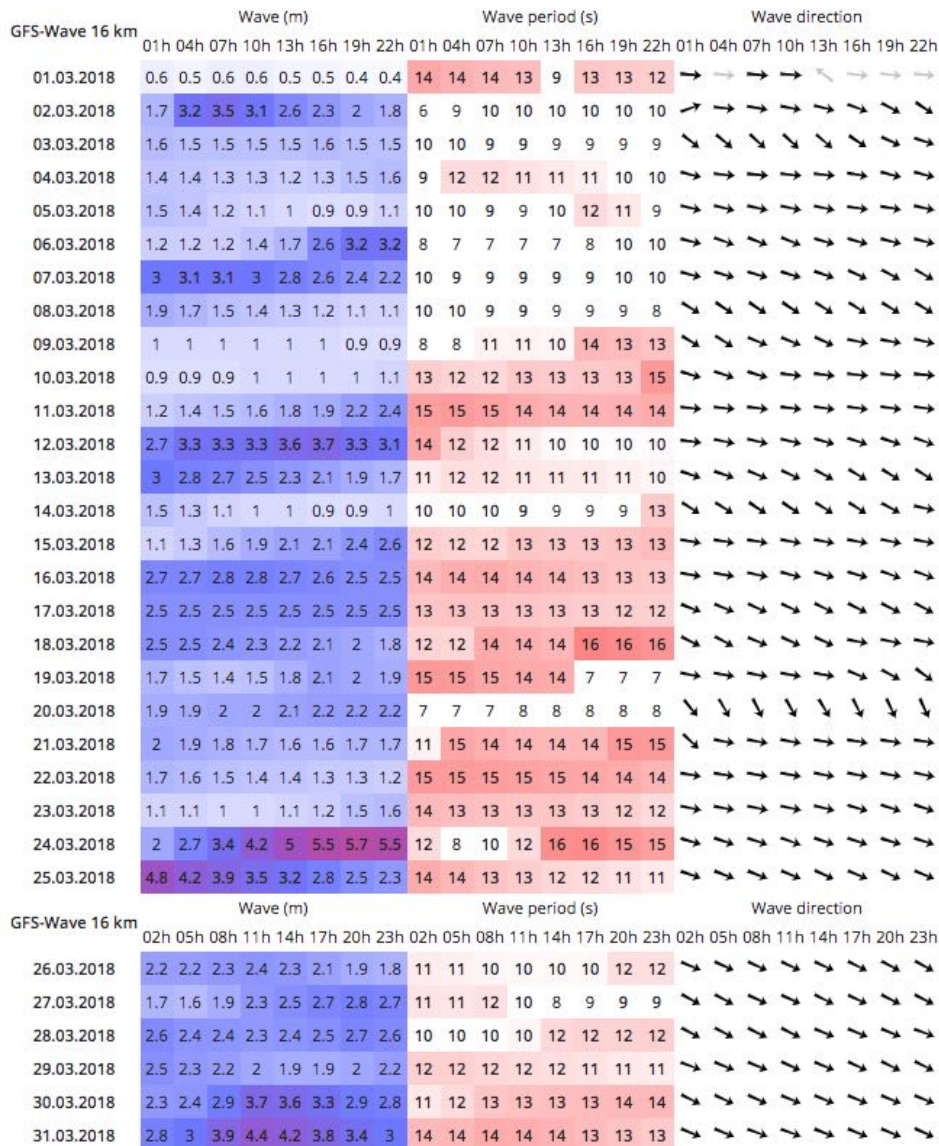


Figure A.1: GFS-Wave wave climate of Capbreton, France, in March 2018 [3, 4]

B

WAVE CLIMATE SAINT-LOUIS, SENEGAL, MARCH 2019

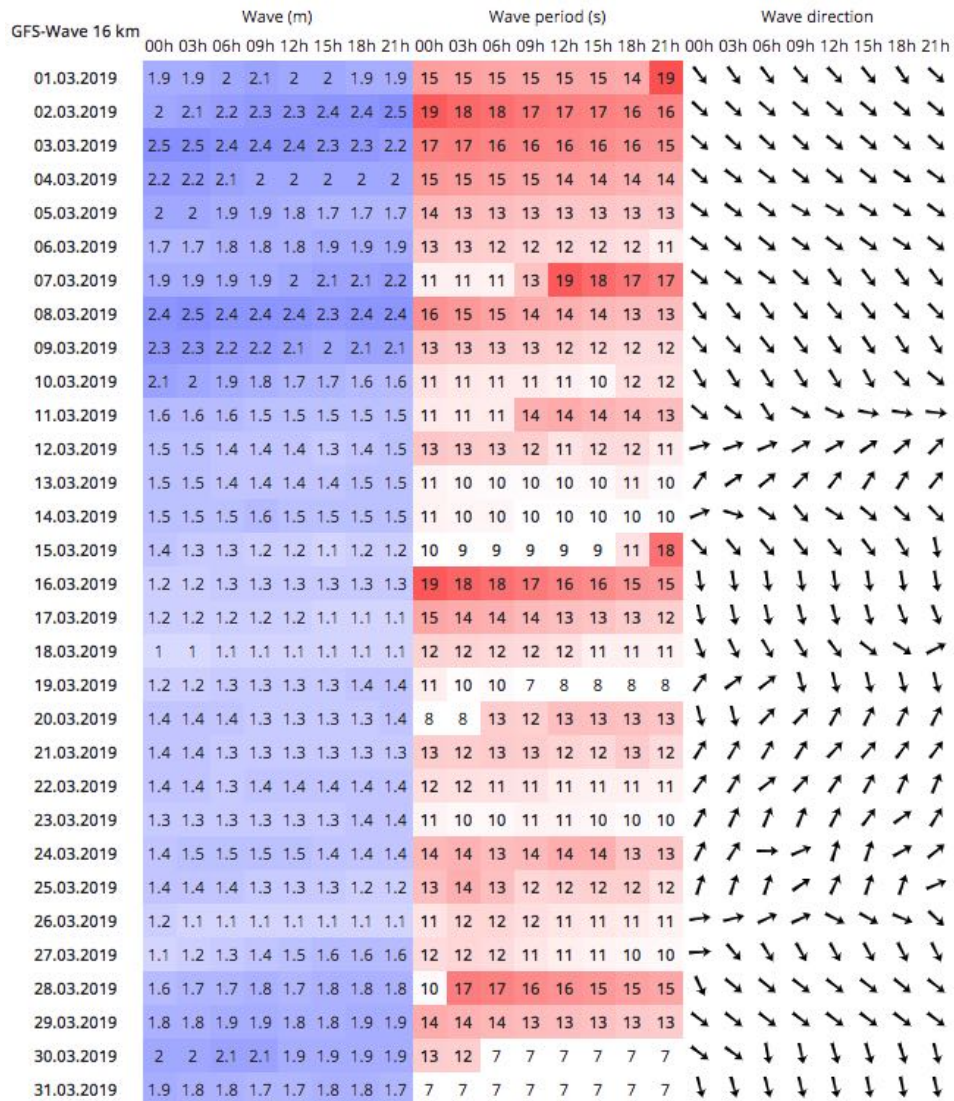


Figure B.1: GFS-Wave wave climate of Dakar, Senegal, a city nearby Saint-Louis, in March 2019 [3, 4]

C

THEORETICAL APPLICATION RANGE OF THE MODEL

A theoretical application range corresponding to the developed spatio-temporal cross-correlation model is defined. The theoretical application range provides insight regarding the performance of the model with respect to existing wave characteristics and is used to support the discussion in Chapter 7. First, the motivation to define a theoretical application range of the model is discussed in Section C.1. The dataset that is used for the purpose, dataset 3, is thereafter introduced in Section C.2. Section C.3 subsequently elaborates upon the specific methodology that is used to develop the theoretical application range, after which Section C.4 presents the results that together define the theoretical application range of the model. Some remarks and conclusions regarding the results are presented in Section C.5.

C.1. MOTIVATION TO DEFINE A THEORETICAL APPLICATION RANGE

The model is expected to be sensitive for existing temporal and spatial wave characteristics: the wave period and wavelength. Research has demonstrated that the restricted temporal range of Sentinel-2 imagery, compared to the wave period, leads to significant complications for the estimation of wave characteristics [72, 73]. The same holds for Sentinel-2's coarse sensing resolution with respect to the wavelength. Almar *et al.* [64] shows that coarser spatial resolutions result in less accurate estimations. Both conclusions are in line with the theory of Nyquist: one needs to observe at least two pixels per wave to recognise wave patterns [104]. In practice, a limit of four to five points per wavelength seems to be even more viable [5]. The expected sensitivity of the model to existing wave characteristics forms the ground to define a theoretical application range corresponding to the model.

C.2. DATASET 3: SET OF SYNTHETIC SINUSOIDAL WAVES

A set of synthetic sinusoidal waves is used to define the theoretical application range of the model. Sinusoidal waves, or sine waves, are the simplest representations of a wave. In a 2D plane (x, η) , according to linear wave theory [65], such a wave is typically represented as a long-crested harmonic wave propagating in positive x-direction:

$$\eta(x, t) = a \sin(\omega t - kx) = a \sin\left(\frac{2\pi}{T}t - \frac{2\pi}{L}x\right) \quad (\text{C.1})$$

in which η is surface height, x is the horizontal direction, t is time, a is wave amplitude, ω is angular frequency, k is wave number, T is wave period and L is wavelength. Since Sentinel-2 images of a water body represent surface height in a 3D plane (x, y, η) , it makes sense to define the sinusoidal waves in the same plane:

$$\eta(x, y, t) = a \sin(\omega t - k_x x - k_y y) \quad (\text{C.2})$$

in which k_x and k_y represent the wave number in x- and y-direction, respectively. The sinusoidal waves propagate in a direction making an angle of -45° with respect to the positive x-direction. This is to ensure that diagonal wave features are included. The dataset is created in such form that the waves more or less mimic Sentinel-2 imagery: the representation of a single propagating sinusoidal wave consists of a certain amount of snapshots of 1920 by 1920 m, with a defined time lag between each snapshot. An example of such a snapshot is provided in Figure C.1. Note that the spatial resolution, temporal time lag and amount of snapshots can vary per representation of a sinusoidal wave. All sinusoidal waves are imposed to have a constant wavelength: $L = 240$ m. By assuming the waves to be in deep water, a constant wave period for each wave follows from $T = \sqrt{\frac{2\pi L}{g}} \approx 12.39\dots$ s and a constant celerity from $c = \frac{L}{T} \approx 19.35\dots$ m/s [65]. The amplitude of the sinusoidal waves is set to be 1 m.

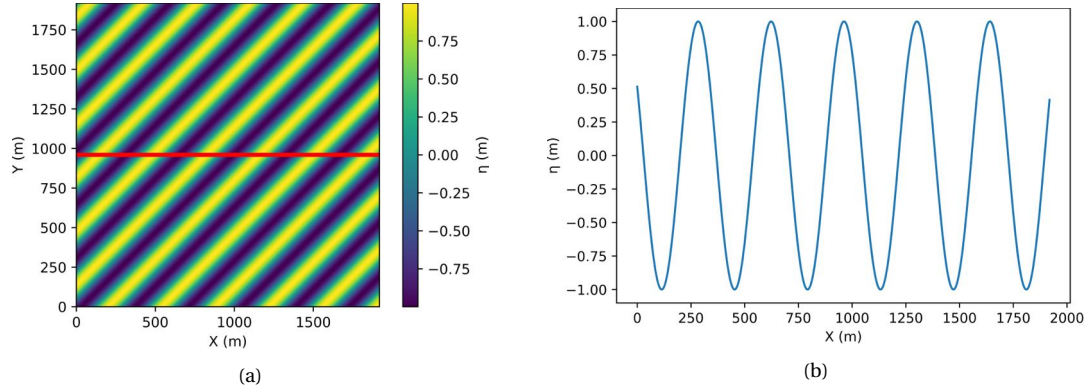


Figure C.1: Example of a sinusoidal wave snapshot ($L = 240$ m) propagating in a direction of -45° with respect to the positive x-direction. (a) Shows the 3D representation (x, y, η). (b) Provides the cross-section of the red line in (a).

C.3. METHODOLOGY: THEORETICAL APPLICATION RANGE OF THE MODEL

A comparison between estimated and actual wave characteristics defines the theoretical application range of the model. Dataset 3, a set of synthetic sinusoidal waves is used for that purpose as it provides for an environment with known ground truth wave characteristics.

C.3.1. PERCENT ERROR AND DIMENSIONLESS PARAMETERS

In the model, the wavelength and celerity are obtained per pixel on a grid. It makes sense to define the estimation accuracies per pixel, by the percent error (PE) [105] in that pixel. For example, related to celerity:

$$PE_{\text{pixel}}[\%] = \frac{|\text{Estimated Value Celerity} - \text{Actual Value Celerity}|}{\text{Actual Value Celerity}} * 100\% \quad (\text{C.3})$$

The analysis of Sentinel-2 imagery is characterised by amongst others four parameters: a burst duration, a time lag, a spatial resolution and a domain radius. The first three parameters are characteristics of the satellite imagery. The last parameter is a design choice of the spatio-temporal cross-correlation model: the radius of the domain that is used to estimate wave characteristics. These two temporal parameters (burst duration and time lag) and two spatial parameters (spatial resolution and domain radius) can be deployed to define the theoretical application range of the model. Dividing by the wave period and wavelength introduces dimensionless forms of these four parameters. An overview of the dimensionless parameters and their proposed abbreviations is shown in Table C.1.

C.3.2. TEMPORAL AND SPATIAL ANALYSIS

Two separate analyses are performed to define the application framework: a temporal and a spatial analysis. The temporal analysis aims to define PE_{pixel} for a range of combinations of the two

Table C.1: Overview of dimensionless temporal and spatial parameters.

Dur/T	Burst Duration / Wave Period
$\Delta t/T$	Time Lag / Wave Period
Res/L	Spatial Resolution / Wavelength
$Radius/L$	Domain Radius / Wavelength

dimensionless temporal parameters: Dur/T and $\Delta t/T$. The spatial analysis does the same for the two spatial parameters: Res/L and $Radius/L$. In practice, the analyses are performed by computing PE_{pixel} while varying the parameters 'Dur' and ' Δt ' or 'Res' and 'Radius' for each sinusoidal wave. The analyses are solely applied to one single pixel in the exact middle of the domain of the dataset (x : 960 m, y : 960 m). The ranges of the parameters per sinusoidal wave are chosen as such that Dur/T varies from 0.01 to 1.0, $\Delta t/T$ varies from 0.01 to 0.1, Res/L varies from 0.01 to 0.25 and $Radius/L$ varies from 0.5 to 3.5. Each of these ranges is the result of empirical fitting and is chosen so that typical ranges of wave periods and wavelengths with respect to Sentinel-2 imagery characteristics easily fit within the resulting graphs. During the spatial analysis - varying Res/L and varying $Radius/L$ - the temporal parameters are chosen exactly like typical Sentinel-2 imagery: $Dur = 2.055$ s and $\Delta t = 0.2935\dots$ s. This is to avoid influence of the temporal parameters to the outcome of the spatial analysis. Within the temporal analysis, the choice of spatial parameters is less straightforward, since especially the parameter $Radius/L$ depends on the settings of the model, instead of the characteristics of the satellite. Therefore, it is decided to use settings of both spatial parameters that correspond with the lowest achieved PE_{pixel} in the spatial analysis.

C.3.3. WAVE PHASE DIFFERENCES

Since the burst duration of Sentinel-2 imagery is relatively short compared to the wave period - $Dur/T \approx 0.10 - 0.67$, for wave periods between 20 s and 3 s -, only a small part of a wavelength is 'observed' by the model. It is therefore expected that PE_{pixel} is influenced by the pixel position with respect to the wave phase. Figure C.2a shows four examples of such pixel positions for a sinusoidal wave propagating in positive x-direction. In this figure the position at $t = 0$ s is indicated by the marker. The part of the wave that is observed during the burst duration is presented by the thicker line. The same four surface paths are plotted in the time domain (t, η) in Figure C.2b. The theoretical application range is defined for eight different pixel positions with respect to the wave phase at $t = 0$ s; the sinusoidal wave of $L = 240$ m, is divided into parts of 30 m. The positions in the (x, η) plane are indicated in Figure C.2c. In practice, the position of interest (x : 960 m, y : 960 m) is kept constant with respect to the x- and y-axis, while the only change that is made is to the spatial phase of the wave, according to:

$$\eta(x, y, t) = a \sin(\omega t - k_x(x + \phi_x) - k_y(y + \phi_y)) \quad (C.4)$$

in which ϕ_x and ϕ_y indicate the spatial phase change of the wave in x- and y-direction.

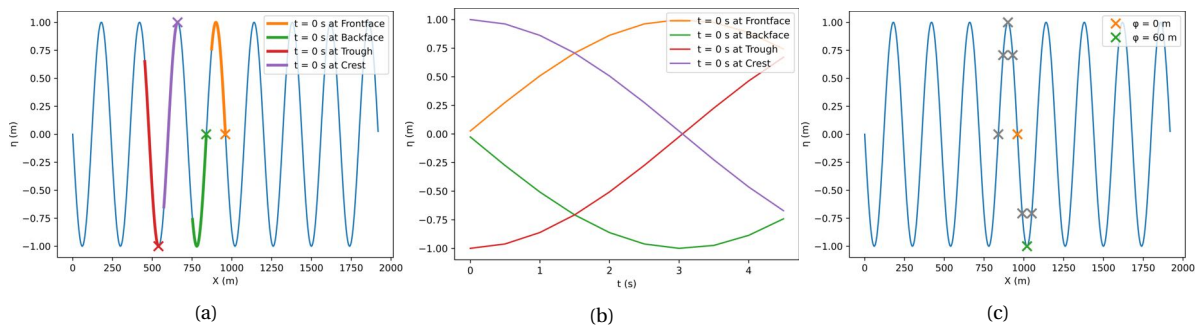


Figure C.2: Example of pixel positions at $t = 0$ s (a) and surface pathways (b) of a sinusoidal wave with wavelength, $L = 240$ m, a burst duration of 4.5 s and a time lag of 0.5 s. In (c) pixel positions with respect to the wave phase of the sinusoidal wave are shown.

C.4. RESULTS: THEORETICAL APPLICATION RANGE

The results of the temporal and spatial analysis are provided in Figures C.3, C.4, C.5 and C.6. The results are projected per pixel position at $t = 0$ s with respect to the wave phase. These positions are presented in Figure C.2c.

C.4.1. RESULTS: TEMPORAL ANALYSIS WAVELENGTH ESTIMATIONS

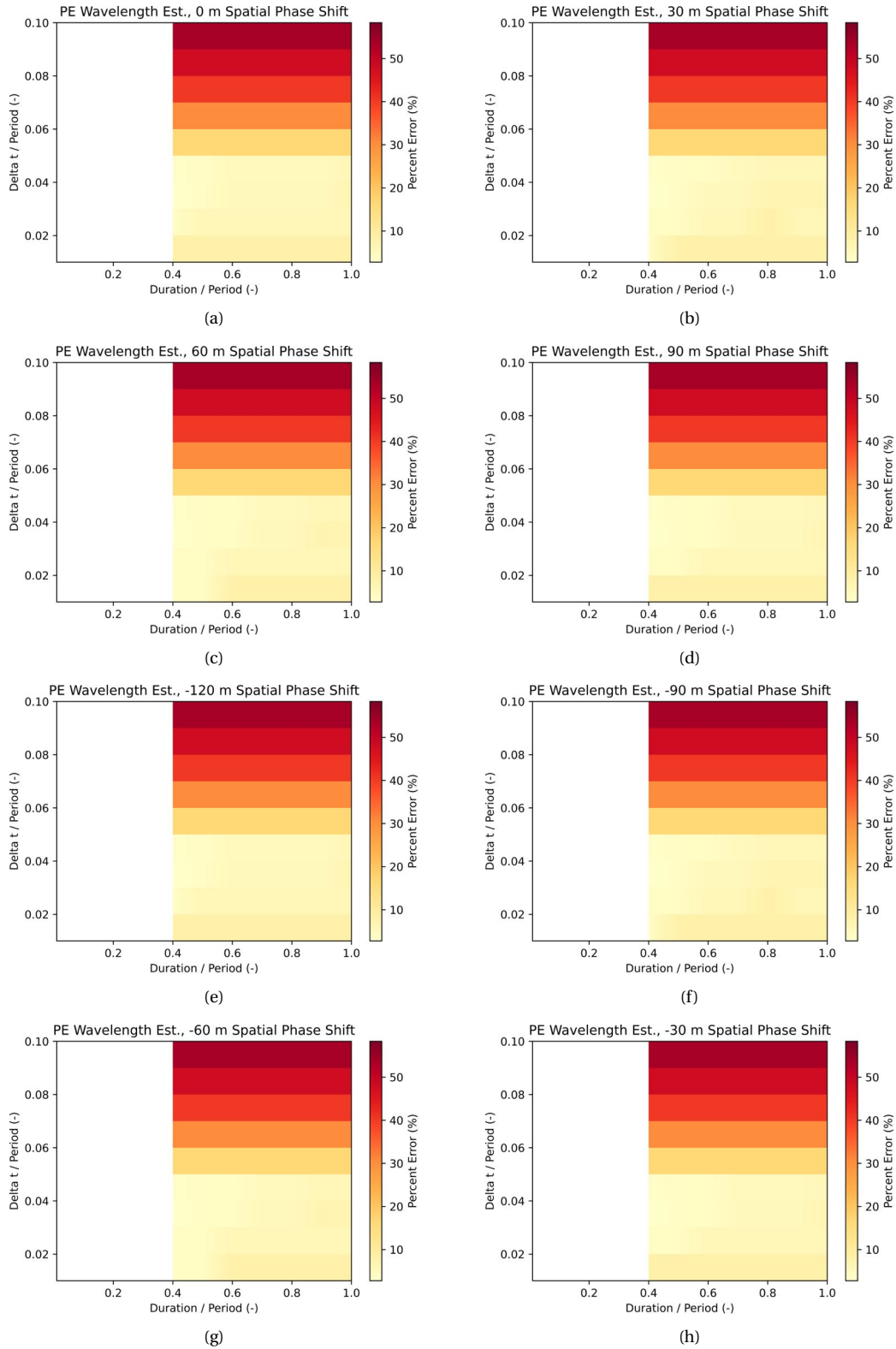


Figure C.3: Overview of results temporal analysis regarding wavelength estimations.

C.4.2. RESULTS: SPATIAL ANALYSIS WAVELENGTH ESTIMATIONS

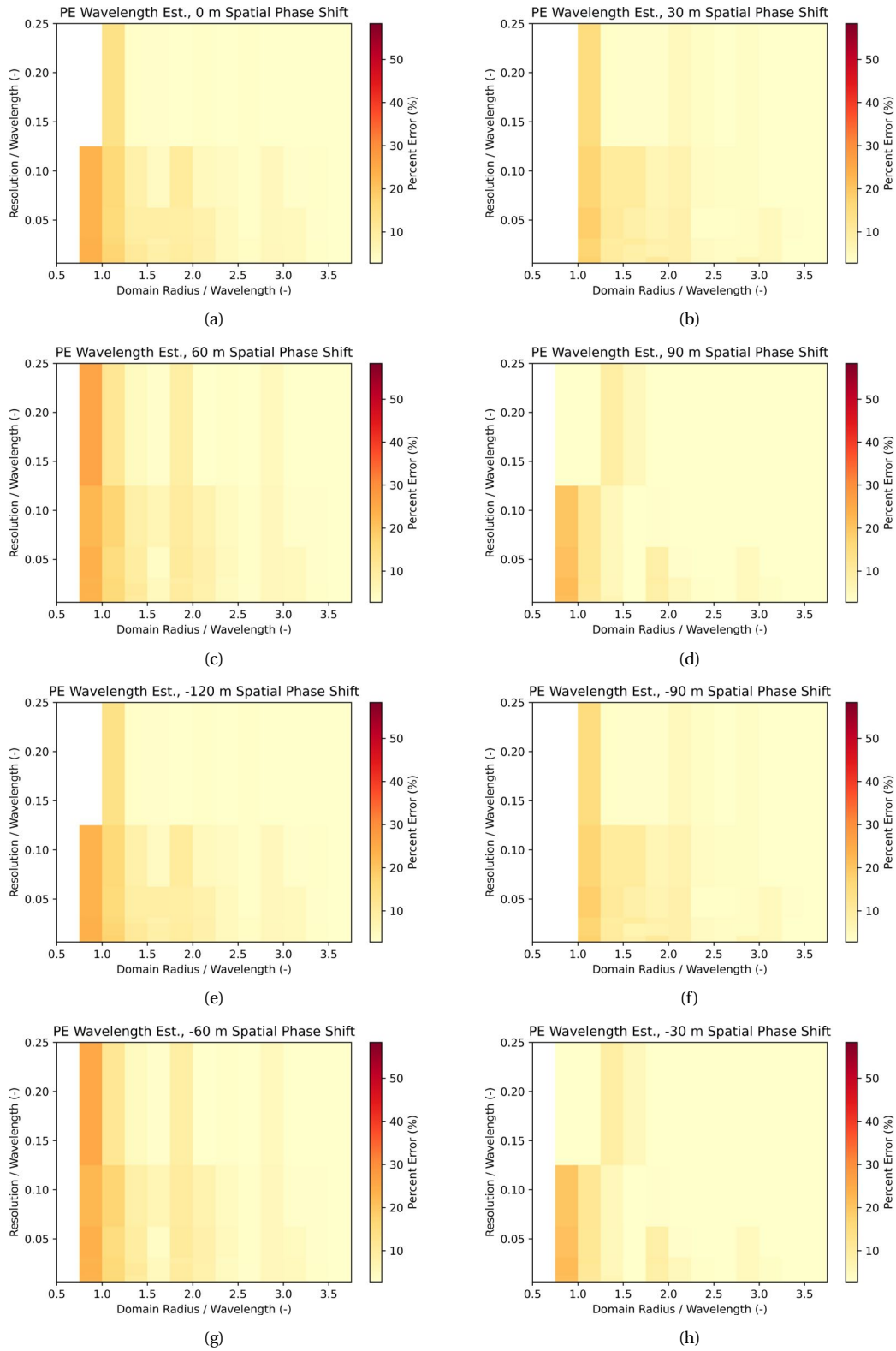


Figure C.4: Overview of results spatial analysis regarding wavelength estimations.

C.4.3. RESULTS: TEMPORAL ANALYSIS CELERITY ESTIMATIONS

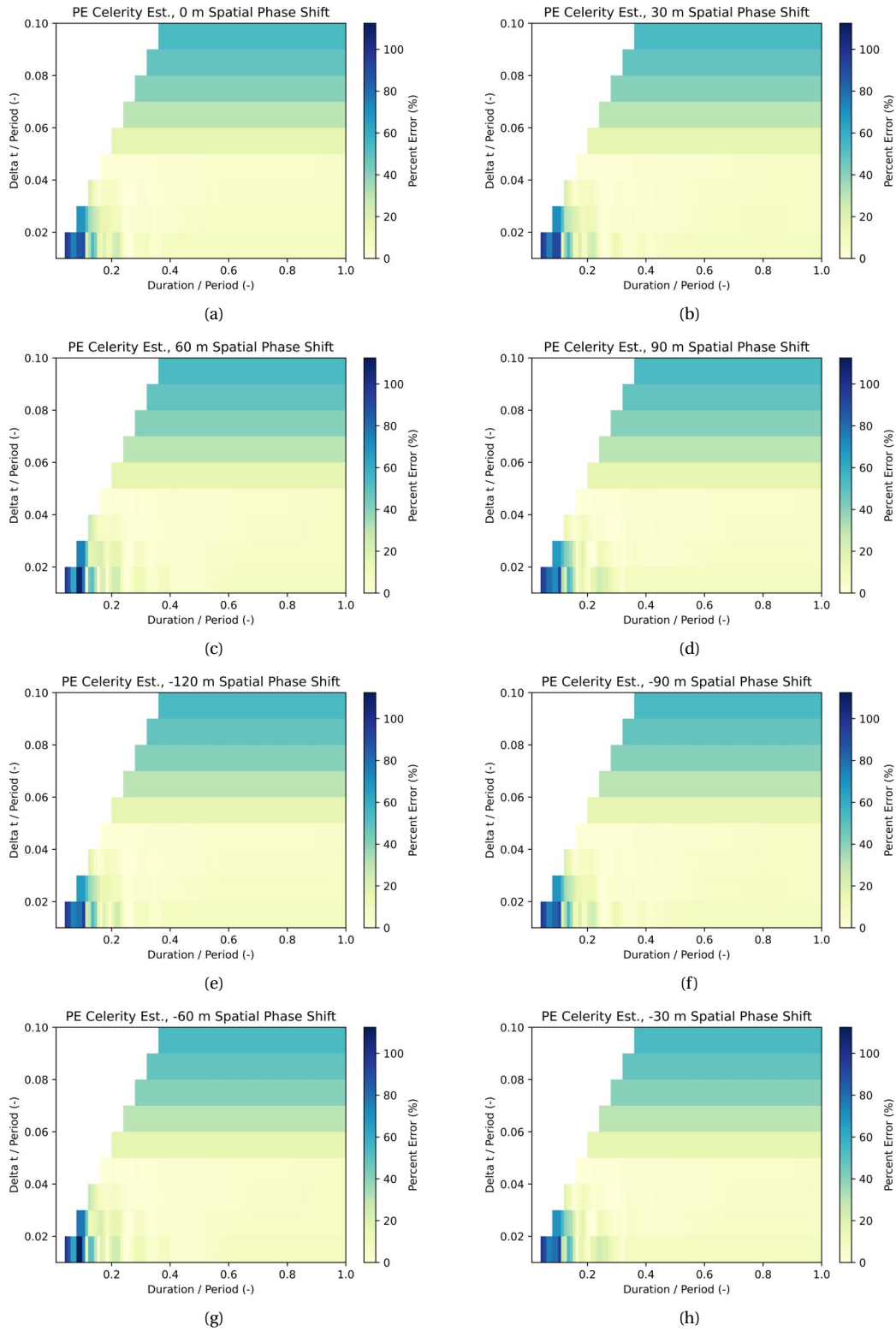


Figure C.5: Overview of results temporal analysis regarding celerity estimations.

C.4.4. RESULTS: SPATIAL ANALYSIS CELERITY ESTIMATIONS

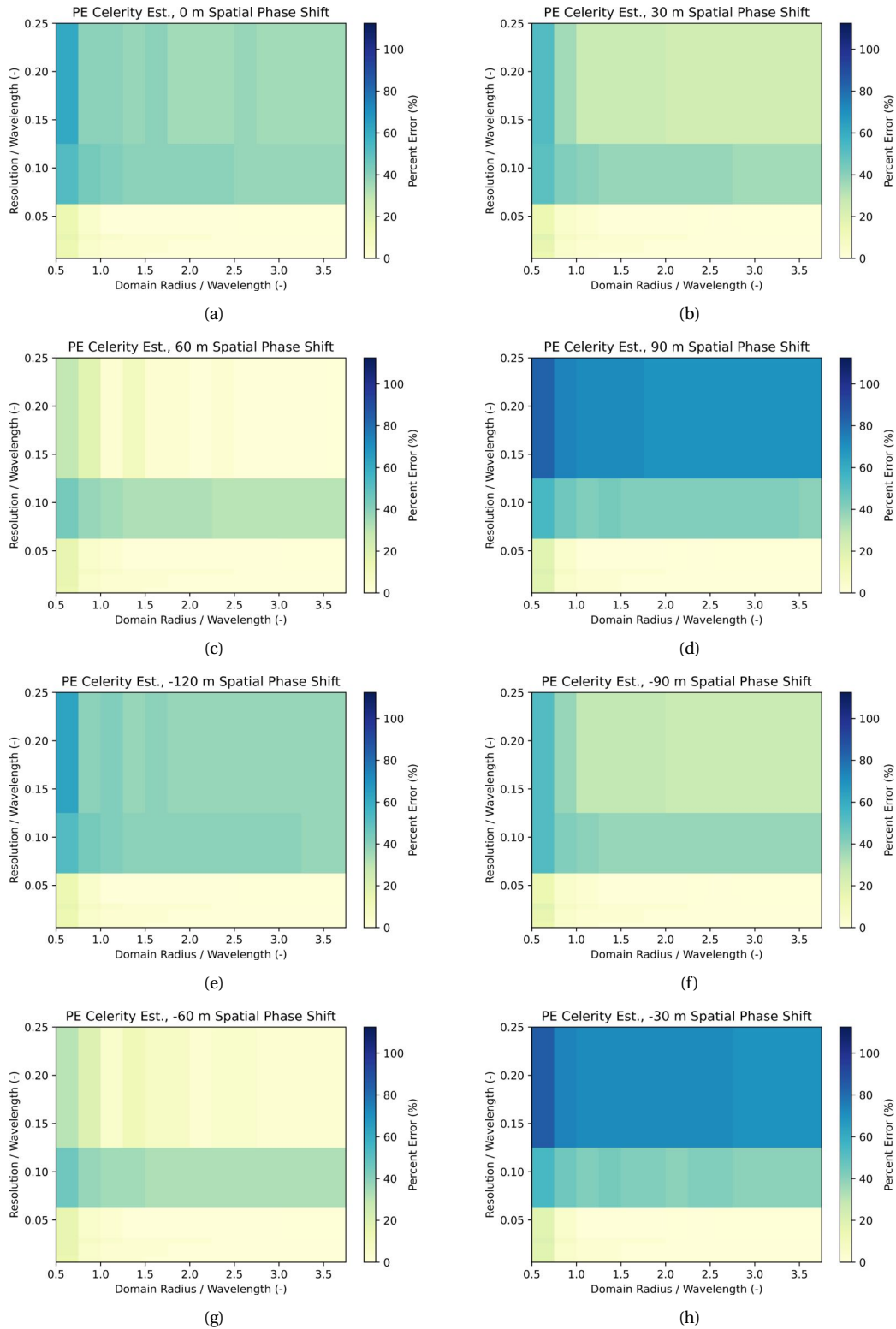


Figure C.6: Overview of results spatial analysis regarding celerity estimations.

C.5. INTERPRETATION OF THEORETICAL APPLICATION RANGE

Figures C.3, C.4, C.5 and C.6 together define the theoretical application range of the developed model. The following aspects are noted:

- All figures present the Percent Error (PE) in relation to temporal and spatial dimensionless values. The colours in the graphs correspond to a certain absolute error;
- Each analysis is performed for 8 different pixel locations with respect to the wave phase. That means, a different part of the wave is observed over the burst duration;
- Some parts of the graphs are blank. That means no results have been obtained for those combinations of dimensionless values. In the case of wavelength estimations, that is due to the lack of one of the separate wavelength estimations (zero-crossings, crests, troughs, see Chapter 5). In most cases, this is the result of a too short isolated wave signal: less than a wavelength is reconstructed in the cross-correlation image. Regarding the blanks in the celerity estimation graphs, those are the result of too few available snapshots.

The relationship between the presented results and the other results in this thesis is discussed in Chapter 7.

D

CELERITY FIELDS IN SAINT-LOUIS

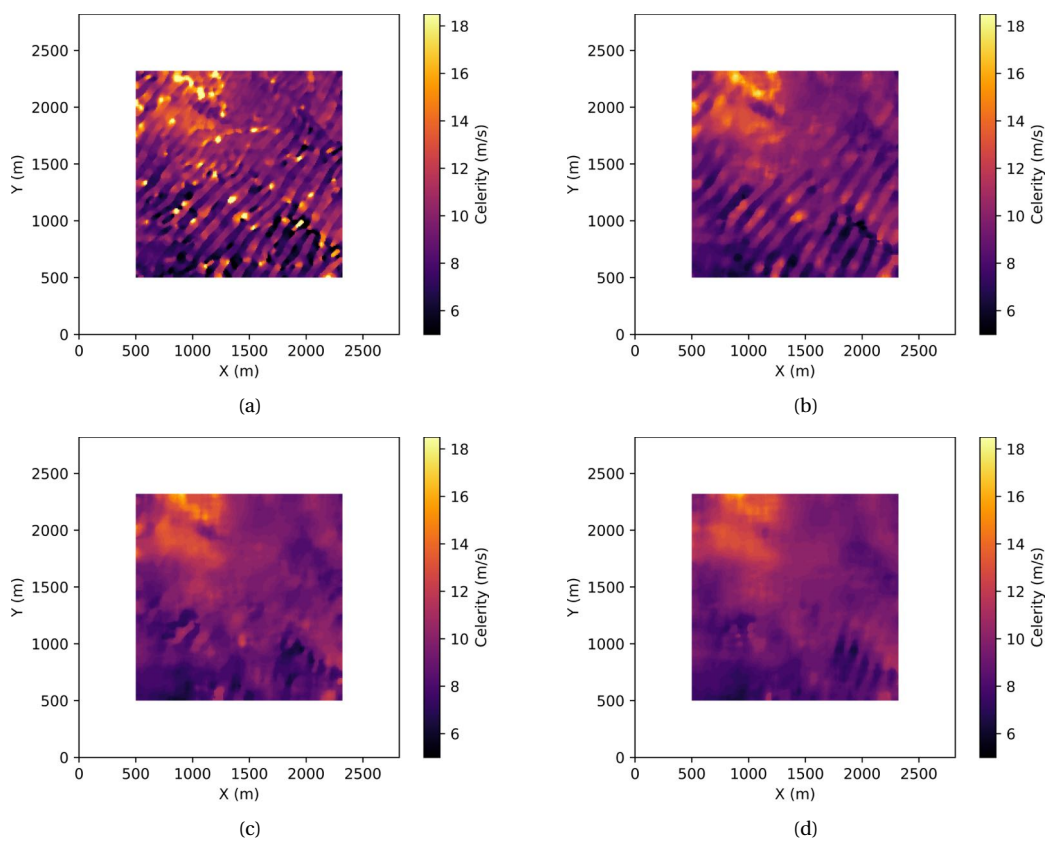


Figure D.1: Celerity Field in Saint-Louis. Median filters: (a) 50 m, (b) 100 m, (c) 150 m, (d) 200 m.

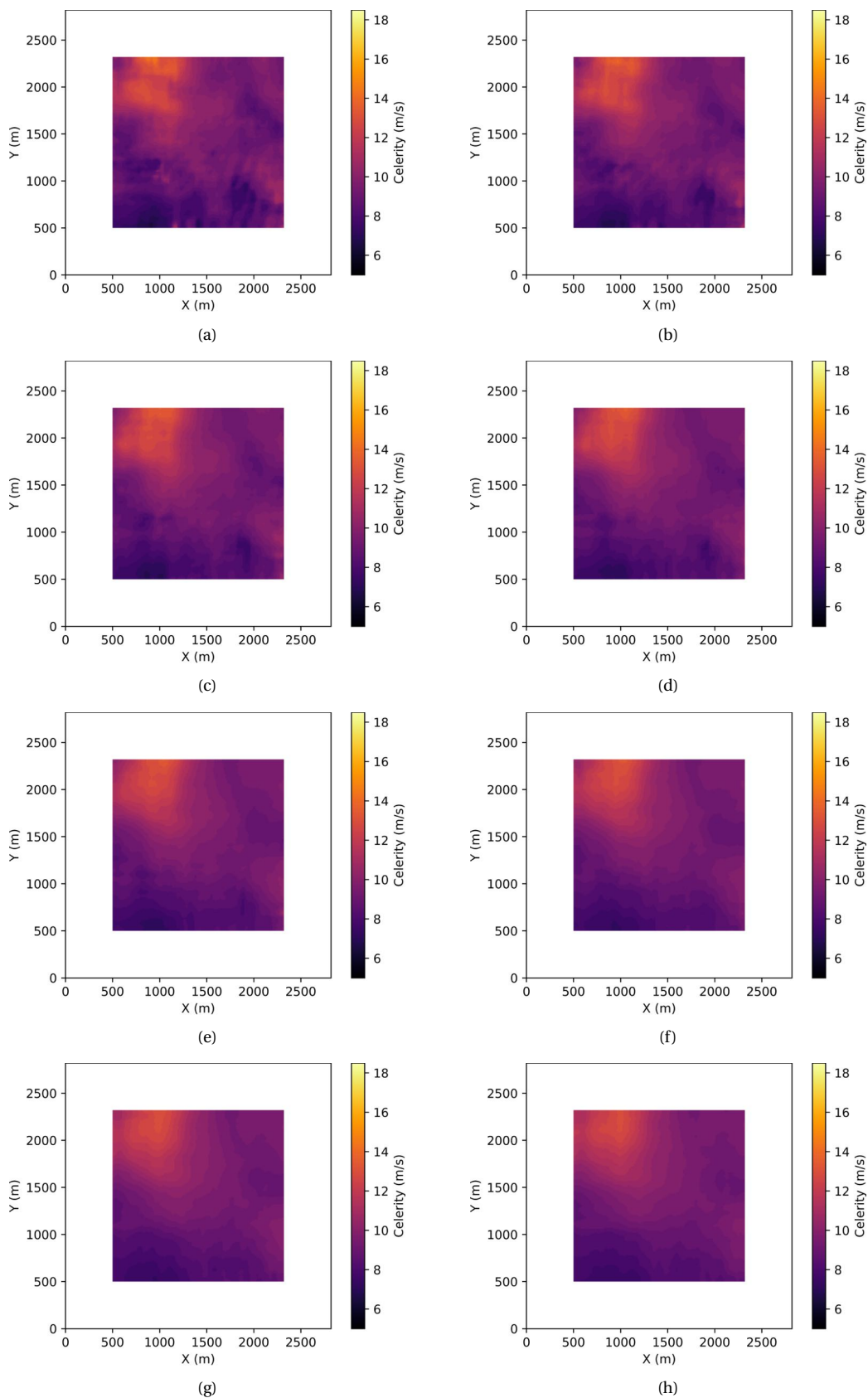


Figure D.2: Celerity Field in Saint-Louis. Median filters: (a) 250 m, (b) 300 m, (c) 350 m, (d) 400 m, (e) 450 m (f) 500 m, (g) 550 m, (h) 600 m.

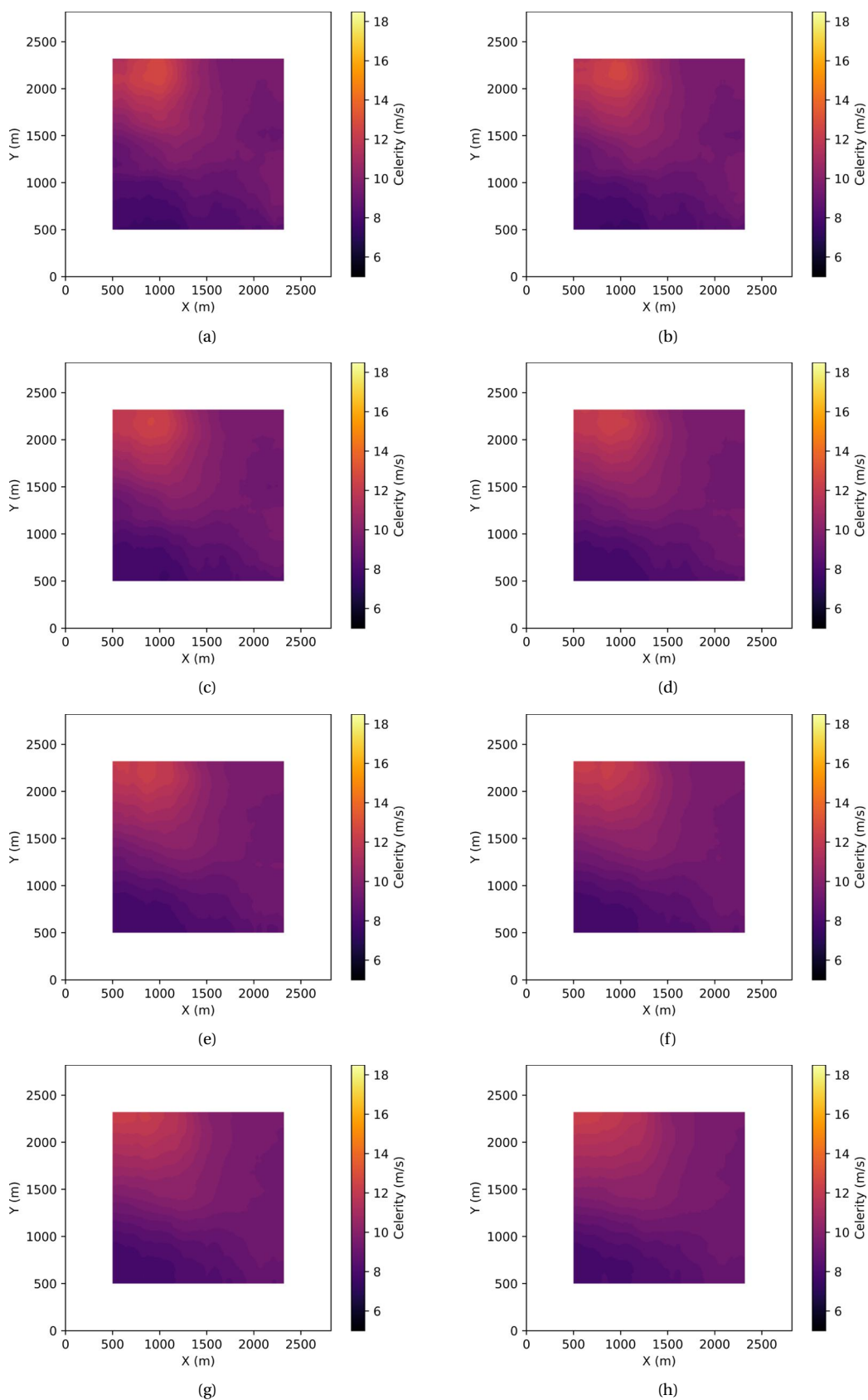


Figure D.3: Celerity Field in Saint-Louis. Median filters: (a) 650 m, (b) 700 m, (c) 750 m, (d) 800 m, (e) 850 m (f) 900 m, (g) 950 m, (h) 1000 m.

E

BATHYMETRY ESTIMATIONS IN SAINT-LOUIS

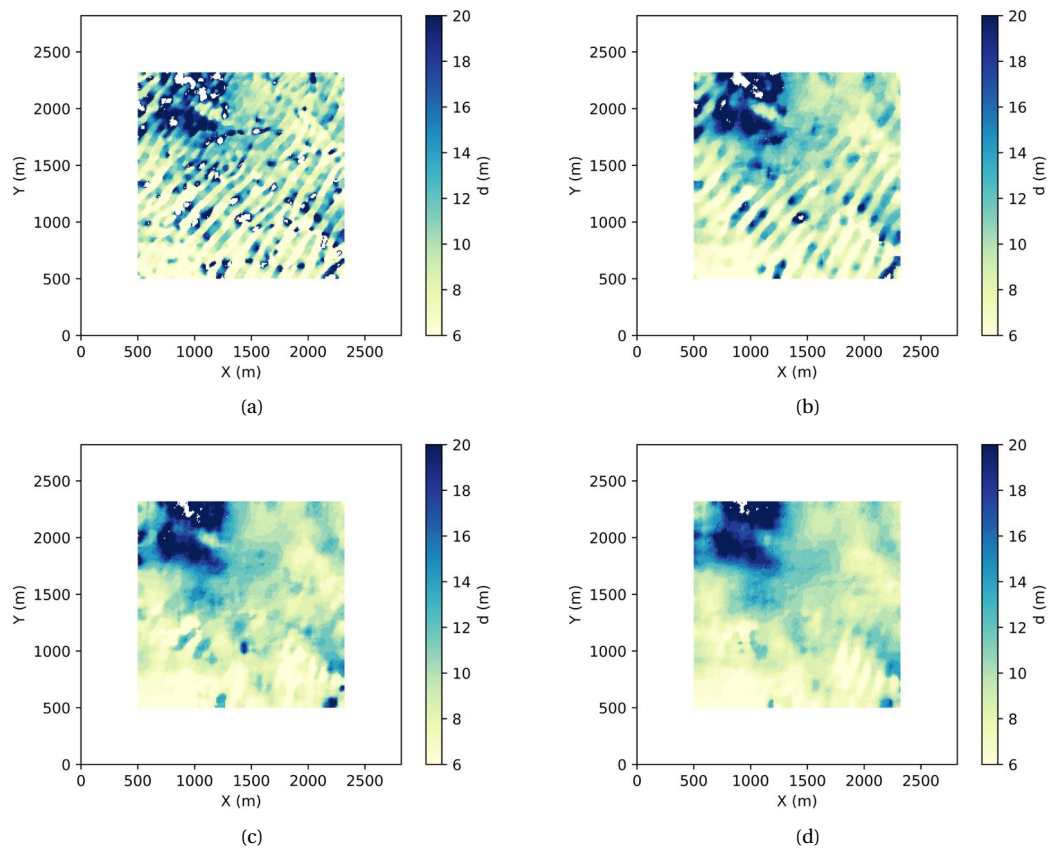


Figure E.1: Bathymetry Estimations in Saint-Louis. Median filters: (a) 50 m, (b) 100 m, (c) 150 m, (d) 200 m.

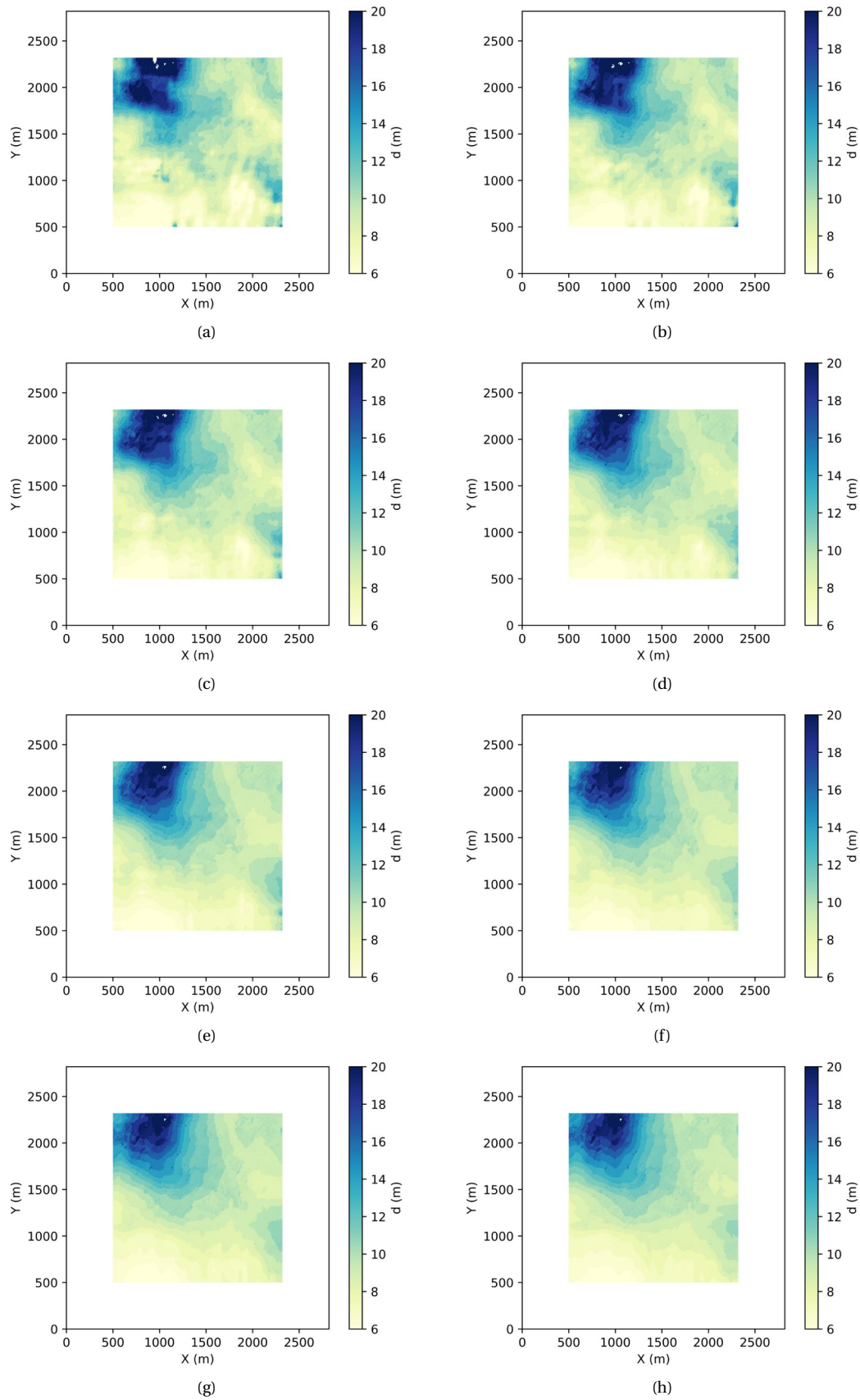


Figure E.2: Bathymetry Estimations in Saint-Louis. Median filters: (a) 250 m, (b) 300 m, (c) 350 m, (d) 400 m, (e) 450 m (f) 500 m, (g) 550 m, (h) 600 m.

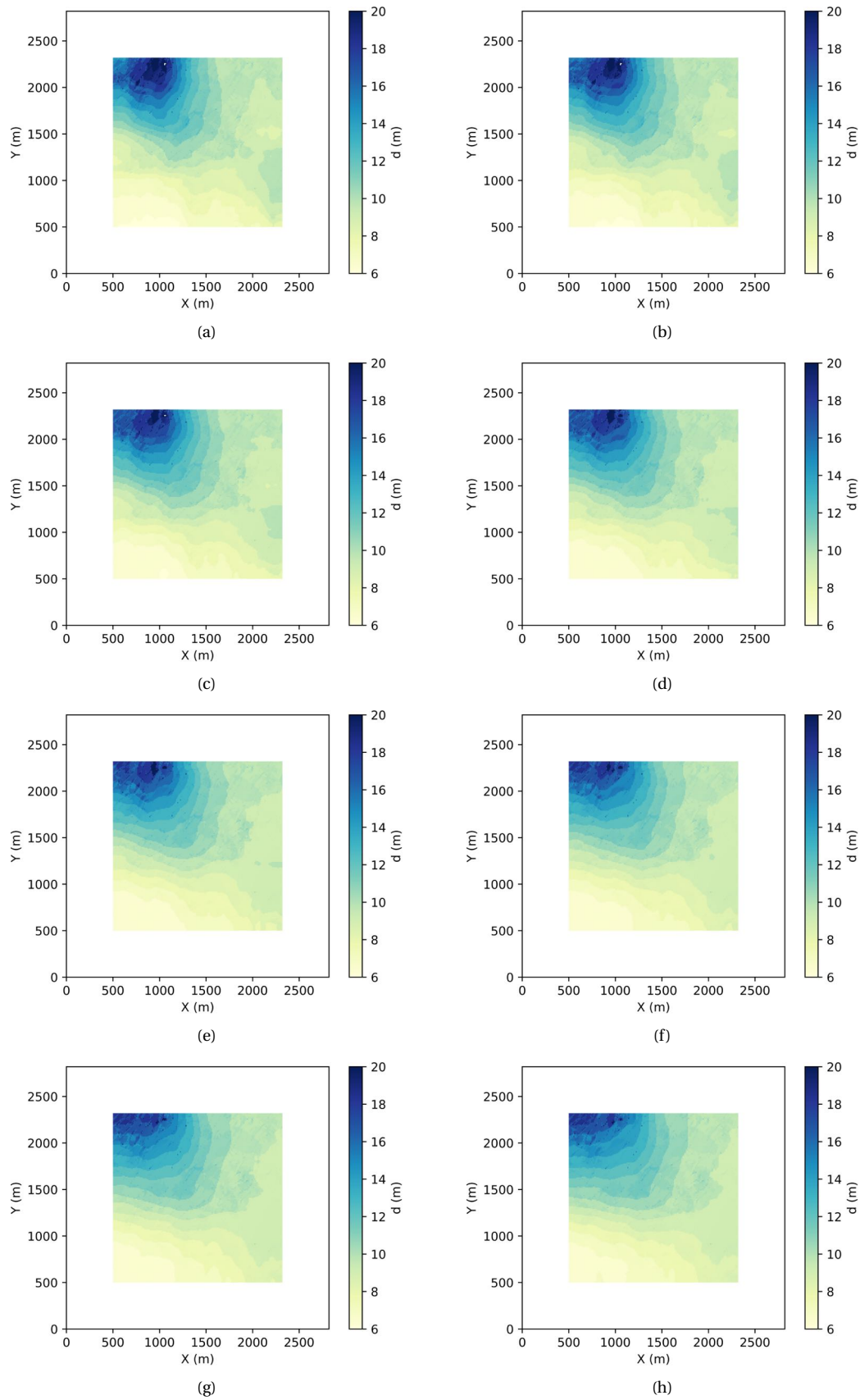


Figure E.3: Bathymetry Estimations in Saint-Louis. Median filters: (a) 650 m, (b) 700 m, (c) 750 m, (d) 800 m, (e) 850 m (f) 900 m, (g) 950 m, (h) 1000 m.